Stephen F. Austin State University
SFA ScholarWorks

Electronic Theses and Dissertations

Winter 12-8-2023

QUANTIFYING CURRENT SOIL BRINE CONTAMINATION WITHIN THE SMACKOVER OIL FIELD IN ARKANSAS USING MULTISPECTRAL DIGITAL IMAGERY

Victoria Williams
Stephen F. Austin State University, williamsv5@jacks.sfasu.edu

Follow this and additional works at: https://scholarworks.sfasu.edu/etds

Part of the Environmental Monitoring Commons, Geographic Information Sciences Commons, Oil, Gas, and Energy Commons, and the Soil Science Commons

Tell us how this article helped you.

Repository Citation

Williams, Victoria, "QUANTIFYING CURRENT SOIL BRINE CONTAMINATION WITHIN THE SMACKOVER OIL FIELD IN ARKANSAS USING MULTISPECTRAL DIGITAL IMAGERY" (2023). *Electronic Theses and Dissertations*. 524.
https://scholarworks.sfasu.edu/etds/524

This Thesis is brought to you for free and open access by SFA ScholarWorks. It has been accepted for inclusion in Electronic Theses and Dissertations by an authorized administrator of SFA ScholarWorks. For more information, please contact cdsscholarworks@sfasu.edu.

QUANTIFYING CURRENT SOIL BRINE CONTAMINATION WITHIN THE SMACKOVER OIL FIELD IN ARKANSAS USING MULTISPECTRAL DIGITAL IMAGERY

Creative Commons License

This work is licensed under a Creative Commons Attribution-Noncommercial-No Derivative Works 4.0 License.

This thesis is available at SFA ScholarWorks: https://scholarworks.sfasu.edu/etds/524

QUANTIFYING CURRENT SOIL BRINE CONTAMINATION WITHIN THE SMACKOVER OIL FIELD IN ARKANSAS USING MULTISPECTRAL DIGITAL IMAGERY

By

Victoria Williams, B.S. in Environmental Science

Presented to the Faculty of the Graduate School of

Stephen F. Austin State University

In Partial Fulfillment

of the Requirements

For the Degree of

Master of Science

STEPHEN F. AUSTIN STATE UNIVERSITY

December, 2023

QUANTIFYING CURRENT SOIL BRINE CONTAMINATION WITHIN THE SMACKOVER OIL FIELD IN ARKANSAS USING MULTISPECTRAL DIGITAL IMAGERY

By

VICTORIA M. WILLIAMS, Bachelor of Science

Approved:

_____
Daniel Unger, Ph.D., Thesis Director

_____
I-Kuai Hung, Ph.D., Committee Member

_____
David Kulhavy, Ph.D., Committee Member

_____
Yanli Zhang, Ph.D., Committee Member

_____
Dr. Lorenzo M. Smith, Ph.D.
Acting Dean of Research and Graduate Studies

ABSTRACT

A remote sensing study was performed to quantify current soil brine contamination across the historic Smackover Oil Field in south-central Arkansas, United States. The oil field was established in 1922 and was not subject to the future waste regulations created by the Arkansas Oil and Gas Commission. Brine is a waste product of oil manufacturing which contains water with high salt levels. The storage and transport of brine in the oil field created landscape scarring across the study area.

Landsat 9 multispectral digital imagery was utilized to create supervised classification maps based on earthen pits and creek scarring across the Smackover Oil Field. The results from these maps were compared to a previously completed brine contamination study which used Landsat 7 digital imagery to quantify brine contamination from oil production in west Texas.

Upon completion of this brine quantification study, it was determined that the scattered small areas of brine contamination identified as training sites for the supervised classifications of brine and non-brine areas of the Smackover Oil Field could not be quantified using the same classification methods as were used for the west Texas study that utilized larger, more uniform training sites representative of brine contamination. Classifications to quantify brine contamination are scene dependent and for oil fields similar to the Smackover Oil Field, a higher spatial resolution dataset than the 30m Landsat data used would be needed to more precisely quantify brine contamination.

ACKNOWLEDGMENTS

First and foremost, I would like to express my appreciation and gratitude to my thesis committee members for providing their knowledge, support, and advice throughout this process. Dr. Daniel Unger, acting as my major advisor, continually provided explanations and guidance to keep me on track. Dr. I-Kuai Hung helped me increase my writing skills and attention to detail. Dr. David Kulhavy facilitated my training and knowledge as a drone operator. Dr. Yanli Zhang pushed me to be a strong and confident graduate student. Dr. Liane Stevens, as my graduate representative, ensured that I was supported and encouraged throughout this process. I would also like to thank Dr. Kenneth Farrish for introducing this project and for the belief that I could succeed in graduate school.

This project could not have been accomplished without the cooperation of the Arthur Temple College of Forestry and Agriculture. All the materials and software necessary for this project were provided by the college. Additionally, funding for this project was provided by the USDA McIntire Stennis grant.

Finally, I would like to express my gratitude to Kirsten Garza and Charles James Heydon. The two of them accompanied and aided me in field research and without their continued support and motivation, I would not have pushed myself to strive to be the best version of myself.

TABLE OF CONTENTS

ABSTRACT i
ACKNOWLEDGMENTS ii
TABLE OF CONTENTS iii
LIST OF FIGURES vi
LIST OF TABLES xvi
INTRODUCTION 1
OBJECTIVES 11
LITERATURE REVIEW 14
History of the Smackover Oil Field Production 14
Oil Waste History 14
Oil Storage 15
Historical Regulation of the Smackover Oil Field 19
History of Smackover Saltwater Production and Storage 20
Brine Effects on the Landscape 20
Brine Regulation of the SOF 27
Brine Validation 28
Soil Sampling 28
Image Acquisition 29
Landsat 29
Landsat-9 OLI/TIRS-2 30
DJI Phantom 4 Multispectral UAV with RTK 30
Image Classification 32
Supervised Classification 32
Unsupervised Classification 33
Accuracy Assessment 33
Error Matrix 33

Kappa Statistic 34
METHODOLOGY 36
Study Area 36
Image Acquisition 39
Landsat 9 OLI/TIRS-2 39
P4M-RTK Sensor 40
Image Corrections 41
Radiometric Corrections 41
Geometric Correction 42
Image Classification 43
Supervised Classification 43
Unsupervised Classification 45
Sample Site Selection 46
Soil Sampling 46
Soil Sample Collection 47
Soil Sample Analysis 48
Accuracy Assessment 48
An Example: Error Matrix 49
An Example: Kappa Statistic 50
RESULTS 52
Landsat 9 Image Acquisition 52
Identifying the Boundary 52
Landsat 9 OLI/TIRS-2 58
Radiometric Corrections 61
Geometric Corrections 61
Landsat 9 Image Classification 64
Reference Data 64
Training Site Acquisition 69
Pit Training Sites 73

Creek Training Sites 77
Supervised Classification 79
Sample Site Selection 87
Louann Park 88
Fishing Area 90
Norphlet Park 91
Soil Sampling 92
Soil Sample Collection 92
Soil Sample Analysis 94
P4M-RTK Image Acquisition 99
Processing the UAV Multispectral Imagery 99
P4M-RTK Image Unsupervised Classification 107
Accuracy Assessment 108
DISCUSSION AND CONCLUSIONS 111
LITERATURE CITED 116
VITA 127

LIST OF FIGURES

Figure 1. The Smackover Oil Field located in south-central Arkansas, United States. 2

Figure 2. 1936 aerial photograph of earthen storage tanks in the Smackover Oil Field which demonstrates the variation in size and shape of earthen storage features (Barrett, 2001). 3

Figure 3. A depiction of data collection in remote sensing. 5

Figure 4. The J.T. Murphy no. 1 crater in the Norphlet District of the Smackover Oil Field. 15

Figure 5. Layers of asphaltic crust are present in the soils near an intermittent creek (Barrett, 2001). 17

Figure 6. Earthen storage and storage scarring in 1936 across the Norphlet District (Culver & Barrett, 2001). 18

Figure 7. Historic photograph of lease pits near an oil well in the Smackover Oil Field (Culver & Barrett, 2001). 19

Figure 8. 1936 aerial photograph taken over part of the Smackover Oil Field (Barrett, 2002). 22

Figure 9. 1996 aerial photograph taken over part of the Smackover Oil Field (Barrett, 2002). 23

Figure 10. Asphaltic crusts and cypress stumps in an intermittent creek (Barrett, 2001). 23

Figure 11. The Phantom 4 Multispectral RTK UAV sensors. 31

Figure 12. A study site map of the Smackover Oil Field with color-infrared imagery. .. 37

Figure 13. The general method performed for the Smackover Oil Field soil brine contamination study. 38

Figure 14. An example of a Landsat 9 OLI/TIRS-2 solid state recorder bad block issue. 42

Figure 15. Land scarring from brine contamination across the Norphlet District in the Smackover Oil Field that was visually present in 1996 (Barrett, 2002). 45

Figure 16. An example error matrix for accuracy assessment on land cover classification. 49

Figure 17. Smackover Oil Field map boundary from the Arkansas Geological Survey, Bulletin 2 (Spooner, 1935). 53

Figure 18. Public Land Survey System sections downloaded for Ouachita and Union counties from the Arkansas GIS Office, n.d.. 54

Figure 19. Public Land Survey System townships downloaded for Ouachita and Union counties from the Arkansas GIS Office, n.d. 54

Figure 20. Merging the four PLSS related areas across the Ouachita and Union County shapefiles into one shapefile in ESRI ArcGIS Pro v. 3.1.0 software..... 55

Figure 21. Projecting the merged PLSS shapefile into the UTM Zone 15 N WGS 1984 in ArcGIS Pro v. 3.1.0 software..... 55

Figure 22. Exporting the PLSS sections that are consistent with sections in the Smackover Oil Field boundary in Figure 17..... 56

Figure 23. Figure 17 is georeferenced to the PLSS sections so that the Smackover Oil Field boundary can be digitized in ESRI ArcGIS Pro v. 3.1.0. 57

Figure 24. Digitized boundary of the Smackover Oil Field based on the historic Smackover Oil Field map boundary in ArcGIS Pro v. 3.1.0. 57

Figure 25. A Landsat 9 OLI/TIRS-2 scene that included the SOF in the online interface, GloVis. 58

Figure 26. The downloaded Landsat 9 scene from USGS in ERDAS IMAGINE® 2022 v. 16.7..... 59

Figure 27. The area that was subset from the Landsat 9 OLI/TIRS-2 image in ERDAS IMAGINE® 2022 v. 16.7 of the Smackover Oil Field..... 59

Figure 28. Creating the subset digital image and including the blue, green, red, near-infrared, and two mid-infrared bands spectral bands in ERDAS IMAGINE® 2022 v. 16.7..... 60

Figure 29. The 6-band multispectral digital image of the Smackover Oil Field. 60

Figure 30. The One Foot Digital Orthophotographs dataset provided by the Arkansas GIS Office (Arkansas GIS Office, n.d.)..... 62

Figure 31. The process of selecting data from each relevant tile in the ESRI ArcGIS Online web map (ESRI, n.d.). 63

Figure 32. The Mosaic to New Raster tool in ESRI ArcGIS Pro v. 3.1.0 was used to mosaic the DOQs and reproject them into the desired spatial reference. 63

Figure 33. A comparison of landscape features between DOQ and Landsat 9 data. 64

Figure 34. The Norphlet District in the eastern portion of the Smackover Oil Field. 65

Figure 35. Norphlet District streams that were discernable in 1996 (Barrett, 2002). 66

Figure 36. The streams of Ouachita and Union counties, Arkansas shown in ESRI ArcGIS Pro v. 3.1.0 and retrieved from the Arkansas GIS Office website. 66

Figure 37. The streams of Union and Ouachita counties were merged into one shapefile using the Merge tool in ArcGIS Pro v. 3.1.0. 67

Figure 38. The Project tool was used in ESRI ArcGIS Pro v. 3.1.0 to project the merged streams into UTM Zone 15 in the datum WGS 1984. 68

Figure 39. The streams across the 1996 map of lease pits and pit scars were georeferenced to the projected streams in Ouachita and Union counties. 68

Figure 40. The reference map to identify potential training sites was georeferenced to the map containing streams across the Norphlet District using ArcGIS Pro v. 3.1.0. 69

Figure 41. The coordinates of pit and creek locations were identified to facilitate locating the scarred areas in CONNECTexplorer™. 70

Figure 42. A potential training site located in CONNECTexplorer™ with coordinates from the reference map (EagleView Technologies, n.d.). 71

Figure 43. A potential training site located in CONNECTexplorer™ that was measured to identify acreage of the area (EagleView Technologies, n.d). 71

Figure 44. The 11 potential training sites which represented pit scarring across the Norphlet District. 72

Figure 45. The ten potential training sites which represented creek scarring across the Norphlet District. 73

Figure 46. The blue and near-infrared bands were chosen to be plotted against each other in a feature space layer in ERDAS IMAGINE® 2022 v. 16.7. 74

Figure 47. The selection of an individal AOI representing a the first pit scar in ERDAS IMAGINE® 2022 v. 16.7. 75

Figure 48. The first pit scar added to the Signature Editor tool in ERDAS IMAGINE® 2022 v. 16.7 75

Figure 49. Each Signature Object based on the added pit AOIs were plotted and labelled at a standard deviation of 2. 76

Figure 50. The Signature Objects of each pit AOI shown in the created feature space layer 76

Figure 51. The Signature Objects of the chosen pit AOIs for the pit-based supervised classification. 77

Figure 52. The Signature Objects of each creek AOI in a feature space layer in ERDAS IMAGINE® 2022 v. 16.7. 78

Figure 53. The Signature Objects of the chosen creek AOIs for the pit-based supervised classification. 78

Figure 54. The decision rules selected for the pit-based and creek-based supervised classifications. 79

Figure 55. The supervised classification based on the chosen pit training sites. 80

Figure 56. The supervised classification based on the chosen creek training sites. 80

Figure 57. The Clump tool in ERDAS IMAGINE® 2022 v. 16.7 used to refine the supervised classifications. 81

Figure 58. The pit-based supervised classification after the “Clump” tool was applied. 82

Figure 59. The creek-based supervised classifcation after the “Clump” tool was applied. 82

Figure 60. The attribute table for the pit-based clumped supervised classification was viewed to ensure each classified polygon was represented by the preselected pit training sites. 83

Figure 61. The Eliminate tool was used to remove island polygons from the clumped supervised classifications. 84

Figure 62. The effects of the Eliminate tool on the clumped pit-based supervised classification in red overlain across the subset Landsat 9 scene. 84

Figure 63. The effects of the Eliminate tool on the clumped creek-based supervised classification overlain in red across the subset Landsat 9 scene. 85

Figure 64. The initial statistics for the histogram of the subset Landsat 9 scene of the Smackover Oil Field indicated a total of 136,725 pixels in the digital image. 86

Figure 65. The statistics for the histogram value of the pit-based clumped and eliminated supervised classification revealed a total of 5,374 classified pixels. 86

Figure 66. The statistics for the histogram value of the clumped and eliminated creek-based supervised classification revealed a total of 3,218 classified pixels. 87

Figure 67. A map representing the three chosen sampling sites in yellow across the Smackover Oil Field. 88

Figure 68. A CONNECTexplorer™ image of the Louann Park sampling site which displayed a lack of vegetation other than the bordering trees and was taken January 7, 2020 (EagleView Technologies, n.d.)..... 89

Figure 69. The boundary of the Louann Park site is delineated in black and brine contamination is indicated with red. The pit-based classification is displayed on the left, while the creek-based classification is displayed on the right. 89

Figure 70. Fishing Area sampling site with the Smackover Creek located toward the southwestern part of the sampling site. Imagery was taken January 8, 2020 (EagleView Technologies, n.d.)..... 90

Figure 71. Norphlet Park sampling site with a lack of vegetation across the surface. A part of the Norphlet Middle School may be identified toward the southern part of the sampling site. The imagery was taken January 20, 2020 (EagleView Technologies, n.d)..... 91

Figure 72. The boundary of the Norphlet Park site is delineated in black and brine contamination is indicated with red. The pit-based classification is located on the left, while the creek-based classification is on the right. 92

Figure 73. The 15 cm length was measured on the shovel to ensure soil samples were taken at a consistent depth. 93

Figure 74. The five soil samples which were collected for the Louann Park sampling site and uploaded with ESRI's Field Maps displayed as red stars. 93

Figure 75. The composite samples from each of the three sampling sites labelled in soil bags August 2, 2023. 94

Figure 76. The soil samples were dried on separate plates. 95

Figure 77. The grinder used to process the soil samples. 95

Figure 78. The saturated pastes were created by adding nano pure water to each sample. 96

Figure 79. The saturated soils placed in a Buchner funnel lined with filter paper. 96

Figure 80. The extraction of the soil samples with a vacuum setup. 96

Figure 81. The Metrohm 914 pH/Conductometer was used to analyze pH and EC of the soil samples. 97

Figure 82. The ICP machine used to identify the concentration of the constituents in the liquid extracts 98

Figure 83. A preprogrammed drone flight mission for Louann Park created in the Ground Station Pro app (DJI, n.d.a). 99

Figure 84. The Ag Multispectral procesing option chosen in PIX4Dmapper. 100

Figure 85. The DSM, Orthomosaic, and Index option was chosen so that an orthophoto mosaic of each band that was captured by the multispectral camera obtained from the flight would be created..... 101

Figure 86. The orthophoto mosaic and easch individual band generated from drone imagery collected during the Louann Park Inner preprogrammed flight. 101

Figure 87. The blue, green, red, and near-infrared bands were combined into a multispectral digital image with the Layer Selection and Stacking tool in ERDAS IMAGINE® 2022 v. 16.7 for each dataset from the preprogrammed flights..... 103

Figure 88. The six preprogrammed drone flights flown with the P4M-RTK each designated by a red letter: A – Louann Park Inner, B- Louann Park Outer, C- Fishing Area Inner, D- Fishing Area Outer, E- Norphlet Park Inner, F- Norphlet Park Inner.... 104

Figure 89. The Indices tool in ERDAS IMAGINE® 2022 v. 16.7 used to create the NDVI of each preprogrammed flight dataset..... 105

Figure 90. The created NDVI of the six preprogrammed drone flights each designated by a red letter: A – Louann Park Inner, B- Louann Park Outer, C- Fishing Area Inner, D- Fishing Area Outer, E- Norphlet Park Inner, F- Norphlet Park Inner. 106

Figure 91. The clustering options chosen for the unsupervised classifications of the P4M-RTK multispectral data..... 107

Figure 92. The created unsupervised classifications of the six preprogrammed drone flights each designated by a black letter: A – Louann Park Inner, B- Louann Park Outer,

C- Fishing Area Inner, D- Fishing Area Outer, E- Norphlet Park Inner, F- Norphlet Park Inner 108

LIST OF TABLES

Table 1. Platforms associated with this study and their sensor resolution characteristics. 9

Table 2. Results of a 1935 water analysis from well drilling in the Meakins producing sands within the Smackover Oil Field depicted in a table from W.C. Spooner in the *Oil and Gas Geology of the Gulf Coastal Plain in Arkansas*. 25

Table 3. Results of a 1935 water analysis from well drilling in the Graves producing sands within the Smackover Oil Field depicted in a table from W.C. Spooner in the *Oil and Gas Geology of the Gulf Coastal Plain in Arkansas*. 26

Table 4. Image resolution characteristics of Landsat-9 OLI/TIRS-2. 30

Table 5. Spectral characteristics of Landsat platforms relevant to the study. 40

Table 6. Spectral characteristics of Phantom 4 Multispectral RTK UAV relevant to the study. 41

Table 7. A table describing the quality ranges of kappa statistics. 51

Table 8. The pH and Electrical Conductivity results for the sampling sites. 97

Table 9. The concentrations of sodium, calcium, and magnesium and the SAR results for the sampling sites. 98

Table 10. The error matrix, and kappa statistic for the pit-based supervised classification of the Smackover Oil Field. 109

Table 11. The error matrix, and kappa statistic for the creek-based classification of the Smackover Oil Field. 110

INTRODUCTION

In Smackover, Arkansas, heavy and light crude oil was produced in the approximately 30,000-acre historic Smackover Oil Field (SOF) during the early 1900s (Figure 1). The data for Figure 1 were compiled from multiple sources including: the Arthur Temple College of Forestry and Agriculture (ATCOFA) Geographic Information Systems (GIS) server, GloVis, and "Bulletin 2: Oil and Gas Geology of the Gulf Coastal Plain in Arkansas" by W. C. Spooner (1935). The SOF comprises two districts: the Louann District on the western side and the Norphlet District on the eastern side. During the first decade of oil production, it was estimated that over one billion barrels of discarded saltwater contaminated the landscape during the oil production process (Barrett 2002). Brine contamination across the SOF resulted in one of the most historically scarred petroleum production areas in the United States. Remote sensing techniques were applied to digital imagery of the area of interest, obtained from Landsat 9 and a DJI Phantom 4 Pro Multispectral RTK (P4RTK) Unmanned Aerial Vehicle (UAV), and were used to identify the spectral signature of soil brine contamination and further quantify the areas affected.

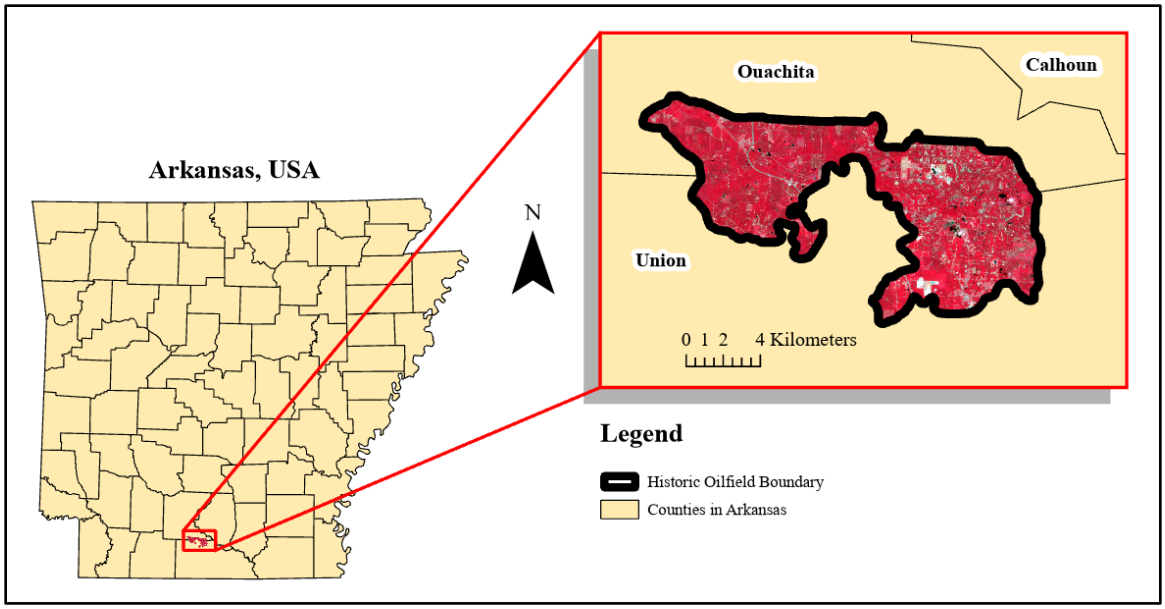

Figure 1. The Smackover Oil Field located in south-central Arkansas, United States.

In 1922 the first oil boom within the SOF occurred, launching the field into its major production era. Official state regulation for oil, gas, and brine related issues did not come into place until 1939 with the Arkansas Conservation Act and subsequent creation of the Arkansas Oil and Gas Commission (AOGC) (Norvell, 2015). As a result, the SOF oil production and waste practices were grandfathered in and did not comply with updated oil and gas conservation regulations (Barrett, 2001). During the SOF's period of operation earthen lease pits and tank farms stored crude oil, oil emulsions, and freshwater. There was a lack of uniformity in the construction of earthen storage pits and tanks. Several earthen storage tanks can be identified as dark rectangular landscape features while scarring that was associated with the pits is identified by the bare white linear features scattered throughout Figure 2. Towards the end of the production era, the

earthen pits previously used for oil were used to store saltwater (Barrett, 2001; Barrett, 2002). This saltwater was left in field pits to evaporate or leach into the surrounding soils until the pits were empty (Barrett, 2002). The effects of saltwater, or brine, on the SOF's landscape are still visually observable a century later.

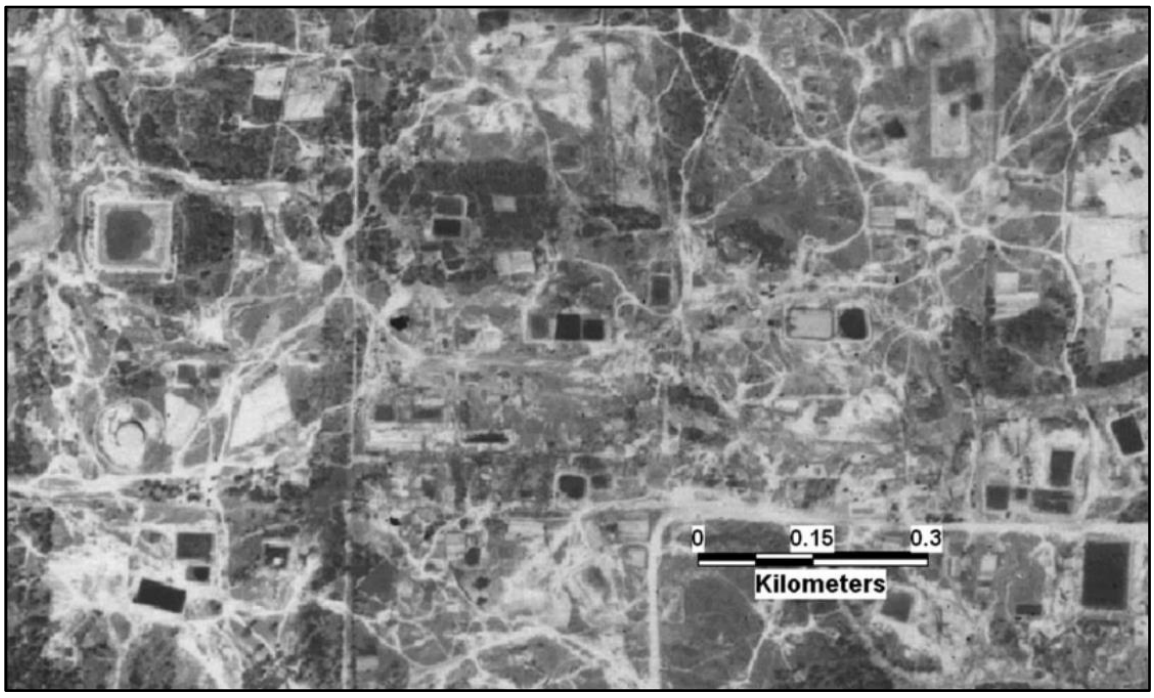

Figure 2. 1936 aerial photograph of earthen storage tanks in the Smackover Oil Field which demonstrates the variation in size and shape of earthen storage features (Barrett, 2001).

The impacts of soil brine contamination are present across all areas where oil and gas are produced. Brine is a waste product of oil and gas manufacturing that contains water with high salt concentrations, primarily sodium chloride (Meehan et al., 2017). Brine is also called produced water and can come from multiple sources including

directly from the geologic formation being drilled into, injection water used to force crude oil to the surface, and emulsions of oil and salts (Meehan et al., 2017). When brine contaminates an ecosystem there may be negative impacts on vegetation and soils as it deteriorates soil texture and is toxic to plant life resulting in soil erosion (Otton, 2006). Brine solutions are characterized by their high electrical conductivities (EC), sodium adsorption ratios (SAR), and more acidic pH (Allison et. al., 1954; Meehan et al., 2017; Sonon et al., 2015). Solutions are considered brine when there is a measured EC greater than 4 deciSiemens per meter (dS/m), an SAR greater than 13, and pH less than 8.5 (Allison et. al., 1954; Sonon et al., 2015). In the SOF, damage to the landscape from brine contamination was documented in a 1936 and 1996 aerial photography comparison (Barrett, 2002).

Remote sensing is the science of obtaining information about the Earth's resources from a distance using reflective and emitted electromagnetic energy. Figure 3 illustrates the data collection process of remote sensing from the source, the Sun, to a platform's sensor (National Space Development Agency of Japan, 1999). Electromagnetic energy from the Sun moves through the atmosphere and interacts with objects on the Earth's surface. The data from the reflective and emitted energy of an object is picked up by a sensor that has been mounted to a platform. Remote sensing has been used to identify soil brine contamination in oil-field sites in west Texas and southern Illinois (Unger et al., 2013; Hensel et al., 1989). Brine contamination on soils may be distinguishable within a landscape due to its unique spectral signature (Panigrahy & Ray,

2005). Each object on Earth has a unique distribution of reflected, emitted, and absorbed electromagnetic energy, known as a spectral signature. Digital remote sensing techniques can be used to identify, interpret, and classify spectral signatures of soil brine contamination across oil fields.

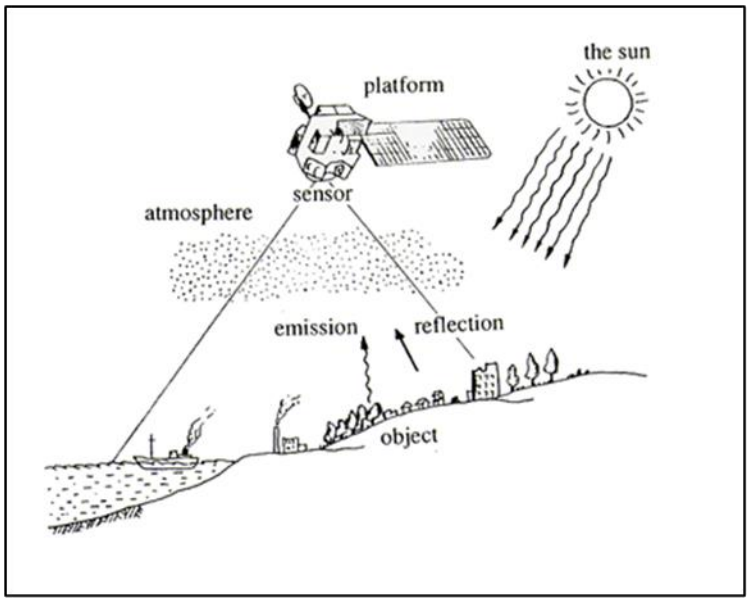

Figure 3. A depiction of data collection in remote sensing.

Four main principles guide remote sensing applications: spectral differentiation, spatial differentiation, radiometric differentiation, and temporal difference. These terms may also be referred to as resolutions, e.g., spectral resolution, and can be used to describe the properties of a sensor that is being used for image acquisition (Hacker & Pickell, n.d.). Sensors are mounted to platforms such as satellites or UAVs. The individual resolution characteristics of sensors will have varying levels of efficacy

depending on their intended use which should be considered during remote sensing applications.

Spectral resolution refers to the different wavelengths across the electromagnetic energy spectrum that a sensor may be able to detect. Electromagnetic energy travels from the Sun to the Earth in waves where it interacts with objects, such as vegetation, on the Earth's surface and is either reflected, emitted, and/or absorbed (Nowatzki et al., 2004). The energy waves are typically measured by length in micrometers (μm) and classified into the electromagnetic spectrum (ES). The spectral resolution of a sensor is determined by the number of spectral bands across the ES that can be discerned in an area of interest (Hacker & Pickell, n.d.). Some sensors are only able to identify visible light waves while others may identify visible, near infrared, and thermal energy wavelengths across the ES.

Spatial resolution is the area of land represented per pixel in a digital image. In a digital image with a spatial resolution of 1 meter (m), each pixel constitutes one square meter of land. The spatial resolution of a sensor is generally classified as low, medium, high, or very high resolutions based on the level of detail that is detected in a digital image (Omali, 2018). Sensors with a low spatial resolution are more suited for classifying larger global areas of interest, while higher spatial resolutions are more suited for smaller local areas (Panigrahy & Ray, 2005). Digital imagery obtained from a sensor with a 30 m resolution will have a lower (coarser) spatial resolution than a sensor with 1 m resolution.

Radiometric resolution involves the level of detail a sensor can capture. Energy differences picked up by a sensor are quantified as digital numbers which represent the amount of energy detected in a pixel (Hacker & Pickell, n.d.). A larger radiometric resolution increases the maximum digital number a pixel may contain. A sensor with a higher radiometric resolution can differentiate brightness levels of objects better than sensors with lower radiometric resolutions (NCERT, 2006). A larger radiometric resolution increases the maximum digital number a pixel may contain making it easier to detect differences in energy reflectance across pixels.

Temporal resolution is the amount of time it takes for a sensor on a platform to complete its orbit over an area (Nowatzki et al., 2004). Temporal resolution influences the choice of a sensor's platform based on how frequent data is needed (Congalton, 2010). Platforms with a higher temporal resolution can complete their orbits in a shorter amount of time and will produce more consecutive data of an area of interest.

In a previous study, Bowes assessed the ability of Landsat 7 ETM+ derived data to identify brine contaminated sites across a petroleum affected area in west Texas (Unger et al., 2013). It was found that the supervised classification technique used in the study successfully identified brine contaminated areas (Unger et al., 2013). With the recent launch of Landsat 9 OLI/TIRS-2 in 2021, digital imagery with a higher radiometric resolution than Landsat 7 is accessible to process for remote sensing studies.

In this study, multispectral digital imagery acquired from two platforms was processed to determine how accurately and precisely current soil brine contamination

would be identified across the SOF. Digital imagery from a mid-spatial resolution Landsat 9 satellite was analyzed to determine and identify the spectral characteristics of soil brine contamination using a supervised classification technique in ERDAS IMAGINE® 2022 v. 16.7. Soil samples were taken from brine and non-brine areas identified in the supervised classification map to validate the brine identification. The sampling sites were further assessed by performing an unsupervised classification on digital imagery obtained from a P4M-RTK UAV to determine if a platform with a higher spatial resolution would be able to validate the results from the supervised classification performed with the Landsat 9 platform.

The remote sensing study to identify the spectral characteristics of soil brine contamination across the SOF was completed using common image classification and accuracy assessment methods. Sensor characteristics for platforms used were considered so that obtained data was able to be compared to the accuracy assessment of a previous remote sensing study. The utilization of Landsat 9 imagery with 14-bit radiometric resolution was assessed to determine if it could provide a more accurate supervised classification result for brine affected oil fields.

The increased radiometric resolution in Landsat 9 compared to Landsat 7 provided an opportunity to analyze how differences in radiometric resolution affect the accuracy of supervised classifications across oil fields with brine contaminated sites. In a previous study mapping oilfield soil brine contamination across a region in west Texas, Unger et. al. (2013), classified contaminated sites using Landsat 7. The most current

Landsat 9 hosts a sensor with a higher radiometric resolution (14-bit) than Landsat 7 (8-bit) (Masek et. al., 2020 and Table 1). Furthermore, digital imagery with a higher spatial resolution (5.26 cm) than Landsat imagery (30 m) was obtained over soil sampling sites in the SOF with a P4M-RTK UAV to identify the presence/absence of soil brine contamination at a more localized scale. Table 1 below was compiled with information from several sources (Chastain et al., 2019; Lulla et al., 2021; Sefercik et al., 2021).

Table 1. Platforms associated with this study and their sensor resolution characteristics.

Platform	Sensor	Spatial	Spectral	Radiometric	Temporal
Landsat 7	ETM+	15m 30m 60m	Panchromatic Blue, Green, Red, *NIR, *MIR, MIR *FIR	8 bit	16 days
Landsat 9	OLI-2/TIRS-2	15m 30m 100m	Panchromatic Aerosol, Blue, Green, Red, NIR, MIR, MIR, Cirrus FIR	14 bit	16 days
Phantom 4 Multispectral UAV	(Six) 1/2.9 CMOS Sensors	5.26 cm	Blue, Green, Red, Red Edge, NIR	16 bit	n/a

*The following spectral bands have been abbreviated as: Near-Infrared (NIR), Mid-Infrared (MIR), and Far-Infrared (FIR).

Additionally, the historic nature of the study area provided a unique opportunity to identify lasting effects of soil brine contamination in regions associated with oil production. To date, landscape scarring from brine in the SOF has only been mapped digitally across the Norphlet District of the SOF by Alison D. Culver and Dr. Mary Barrett (Barrett, 2001; Culver & Barrett, 2001; Barrett, 2002). A supervised classification

of both the Louann and Norphlet Districts provided the ability to create a more current identification of brine-affected areas within the SOF. Earthen pits within the SOF are the last unaltered pits in the United States and, because of the delayed regulations to maintain the SOF, the landscape of the study area was considered to be one of the most historically brine-damaged petroleum production areas in the U.S. (Barrett, 2001; Barrett, 2002).

Furthermore, soil brine contamination continues to affect the Earth's surface as oil production continues throughout the world. In the United States it is estimated that five percent of the wastewater or brine from oil and gas industries are unintentionally or illicitly introduced into the environment (Konkel, 2016). Common sources of spillage occur during transportation or addition/removal of brine from storage tanks (Lauer et al., 2016). The completed image classification technique may provide natural resource managers with a method to efficiently locate and quantify soil brine contamination in areas related to ongoing brine production, transport, and storage.

OBJECTIVES

The purpose of this study was to determine if soil brine contamination may be identified across the SOF using multispectral digital data obtained from Landsat 9. A supervised classification map was created with data acquired from the satellite to determine if soil brine contamination was able to be classified from its spectral signature. Soil samples were randomly collected from three sites to validate whether areas classified as brine contaminated in the supervised classification were accurate. A P4M-RTK drone was operated to obtain digital imagery for a more precise and highly detailed analysis of the three sampling sites. The results from this study were used as an example to determine the robustness of the techniques used to identify soil brine contamination previously quantified in a similar remote sensing study (Unger et al., 2013).

Specific objectives of this study were:

1. To determine if the spectral signature of soil brine contamination was able to be identified in a supervised classification of Landsat 9 remotely sensed data.
2. To ascertain the accuracy of the brine and non-brine areas identified in the SOF by comparing the classification to random soil sampling results.

3. To evaluate the presence or absence of brine contamination across the sampling sites with high spatial resolution imagery obtained from a P4M-RTK drone.
4. To confirm the validity of the method of soil brine contamination identification used in the Landsat 7 study conducted over petroleum producing regions in west Texas (Unger et al., 2013).
5. To determine if the higher radiometric resolution of Landsat 9 impacts the accuracy of soil brine contamination mapping across oil fields compared to results from Cindy Bowes Landsat 7 study (Unger et al., 2013).
6. To quantify the current amount of soil brine contamination within the SOF to compare with previously documented soil brine contamination from the study, "*Landscape Modification of the Smackover Field, Arkansas"* (Culver & Barrett, 2001).

Hypotheses:

H_{01}: A supervised classification of Landsat 9 data will not significantly differentiate between brine and non-brine contaminated sites across the Smackover Oil Field.

H_{a1}: A supervised classification of Landsat 9 data will be able to clearly differentiate between brine and non-brine contaminated sites across the Smackover Oil Field.

H_{02}: The higher spatial resolution of the P4M-RTK will not have a significant effect on precisely identifying the presence or absence of soil brine contamination within sampling sites.

H_{a2}: The higher spatial resolution of the P4M-RTK will more precisely identify the presence or absence of soil brine contamination within sampling sites.

H_{03}: The higher radiometric resolution (14-bit) of the obtained Landsat 9 data will not significantly affect the accuracy of soil brine identification results across petroleum affected fields compared to results from Landsat 7 data (8-bit).

$H_{a3:}$ The higher radiometric resolution (14-bit) of the Landsat 9 will produce a more accurate soil brine identification across petroleum affected fields compared to accuracy results from Landsat 7 (8-bit).

LITERATURE REVIEW

History of the Smackover Oil Field Production

> *"The manner in which the El Dorado and Smackover fields were operated is a disgrace to the industry. Millions of barrels of oil were allowed to escape, polluting the waters of Smackover Creek and thereafter the Ouachita River."*
>
> - W. Henry Rector in *Legal History of Conservation of Oil and Gas 16* (Norvell, 2015)

Oil Waste History

The SOF is a distinctive oil field because of how wasteful petroleum practices were during its era. In April 1922 the J. T. Murphy No. 1 oil well exploded, resulting in the SOF's first oil boom and a lasting crater (Barrett, 2001). The crater is pictured in Figure 4, based on coordinates and location descriptions from Van Zbinden's approved National Register of Historic Places Inventory/Nomination Form for the J.T. Murphy No. 1 crater (2008). Figure 4 was taken by Victoria Williams July 23, 2022, with a DJI Mini 2 UAV at the following coordinates: 33° 20' 32.6219" N and 92° 40' 6.3775" W. The oil field is divided into two districts: the western Louann District and the eastern Norphlet District (Barrett, 2001). The Louann District principally produced light oil (23° to 28° American Petroleum Institute gravity (API)) while the Norphlet District produced heavy oil (18° to 23° API) (Barrett, 2001). In the first decade of oil production, between 5 to 10

million barrels of oil were estimated to be lost because of leaching into the ground, storage issues, and spills which occurred during floods and fires (Barrett, 2001). According to Dr. Mary Barrett in *The Oil Waste History of Smackover Field, Arkansas*, the Norphlet District was more impacted by oil wastes than the Louann District (2001). The lack of regulation during the early stages of production allowed oil, gas, and saltwater to stream openly onto the surface of the land (McEwen, 1970).

Figure 4. The J.T. Murphy no. 1 crater in the Norphlet District of the Smackover Oil Field.

Oil Storage

The SOF was the final oil field in the United States to utilize earthen tank farm storage, storage carved directly into the Earth's surface, for oil production, the other two

fields were in southeast Texas and central California (Barrett, 2001). Most crude oil was purchased by the Standard Oil Company of Louisiana, which also built the majority of earthen storage in the SOF (Barrett, 2001). Earthen tank storage varied in size and purpose and within the first year over 5 million barrels of oil were stored in earthen tank storage (Barrett, 2001). Most of the earthen tanks in the United States were constructed 7 ft below the surface with 6 ft walls encircling the pit (Barrett, 2001). Much of the earthen storage was constructed in silty and sandy soils in the lower elevations towards the center of the field, while earthen storage at the field edge was constructed in soils with a higher abundance of clay (Barrett, 2001). In earthen storage and drainage areas across the oil field, asphaltic crusts formed as the crude oil began to break down and aggregate (Barrett, 2001). Near drainage areas across the SOF, narrow layers of asphaltic crusts from oil waste material are still present at and below the surface (Figure 5) (Barrett, 2001). The arrows in figure 5 point to thin layers of asphaltic crusts in the soils, which originated from waste oil materials. In Figure 6, the location of earthen storage visible across the Norphlet District in 1936 is depicted from a previous study over landscape change within the SOF (Culver & Barrett, 2001). The “Lease Pits” and “Pit Scars” digitized in Figure 6 were identified from a culmination of 1936 aerial photographs over the SOF (Culver & Barrett, 2001). More productive areas of the Norphlet District during can be identified by higher densities of lease pits and pit scarring, such as seen in areas of higher elevation in Figure 6 (Culver & Barrett, 2001).

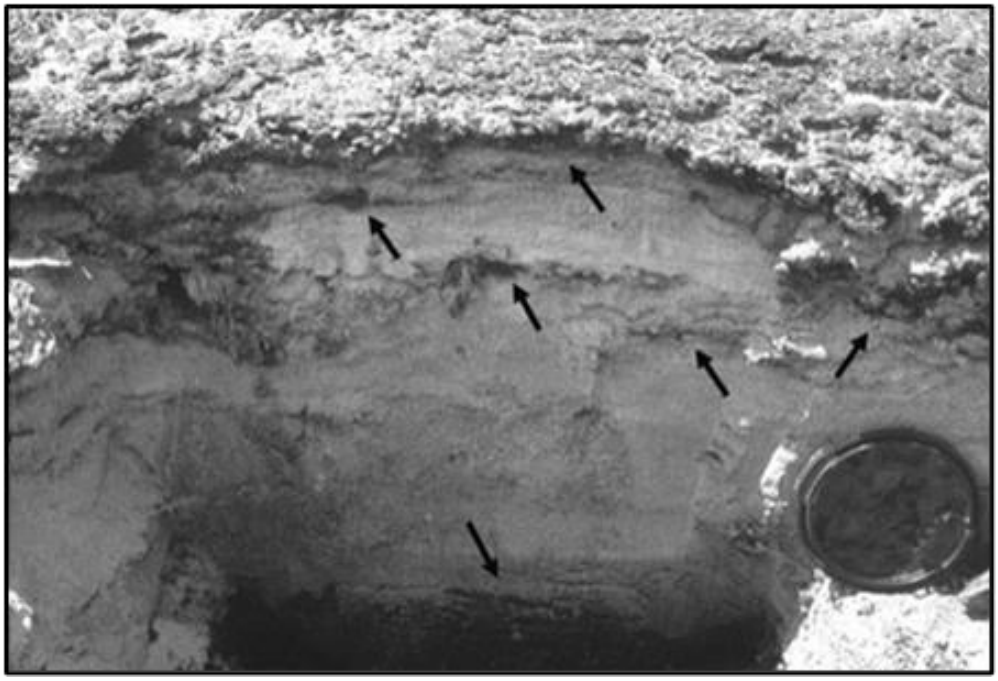

Figure 5. Layers of asphaltic crust are present in the soils near an intermittent creek (Barrett, 2001).

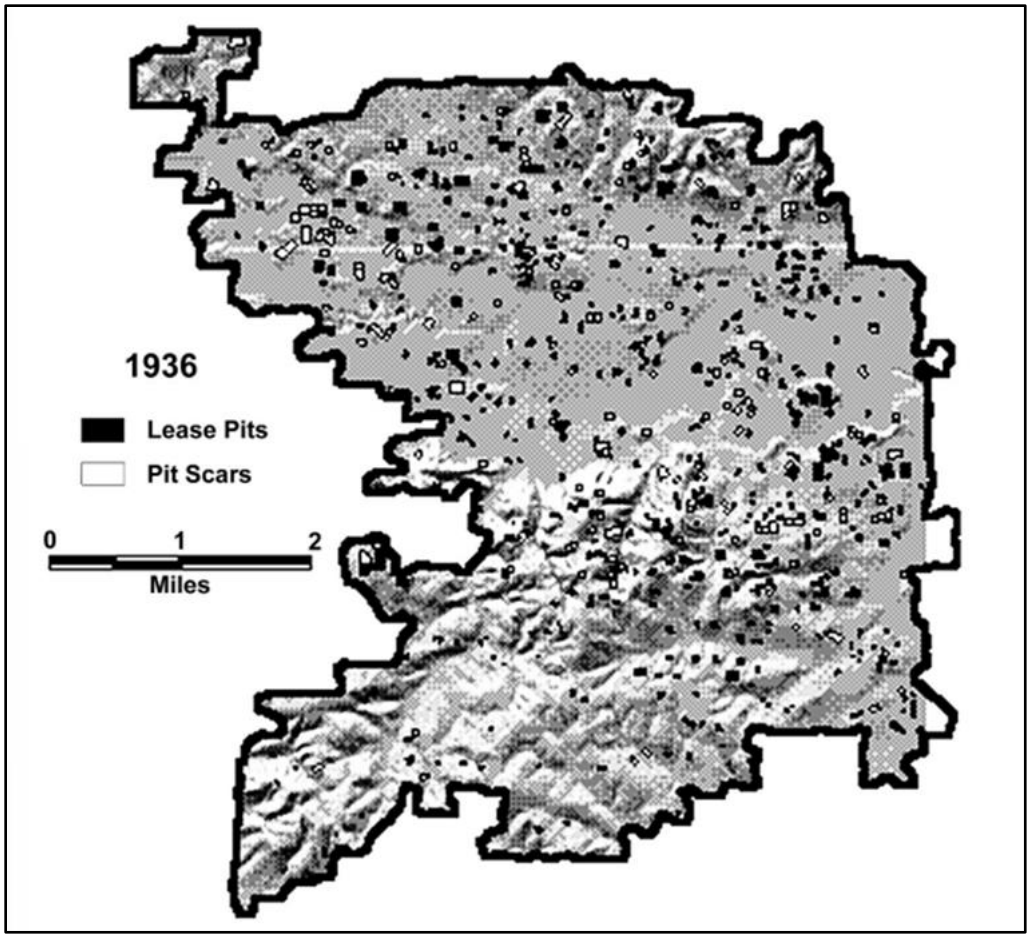

Figure 6. Earthen storage and storage scarring in 1936 across the Norphlet District (Culver & Barrett, 2001).

In the SOF two main kinds of earthen storage were utilized to store oil depending on their purpose. Larger earthen pits were built in areas of higher elevation towards the field edge to store oil more safely for longer periods of time and were collectively referred to as "tank farms" (Culver & Barrett, 2001). While smaller earthen pits, known as "lease pits," were located closer to well sites to store oil temporarily such as pictured in Figure 7 (Culver & Barrett, 2001). Towards the end of 1925 there were nearly 23 million barrels of crude oil in earthen tank storage in the SOF (Barrett, 2001).

Crude oil was stored in earthen storage until it was finally extracted from the tanks in 1933 (Barrett, 2001). The SOF continues to produce oil and, as of 2016, over 606,627,681 barrels of crude oil had been produced (Office of the State Geologist, n.d.).

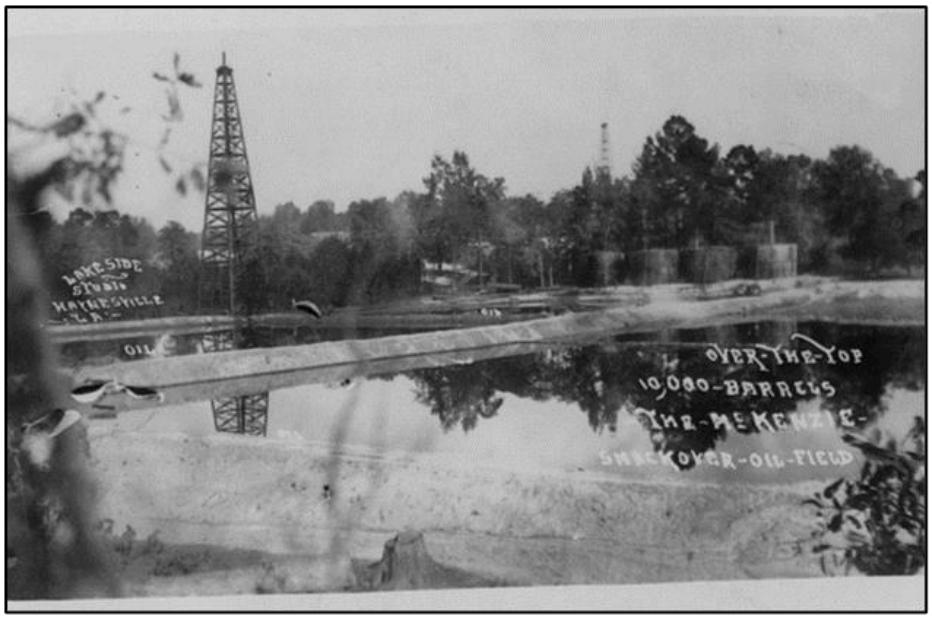

Figure 7. Historic photograph of lease pits near an oil well in the Smackover Oil Field (Culver & Barrett, 2001).

Historical Regulation of the Smackover Oil Field

As mentioned in the introduction, the SOF was not subject to the regulations of the AOGC. Arkansas oil and gas fields that were in production prior to January 1, 1937, are referred to as "uncontrolled", and fields created after this time are referred to as "controlled" (McEwen, 1970). Based on this terminology the SOF is considered an "uncontrolled field", which prevented the AOGC from exercising authority over production and waste practices in the SOF (McEwen, 1970). An example of a detrimental

waste practice of the SOF production era can be identified in the removal process of saltwater or brine. Oil field operators would send brine from their wells through sloughs, shallow swamp-like areas, into Smackover Creek which eventually flowed into the Ouachita River introducing brine contamination into these freshwater bodies (McEwen, 1970).

Eventually the effects of brine contamination on freshwater bodies were acknowledged. The first pushback towards this contamination was delivered by the Arkansas Pollution Control Commission (APCC). In 1958 the Ouachita River was estimated to be contaminated by 185 million pounds of chlorides per month, with much of the contamination being traced back to the contaminants entering the Smackover Creek within the SOF (McEwen, 1970). After 1958, APCC issued pollution controls that granted oil producers a five-year period to terminate their release of brine into any surface waters, i.e., above ground water sources (McEwen, 1970). The pollution controls enacted by the APCC resulted in the SOF oil operators shifting to other methods of brine disposal. Most of the brine was reinjected into the geologic formation it originated from, while other brine waste products were stored in earthen tanks (McEwen, 1970).

History of Smackover Saltwater Production and Storage

Brine Effects on the Landscape

The mismanagement of saltwater produced from the SOF resulted in lasting landscape changes. As the production of oil declined from the SOF, the earthen pits previously used for oil storage transitioned into storing the increasing amount of

production water (Barrett, 2002). For petroleum fields located in non-coastal areas it was routine to dispose of saltwater into earthen pits, and in the SOF, pits were constructed to store the increasing amount of produced saltwater (Barrett, 2002).

Lasting effects of soil brine contamination across the SOF are identified by the damage to vegetation and changes in the structure of linear water features, such as seen in a comparison of 1936 to 1996 aerial photographs in Figures 8 and 9 (Barrett, 2002). Four common features from the aerial photographs were labeled as A, B, C, and D. Prior to oil production in 1922, the land was originally a wetland mainly dominated by cypress trees and multiple intermittent creeks which followed a "natural meandering pattern," (Barrett, 2002). The natural stream patterns, shown at A in Figure 8, transformed as erosion in drainage areas created sand bars and narrow braided waterways (shown at A in Figure 9). Feature B in Figures 8 and 9 illustrates the recovery and transformation of a 1936 barren drainage scar to smaller landscape scar capable of hosting salt tolerant vegetation in 1996 (Barrett, 2002). In Figure 8, features C and D hosted visible landscape scarring related to earthen storage pits (Barrett, 2002). The outlines of earthen pits seen at C and D were still identifiable in 1996 aerial photography in Figure 9 (Barrett, 2002). In Figure 10, remnants of cypress stumps and asphaltic crusts are visible in an altered intermittent stream in the SOF due to low levels of water (Barrett, 2001).

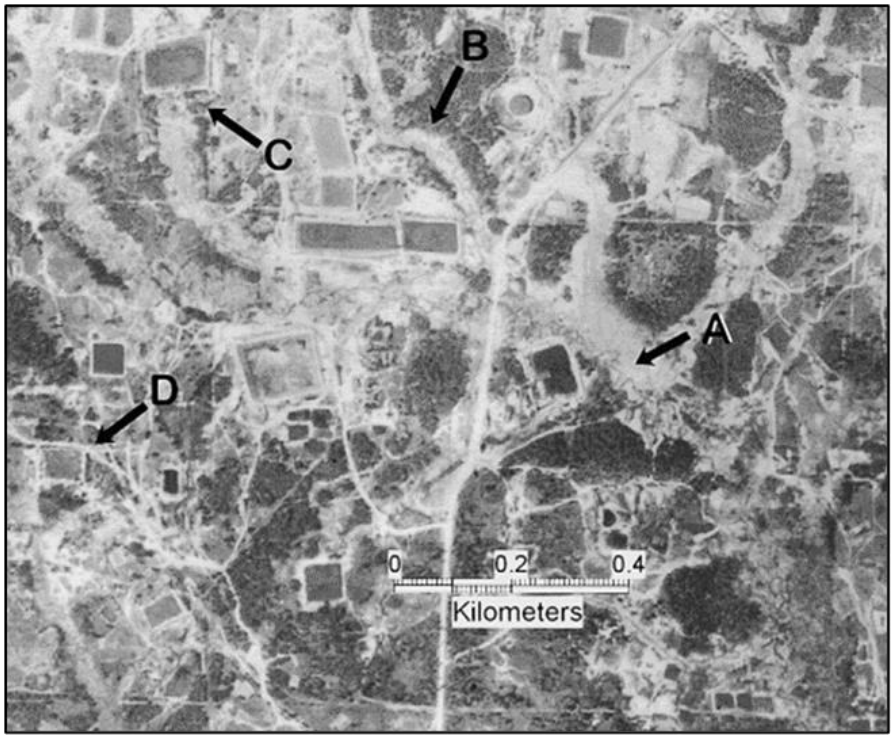

Figure 8. 1936 aerial photograph taken over part of the Smackover Oil Field (Barrett, 2002).

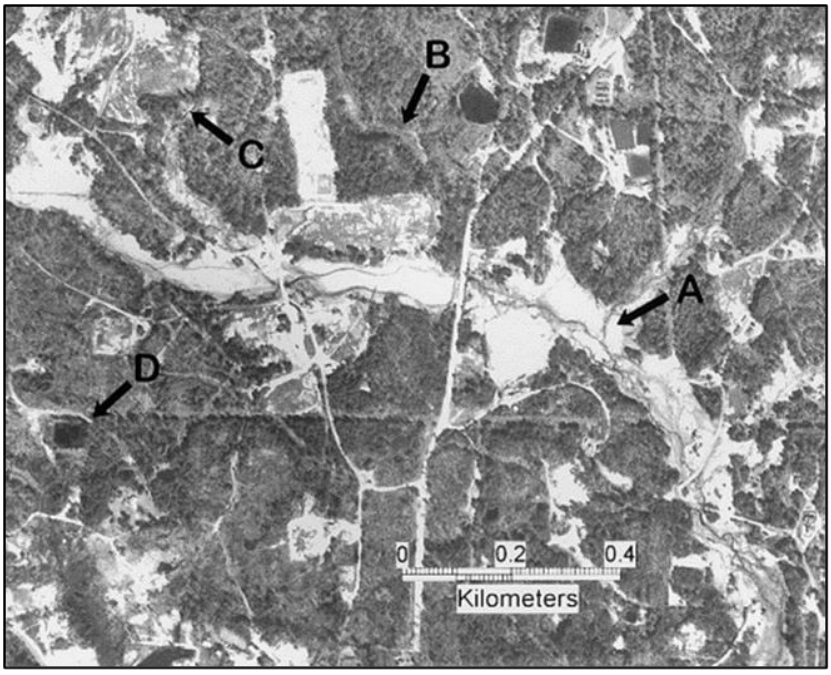

Figure 9. 1996 aerial photograph taken over part of the Smackover Oil Field (Barrett, 2002).

Figure 10. Asphaltic crusts and cypress stumps in an intermittent creek (Barrett, 2001).

In 1935, information to accurately quantify the amount of produced water coming from the SOF was not available, but it is approximated by W.C. Spooner in the *Oil and Gas Geology of the Gulf Coastal Plain in Arkansas* that, “not less than 75 percent of the fluid produced is water”, which is estimated to be equivalent to one billion barrels of brine produced between 1922 and 1933 (Barrett, 2002). Historical water sample analysis for wells in two types of the producing sands within the SOF revealed that they both were producing water with a primary salinity greater than 75% and that the three main constituents found in the wells were sodium, calcium, and chloride (Spooner, 1935) (Tables 2 and 3). The constituents identified in the production water from the water samples were believed to have been combined chemically as sodium chloride, magnesium chloride, calcium sulfate, and calcium carbonate (Tables 2 and 3).

Table 2. Results of a 1935 water analysis from well drilling in the Meakins producing sands within the Smackover Oil Field depicted in a table from W.C. Spooner in the *Oil and Gas Geology of the Gulf Coastal Plain in Arkansas*.

Analysis of water from the Meakin sand in the Smackover field

(Analyst, Fort Worth Laboratories)

Marked wells A-2 salt water sample from northwest corner SW¼ SE¼ sec. 25, T. 15 W., R. 17 S., Union County, Arkansas, received from Atlantic Oil Producing Company, Dallas, Texas.

Properties of reaction	Per cent
Primary salinity	78.22
Secondary salinity	21.68
Primary alkalinity	None
Secondary alkalinity	0.10
Per cent SO_4 in SO_4 plus Cl	0.18
Ratio CO_3 to SO_4	0.55

Constituents	Parts per million
Sodium (Na)	19,388.7
Calcium (Ca)	3,280.0
Magnesium (Mg)	850.0
Iron and aluminum oxides (Fe_2O_3, Al_2O_3)	50.0
Sulphate (SO_4)	94.6
Chloride (Cl)	38,000.0
Carbonate (CO_3)	33.6
Silica (SiO_2)	35.0

	Reacting value	Per cent
Alkalies		
Sodium (Na)	853.40	39.11
Alkaline earths		
Calcium (Ca)	163.67	7.64
Magnesium (Mg)	69.87	3.25
Strong acids		
Sulphate (SO_4)	19.67	0.09
Chloride (Cl)	1,071.60	49.86
Weak acids		
Carbonate (CO_3)	1.12	0.05

Hypothetically combined as	Parts per million	Grains per U. S. gallon
Calcium carbonate ($CaCO_3$)	56.0	3.25
Calcium sulphate ($CaSO_4$)	134.0	7.77
Calcium chloride (CaCl)	8,914.4	517.20
Magnesium chloride ($MgCl_2$)	3,325.0	192.95
Sodium chloride (NaCl)	49,217.5	2,855.00
	61,646.9	3,576.17

Table 3. Results of a 1935 water analysis from well drilling in the Graves producing sands within the Smackover Oil Field depicted in a table from W.C. Spooner in the *Oil and Gas Geology of the Gulf Coastal Plain in Arkansas*.

Analysis of water from the Graves sand in the Smackover field

(Analyst, Fort Worth Laboratories)

Water sample 2631 from Marked Murphy A-8, sec. 8, T. 16 W., R. 15 S., Union County, Arkansas, received from Lion Oil Refining Company El Dorado.

Properties of reaction	Per cent
Primary salinity	78.06
Secondary salinity	21.74
Primary alkalinity	None
Secondary alkalinity	0.20
Per cent SO_4 in SO_4 plus Cl	0.02
Ratio CO_3 to SO_4	0.10

Constituents	Parts per million
Sodium (Na)	21,851.8
Calcium (Ca)	3,802.0
Magnesium (Mg)	943.5
Iron and aluminum oxides (Fe_2O_3, Al_2O_3)	12.0
Sulphate (SO_4)	11.1
Chlirode (Cl)	42,800.0
Carbonate (CO_3)	69.6
Silica (SiO_2)	20.0

	Reacting value	Per cent
Alkalies		
Sodium (Na)	948.56	39.03
Alkaline earths		
Calcium (Ca)	189.72	7.80
Magnesium (Mg)	77.55	3.17
Strong acids		
Sulphate (SO_4)	0.23	0.01
Chloride (Cl)	1,206.96	49.89
Weak acids		
Carbonate (CO_3)	2.32	0.10

Hypothetically combined as	Parts per million	Grains per U. S. gallon
Calcium carbonate ($CaCO_3$)	116.0	6.72
Calcium sulphate ($CaSO_4$)	15.7	0.91
Calcium chloride ($CaCl_2$)	10,366.5	602.42
Magnesium chloride ($MgCl_2$)	3,694.7	214.00
Sodium chloride (NaCl)	55,265.1	3,205.67
	69,458.0	4,029.72

Brine Regulation of the SOF

After regulations in 1958 required oil producers to cease disposing of brine into surface waters within five years, the most intense period of brine pollution in freshwater occurred in 1962 when it was estimated that Smackover Creek was transporting 275 million pounds of chlorides per month (Barret, 2002). Eight years later the brine contamination transported by the creek had decreased to 25 million pounds, which was attributed to salts from contamination leaching into the soil rather than directly being poured into surface waters (Barrett, 2002). In the 1970s, brine was no longer released into surface waters but was directly reinjected into producing sands, or deposited in earthen pits, and in the 1980s the state of Arkansas began terminating the practice of storing saltwater in older unlined earthen pits (Barrett, 2002). In 1993, the Arkansas Pollution Control and Ecology Commission (APCEC) further restricted the disposal of brine into earthen pits by requiring pits be constructed in an area with highly compacted soils or with a liner made of impermeable materials such as asphalt to prevent the leaching of the pit contents into the surrounding soils (Barrett, 2002). Also, in 1993, the APCEC required that any earthen pits within the 100-year floodplain of streams in Arkansas must be discontinued to prevent brine contamination from overflowing earthen pits (Barrett, 2002).

Brine Validation

Soil Sampling

Soil sampling may follow many methods and can be altered to cater towards the purpose of a study. In Cindy Bowes thesis, "*Detecting Oilfield Brine Contaminated Sites Using Satellite Remote Sensing"*, the electrical conductivity (EC), pH, and sodium adsorption ratio (SAR) levels of soil samples were assessed to determine the presence of soil brine contamination (2007). When taking soil samples related to plant vigor, measuring the conductivity of a soil sample extract is preferred (Allison et. al., 1954). Soil extracts characterized as "saline" are associated with EC levels greater than 4 mmhos/cm (Allison et. al., 1954). The pH of saline soils is closer to the acidic end of the pH spectrum with levels less than 8.5 (Allison et. al., 1954). As concentrations of electrolytes increase in the soil, the pH of soils becomes more acidic (Sparks et al., 2024). The concentrations of sodium, calcium, and magnesium are quantitatively assessed in Equation 1 below to determine the SAR of a soil extract (Gharaibeh et al., 2021).

$$SAR = \frac{Na}{\sqrt{\frac{Ca + Mg}{2}}} \quad (1)$$

Soil extracts with SAR levels higher than 13 indicate there is an overabundance of sodium present in the samples, which contributes to soil erosion as soil particles are unable to aggregate together (Sonon et al., 2015).

Image Acquisition

Landsat

In 1972, the Landsat-1 was launched, beginning the decades-long collection of remotely sensed data available by collaboration between the National Aeronautics and Space Administration (NASA) and the US Geological Survey (USGS) (Masek et al., 2020). In 2001, the USGS launched the Global Visualization Viewer (GloVis) website, which made remotely sensed data available to the public via the internet (Educational Resources, n.d.). Landsat 1-5 and Landsat 7-9 data bundles are available to download for no cost through GloVis. Landsat imagery may be used in remote sensing studies to create land-cover classification maps of Areas of Interest (AOI).

An advantage to the utilization of Landsat data is that, prior to image collection, the radiometric and geometric effects on Landsat scientific instruments and satellites are already considered. For Landsat related devices, the Earth Resources Observation and Science (EROS) CalVal Center of Excellence (ECCOE) are the main authority for radiometric and geometric calibration (Haque et al., 2023). ECCOE regularly updates Landsat instruments based on identified radiometric and geometric effects (Haque et al., 2023). Information about the performance if the most recent mission, Landsat 9, is not available yet, but the ECCOE publishes "*ECCOE Landsat Quarterly Calibration and Validation Report(s)*" (n.d.) on the USGS.gov webpage, *Landsat Calibration and Validation* regarding the radiometric and geometric performance of Landsat missions.

Landsat-9 OLI/TIRS-2

Landsat 9 scenes became available in GloVis on June 15, 2022, when the Landsat Collection 2 Level-1 data was integrated into the interface (Landsat Missions, n.d.$_c$). The Landsat 9 Platform bears two imaging sensors, the Operational Land Imager 2 (OLI-2) and the Thermal Infrared Sensor 2 (TIRS-2) with varying sensor characteristics which can be seen in Table 4 below (Lulla et al., 2021). Landsat 9 collections were updated in early 2023 to account for calibration improvements based on data collection from the first year (Landsat Missions, n.d.$_c$).

Table 4. Image resolution characteristics of Landsat-9 OLI/TIRS-2.

Platform	Sensor	Spatial	Spectral	Radiometric	Temporal
Landsat 9	OLI-2	15m	Panchromatic	14 bit	16 days
		30m	Aerosol, Blue, Green, Red, *NIR, *MIR-1, MIR-2, Cirrus		
	TIRS-2	100m	*FIR-1, FIR-2		

*The following spectral bands have been abbreviated as: Near-Infrared (NIR), Mid-Infrared (MIR), and Far-Infrared (FIR).

DJI Phantom 4 Multispectral UAV with RTK

The utilization of UAVs has been integrated into the science of remote sensing. UAVs act as efficient tools to collect high spatial resolution data, can be maneuvered in a variety of landscapes and allow for prompt data acquisition (Lu et. al, 2020). A UAV is capable of conveying information to its remote controller to deliver important information about the vehicle's status such as battery performance, altitude, and Global

Positioning System (GPS) coordinates (Austin, 2011). UAVs can collect data with higher spatial resolution and possess a more immediate temporal acquisition than satellites.

The P4M-RTK is a DJI brand quadcopter with DJI Onboard D-RTK™ (Real-Time Kinematic), which produces a more precise positioning accuracy (DJI, n.d.$_b$). The UAV hosts six 1-/2.9” CMOS (complementary metal oxide semiconductor) sensors which separately collect visible light (RGB), blue, green, red, red-edge, and near infrared spectral bands (DJI, n.d.$_b$). The six sensors and their associated bands are depicted in Figure 11. In Figure 11, the range of each spectral band is also included if applicable. The P4M-RTK can participate in pre-programmed flights to collect data for orthomosaiced digital images. Multiple images taken from different angles during a pre-programmed flight can be mosaiced together based on tie points in overlapping images to create a final orthophoto mosaic of the AOI (Sefercik et al., 2021).

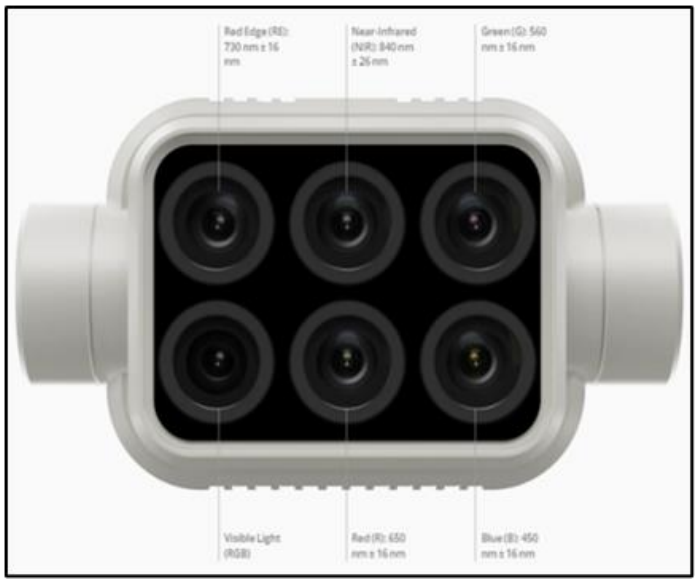

Figure 11. The Phantom 4 Multispectral RTK UAV sensors.

Image Classification

Once remotely sensed data has been collected, the imagery may be classified into various groups based on the need of the project. Groups of pixels within a digital image may be aggregated to delineate land cover classes in an AOI (Sathya & Deepa, 2017). Primarily, three image classification methods are utilized in remote sensing studies to classify digital images: supervised, unsupervised, and object-based classification (Sathya & Deepa, 2017). A supervised classification approach to remotely sensed data allows natural resource managers to select pixels that should be classified together before the chosen software processes the image into classes (Sathya & Deepa, 2017). In an unsupervised classification, a computer groups together pixels with similar digital values into distinct classes, allowing users to determine what each class represents after the classes are created (Li et al., 2017). Finally, object-based classification relies on object-based models which delineate classes from features such as groups of roads or trees, to classify objects across digital imagery rather than analyzing pixels like the previously mentioned classification schemes (Li et al., 2017). An Object-based classification approach was not used in the study as the presence of soil brine contamination may not be specific to groups of land features.

Supervised Classification

In supervised classification a user actively selects groups of pixels called training sites to represent known classes (Perumal & Bhaskaran, 2010). A spectral signature is created based on the training sites and is unique for each class (ERDAS, 2005). Untrained

pixels in a digital image are compared to the spectral characteristics of training sites to determine how they should be classified. The accuracy of this classification method is affected by the selection of training sites (Sathya & Deepa, 2017). If selected training sites are not representative enough of the desired classes, the spectral signature based on the training sites may cause pixels across the image to be misrepresented in the produced classification map. A user collects remotely sensed data, e.g., a Landsat scene, and selects training sites to represent user desired classes. The computer completes the classification by grouping pixels in the most comparable class based on the prior delineated training sites. The output is evaluated by the user to determine its accuracy and present a final classified map.

Unsupervised Classification

In an unsupervised classification, a computer creates multiple classes across a digital image and requires a user to determine what the computer-generated classes are after the unsupervised classification has been completed. The computer will group together pixels with similar spectral characteristics to create a predetermined number of classes the user defines (ERDAS, 2005). All pixels within a digital image will be forced into a class with the most similar spectral characteristics available (Congalton, 2010).

Accuracy Assessment

Error Matrix

A standard measure of accuracy assessment is performing an error matrix. An error matrix is a table that compares samples from a classified map to samples taken from

a validated reference data source (Congalton, 2010). Data such as user accuracy, producer accuracy, overall accuracy, and Kappa statistics can be obtained from an error matrix (Congalton, 2010). According to Klaus Tempfli et al., 2009 in *Principles of Remote Sensing: an introductory textbook*, user accuracy is "the probability that a certain reference class has also been labeled that class" and producer accuracy is "the probability that a sampled point on the map is that particular class." The overall accuracy of an error matrix is determined by calculating how many pixels in a map were classified accurately compared to the overall quantity of pixels examined (Tempfli et al., 2009).

Kappa Statistic

Another standard measure of accuracy assessment is the Kappa statistic or $\widehat{K}$-statistic, which can be calculated from an error matrix (Rwanga & Ndambuki, 2017). The $\widehat{K}$-statistic quantifies the amount of error produced from the utilized classification process in a study compared to the amount of error a user may expect when using any arbitrary classification scheme (ERDAS, 2005). An advantage of the calculation of the $\widehat{K}$-statistic is that it enables natural land use resource managers to determine if there are significant differences between to error matrices in remote sensing studies (Congalton, 2010; Tempfli et al., 2009). The calculation and variables for the $\widehat{K}$-statistic are as follows in Equation 2 from the study, *A Review of Assessing the Accuracy of Classifications of Remotely Sensed Data* (Congalton, 1991):

$$\widehat{K} = \frac{N\sum_{i=1}^{r} x_{ii} - \sum_{i=1}^{r}(x_{i+} \times x_{+i})}{N^2 - \sum_{i=1}^{r}(x_{i+} \times x_{+i})}$$

(2)

Congalton (1991) described the variables for this equation as, "*r* is the number of rows in the matrix, x_{ii} is the number of observations in row *i* and column *i*, x_{i+} and x_{+i} are the marginal totals of row *i* and column *i*, respectively, and N is the total number of observations."

METHODOLOGY

Study Area

The SOF historically encompassed 29,505 acres and was in south-central Arkansas in the Ouachita and Union counties (Figure 12). Due to the large size of the study area, it encompasses both private and public lands. In Arkansas, the precipitation is ample throughout the year and fluctuates frequently, but the seasons which experience the most moisture throughout the year are spring and winter (Runkle et al., 2022).

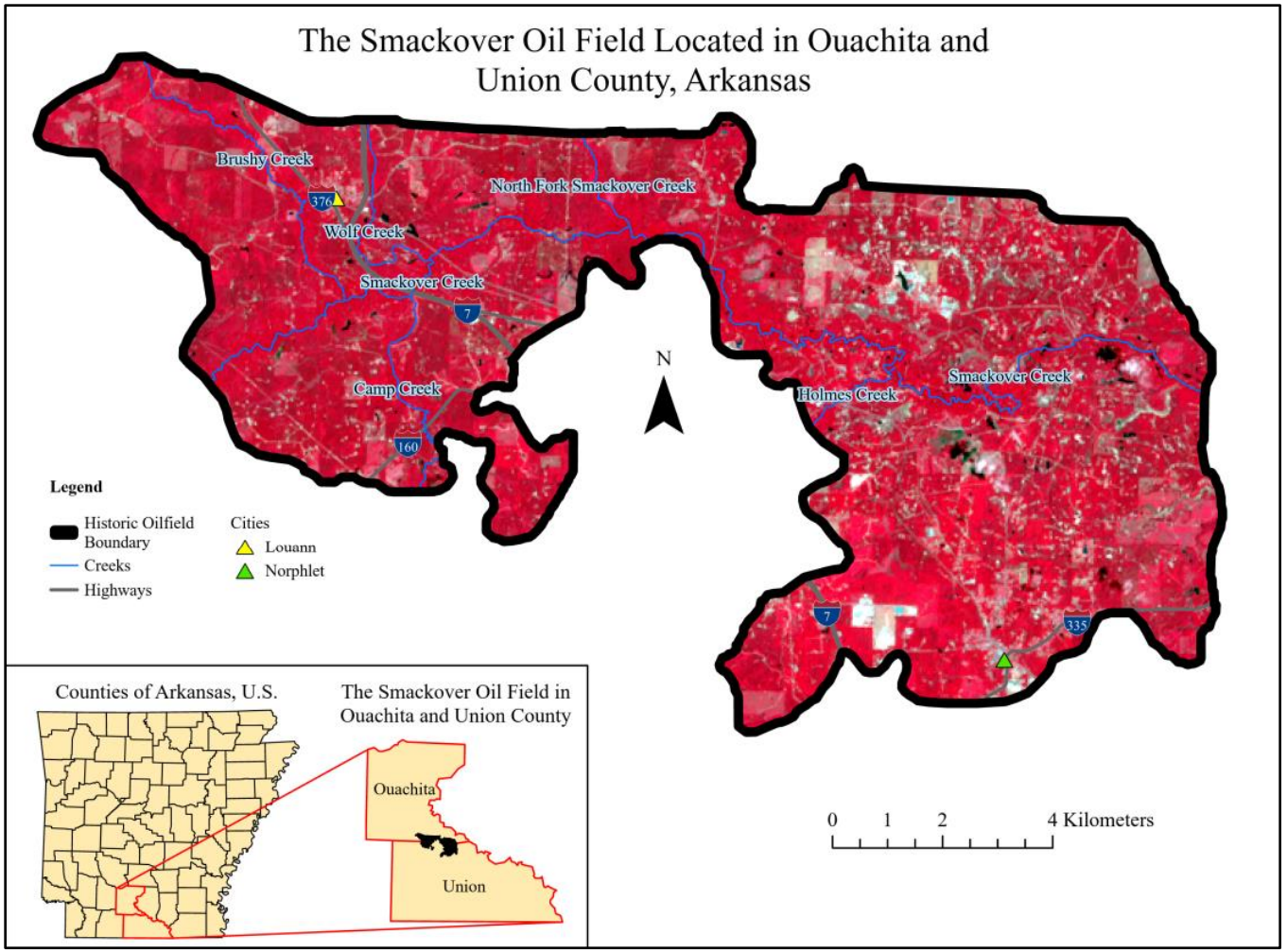

Figure 12. A study site map of the Smackover Oil Field with color-infrared imagery.

A general model for the completed study to identify current soil brine contamination within the SOF is illustrated in Figure 13. The study includes three main processes. The main process was the creation of two supervised classifications of Landsat 9 OLI/TIRS-2 imagery, one which represented pit scarring and one which represented creek scarring. The soil sampling process and image acquisition process using a P4M-RTK UAV were dependent upon the completion of the supervised classification of Landsat 9 OLI/TIRS-2 digital imagery. Once the three main processes were completed, an accuracy assessment and data comparison occurred.

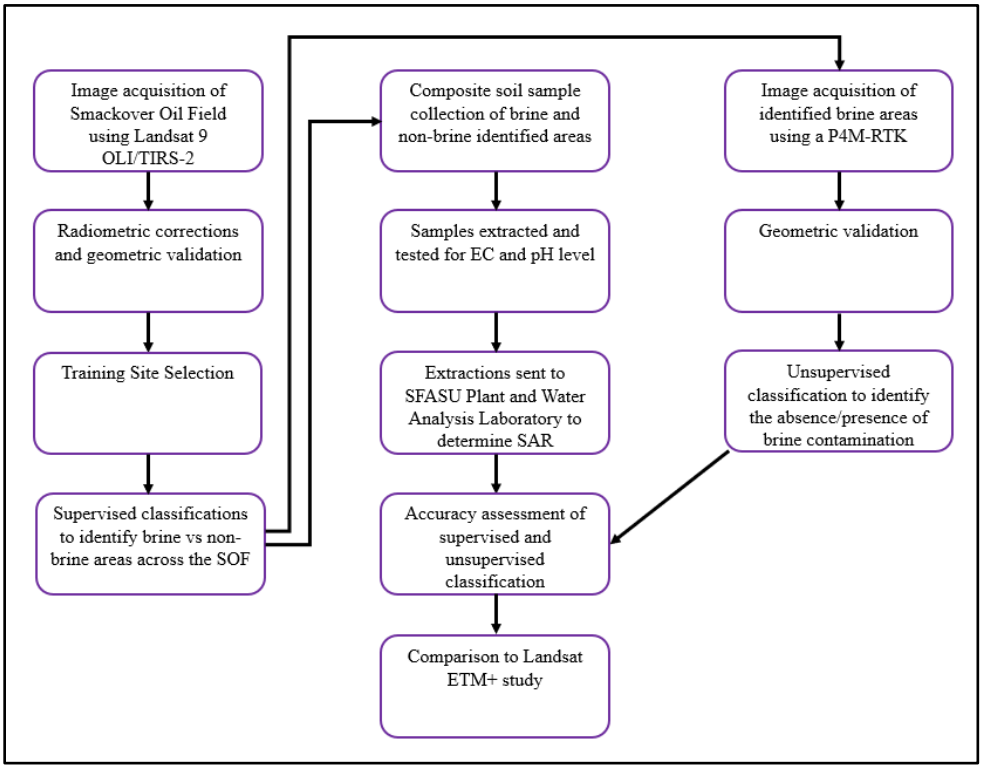

Figure 13. The general method performed for the Smackover Oil Field soil brine contamination study.

Image Acquisition

The characteristics of brine were considered to determine the optimum time for image acquisition. The buildup of salts from soil brine contamination are more apparent across the surface of a landscape during periods where there is an absence of moisture (Sukchan & Yamamoto, 2002). Digital image acquisition of the SOF was restricted to data obtained during a summer month (July) in Arkansas. A summer acquisition date ensured less moisture was present across the study area, which allowed for more accurate identification of brine contaminated soils.

Landsat 9 OLI/TIRS-2

Digital images for the proposed study were obtained from two different platforms: Landsat 9 and the P4M-RTK. A single Landsat 9 scene was acquired to create two supervised classifications of the SOF. The spectral bands from Landsat 9 data used for landcover/land use classification were kept consistent with bands used in the remote sensing study, *Mapping Oilfield Brine Contaminated Sites with Mid-spatial Resolution Remotely Sensed Data*, to test the effect of radiometric difference on classification accuracy (Unger et al., 2013). The spectral characteristics of bands from Landsat 7 and Landsat 9 relevant to the proposed study are listed in Table 5 and were compiled with information from "Landsat 7" by Landsat Missions, n.d.$_a$ and "Landsat 9" by Landsat Missions, n.d.$_b$.

Table 5. Spectral characteristics of Landsat platforms relevant to the study.

Platform and Sensor	Spectral Band	Band Length (μm)
Landsat 7 ETM+	Blue	0.45 - 0.52
	Green	0.52 - 0.60
	Red	0.63 - 0.69
	*NIR	0.75 - 0.90
	*MIR	1.55 - 1.75
	MIR	2.09 - 2.35
Landsat 9 OLI/TIRS-2	Blue	0.45 - 0.51
	Green	0.53 - 0.59
	Red	0.64 - 0.67
	NIR	0.85 - 0.88
	MIR	1.57 - 1.65
	MIR	2.11 - 2.29

*NIR: Near Infrared, MIR: Mid Infrared

P4M-RTK Sensor

After a supervised classification of the SOF was completed, sites identified in both brine and non-brine areas were further assessed with soil sampling to determine if the presence/absence of contamination was identified correctly in the classification. Additionally, preprogrammed flights across the soil sample sites were conducted using a P4M-RTK to obtain multispectral digital imagery. Orthophoto mosaics of the sampling sites were created from a pre-programmed flight orchestrated using the DJI Ground Station Pro (GS Pro) app on iPad (DJI, n.d.$_a$).

The imagery was assessed to determine if the presence/absence of soil brine contamination would be more precisely identified in datasets with higher spatial resolution compared to the mid-spatial resolution dataset from Landsat 9. To maintain

consistency throughout this proposed study, the blue, green, red, and near infrared spectral bands were layer-stacked in ERDAS IMAGINE® 2022 v. 16.7 to create a multispectral digital image (Table 6). Information for Table 6 was compiled from DJI's P4 Multispectral User Manual v1.0, 2019.

Table 6. Spectral characteristics of Phantom 4 Multispectral RTK UAV relevant to the study.

Spectral Band	Band Length (μm)
Blue	0.434 - 0.466
Green	0.544 - 0.576
Red	0.634 - 0.666
*NIR	0.814 - 0.866

*NIR: Near Infrared

Image Corrections

Radiometric Corrections

It is sometimes necessary to perform radiometric corrections on a multispectral digital image before conducting an image classification. In remote sensing studies where, multiple multispectral images are compared across time such as in a landscape change study, radiometric corrections are needed to nullify the effects of detector errors and atmospheric conditions (Chen et al., 2005). Previously, Landsat Missions, an author for USGS, has identified a detector error known as the "solid state recorder (SSR) bad block issue," pictured in Figure 14 (Landsat Missions, n.d.$_b$). The Landsat scene in Figure 14 was in WRS Path 225 WRS Row 64 and was acquired on November 13, 2021. Although

uncommon, this error results in loss of data and can be identified by missing sections of data in a Landsat 9 scene (Landsat Missions, n.d.$_b$).

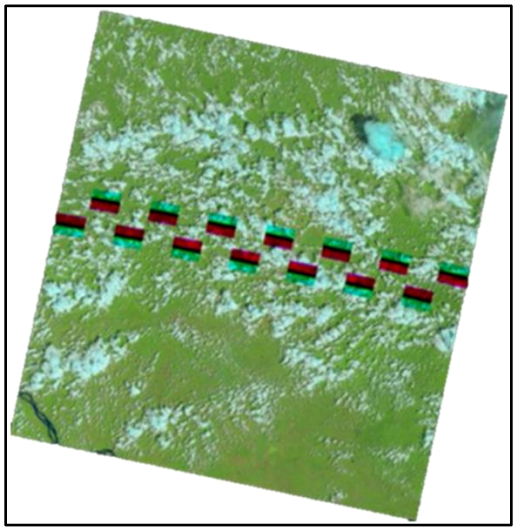

Figure 14. An example of a Landsat 9 OLI/TIRS-2 solid state recorder bad block issue.

The Landsat 9 scene in consideration for the SOF study was visually inspected and was not affected by the SSR Bad Block Issue. Additionally, the multispectral data acquired from Landsat 9 was not compared to other multispectral digital imagery, thus radiometric corrections did not have a significant effect on the SOF study and were not performed on the data acquired from Landsat 9.

Geometric Correction

Errors in digital imagery may also be caused by differences in terrain and the Earth's arc across an area of interest (ERDAS, 2005). Geometric correction ensures that coordinates of features identified in raw data are representative of the actual coordinates of those features (Dave et al., 2015). Geometric correction on images should be

performed if multiple images are going to be compared in remote sensing study (Dave et al., 2015). Although only one image was used for the SOF study, a relevant aspect of geometric correction is image rectification. Rectification ensures that the coordinates of an image match the coordinates on a mapping or coordinate system, such as the Universal Transverse Mercator (UTM) coordinate system (Dave et al., 2015). The Landsat 9 imagery relevant and available for the SOF study is projected as UTM Zone 15 with the World Geodetic System (WGS) 1984 datum. The imagery of the SOF was compared to digital orthophoto quarters (DOQs) from the Arkansas GIS Office to visually assess and confirm there were no geographic differences between major land features.

Image Classification

Supervised Classification

A Landsat 9 scene was processed using ERDAS IMAGINE® 2022 v. 16.7 software (ERDAS, 2022). The scene was subset so that only areas relevant to the SOF study were classified. Two supervised classifications were executed on the subset image based on identified pit and creek scars and were restricted by the following decision rules: non-parametric rule- parallelepiped, overlap rule- parametric, unclassified rule- unclassified, and a parametric rule- maximum likelihood. A nonparametric signature does not originate from digital image statistics, but rather from defined objects such as training sites which means when a parallelepiped algorithm is used, the classification considers the mean value of pixels which comprise the training sites for each class (ERDAS, 2005; Sathya & Deepa, 2017). With the overlap rule of parametric, if training sites have

overlapping spectral characteristics in a feature space, pixels will be assigned to the appropriate class according to the statistic distribution of the dataset (ERDAS, 2005). The unclassified rule determines the standard deviation of the pixels from the mean value creates boundaries to delineate what class unclassified pixels should be grouped into (Sathya & Deepa, 2017). For the parametric rule, maximum likelihood was chosen so that pixels were assigned to the class they had the highest probability of being in based on the statistic distribution of the dataset (Sathya & Deepa, 2017). Only one class was created to delineate brine contaminated areas, so only pixels with values that coincide with the previously mentioned decision rules were classified.

Selected training sites were chosen based on the 346 known brine affected areas that were mapped and digitized in 1996 for the study, *Saltwater Waste and Landscape Change, Smackover Field, Arkansas* (Figure 15) (Barrett, 2002). Eleven training sites were selected based on 1996 pit scars for one supervised classification and ten training sites were selected based on 1996 pit scars for the second supervised classification.

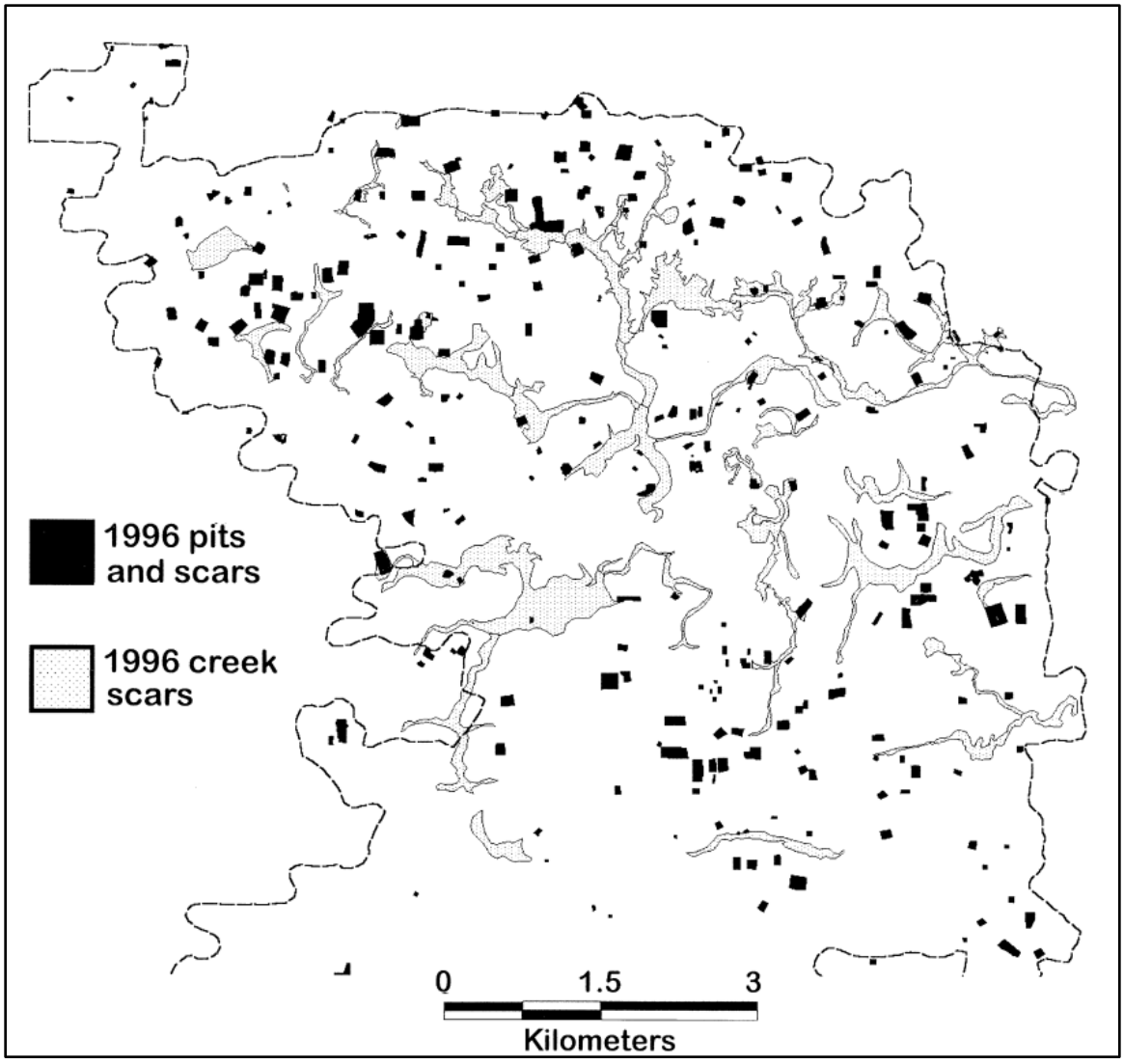

Figure 15. Land scarring from brine contamination across the Norphlet District in the Smackover Oil Field that was visually present in 1996 (Barrett, 2002).

Unsupervised Classification

Areas of soil brine contamination identified in the supervised classifications were further assessed with an unsupervised classification. P4M-RTK imagery was taken over brine affected areas at an altitude which maintained a spatial resolution of 5.26 cm per

pixel. Imagery was acquired within two weeks of the time soil samples were taken in the SOF to ensure the temporal (summer/low moisture) conditions needed for multispectral digital imagery in this study were met. An unsupervised classification created classes within the multispectral data that were assessed to determine if unique classes of soil brine contamination were absent/present.

Sample Site Selection

Three sites located within the SOF were chosen as sampling sites. Initially the eight training sites used in the supervised classifications were attempted to be sampled but access to these areas was prohibited by the landowners. To locate appropriate sampling sites, publicly accessible sites within the SOF were selected and assessed visually prior to conducting field research in CONNECTexplorer™ (Eagle view Technologies, n.d.). CONNECTexplorer™ provides high spatial resolution datatsets with spatial resolutions of one to six inches. The sites were designated as: Louann Park, Norphlet Park, and Fishing Area. Louann Park and Norphlet Park were chosen to represent areas that had been classified as brine-contaminated following the supervised classification. The Fishing Area was chosen to act as a control as it was not deemed to be brine contaminated based on the supervised classifications.

Soil Sampling

An important aspect of this study is the validation of the supervised classification results. Composite sampling of soil in identified brine and non-brine areas was conducted

to assess the accuracy of the supervised classification (Tempfli et al., 2009). Soil sampling was also used to validate the results of the unsupervised classifications over the P4M-RTK imagery at higher spatial resolution. The methodology for soil sampling is based on techniques used in "*Detecting Oilfield Brine Contaminated Sites Using Satellite Remote Sensing*," a thesis authored by Bowes in 2007. Bowes' methodology was simulated as her study also involved identifying soil brine contamination across a petroleum affected field. Additionally, the accuracy of the SOF study was compared to the accuracy of Bowes' study to compare the effects of radiometric resolution. By minimizing the differences between the soil validations in the two studies, a more definitive conclusion can be given about the effects of radiometric differences on supervised classification accuracy. The general methodology for soil sampling in the SOF study is outlined in Figure 13.

Soil Sample Collection

A composite soil sample was taken for each of the three sites. Prior to soil sample collection the boundaries of each sampling site were identified and uploaded in ArcGIS Online so that they could be accessible on ESRI's Field Maps app when field research was conducted (ESRI, n.d.). This allowed for the boundary of each site to be viewed when soil samples were collected and ensured that the soil samples taken to create the composite soil sample would be collected within the site boundaries. Five soil samples were collected with a sharp-nosed shovel at each site to create a composite sample. This composite sample and two duplicates of the sample were stored in soil bags labelled with

a sharpie to indicate where and when the samples were taken. The location of each sample was taken and stored in ESRI's Field Maps app. Each soil sample was collected 15 cm below the surface to determine if the presence of brine contamination was near the surface of the soil and able to be detected with remote sensing methods. The collected soil was mixed in a clean bucket with other samples from the site to create the composite sample.

Soil Sample Analysis

The soil samples were processed at the SFASU Soil, Plant, and Water Analysis Laboratory. The samples from each soil bag were dried on plates in a well-ventilated room based on guidance from the laboratory employees. After the soil samples were dried, they were ground and sieved to remove excess debris and create a finer consistency and 250 mg of each sieved soil sample were measured out into beakers. Nanopure water was added to each beaker and the soil samples were mixed to create a saturated soil paste. Following this, the samples were transferred into a Buchner funnel that contained filter paper at the bottom. The liquids from the soil samples were pulled through the filter with a vacuum so that electric conductivity, pH and sodium adsorption ratio information could be obtained from the extracts.

Accuracy Assessment

Soil sample results were used to validate the supervised classification results to determine how accurately brine and non-brine areas were classified across the SOF. Two

error matrices for the classifications of brine in the SOF were created based on the results from soil sampling which serve as reference data. Once the error matrices were completed, two $\widehat{K}$-statistics were calculated to determine the accuracy of the SOF supervised classification and to compare to the results of Cindy Bowes' Landsat 7 study identifying brine contaminated sites (Bowes, 2007; Unger et al., 2013).

An Example: Error Matrix

An example of an accuracy assessment of a land cover classification used in this study is given by Dr. Russell G. Congalton in, *A Review of Assessing the Accuracy of Classifications of Remotely Sensed Data* (1991). In his error matrix example, shown in Figure 16, a hypothetical land cover classification study has been conducted using four different classes: deciduous, conifer, barren, and shrub. Classified data is compared to reference data in the error matrix.

Reference Data

	D	C	BA	SB	row total
D	65	4	22	24	115
C	6	81	5	8	100
BA	0	11	85	19	115
SB	4	7	3	90	104
column total	75	103	115	141	434

Land Cover Categories
D = deciduous
C = conifer
BA = barren
SB = shrub

OVERALL ACCURACY = 321/434 = 74%

PRODUCER'S ACCURACY
D = 65/75 = 87%
C = 81/103 = 79%
BA = 85/115 = 74%
SB = 90/141 = 64%

USER'S ACCURACY
D = 65/115 = 57%
C = 81/100 = 81%
BA = 85/115 = 74%
SB = 90/104 = 87%

Figure 16. An example error matrix for accuracy assessment on land cover classification.

The overall accuracy for the SOF error matrix was determined by dividing the sum of correctly identified pixels in each category by the total number of pixels in the study area. The overall accuracy derived from the error matrix in Figure 16 reveals that the overall accuracy of the classified map was only calculated to be 74%, which was regarded as fair quality by Dr. Congalton.

The user's accuracy for the SOF error matrix was calculated by dividing the correctly classified number of pixels for a specific class over the total amount of pixels assigned to that class. In Figure 16, 90 pixels were correctly classified as shrub by the classified data while a total of 104 pixels were categorized as shrub by the classification, resulting in a user's accuracy of 87%.

The producer's accuracy for the SOF error matrix was calculated by dividing the correctly classified number of pixels for a specific class over the actual total amount of pixels for the class based on the reference data. In the example shown in Figure 16, 90 pixels from the classified data were in the shrub category while in fact a total of 141 pixels were identified in the reference data as shrub, making the producer's accuracy for the barren class of 64%.

An Example: Kappa Statistic

A $\widehat{K}$-statistic for the SOF was evaluated using the example by Rwanga and Ndambuki's study (2017), *Accuracy Assessment of Land Use/Land Cover Classification Using Remote Sensing and* GIS. The calculated value of the $\widehat{K}$-statistic for the SOF was

evaluated for strength of agreement, a measure of agreement beyond random chance assignment (Table 7).

Table 7. A table describing the quality ranges of kappa statistics.

S.No	Kappa statistics	Strength of agreement
1	<0.00	Poor
2	0.00 - 0.20	Slight
3	0.21 - 0.40	Fair
4	0.41 - 0.60	Moderate
5	0.61 - 0.80	Substantial
6	0.81 - 1.00	Almost perfect

RESULTS

Landsat 9 Image Acquisition

Identifying the Boundary

The boundary for the SOF was georeferenced from the map boundary depicted in Arkansas Geological Survey, Bulletin 2 illustrated in Figure 17 (Spooner, 1935). Although there is no formal boundary designating the difference between the Louann District and the Norphlet District within the SOF, in Figure 17, the Louann District encompasses the western portion of the SOF while the Norphlet District encompasses the eastern portion of the field. This boundary was georeferenced in Environmental Systems Research Institute, Inc. (ESRI) ArcGIS Pro v. 3.1.0 to determine the full extent of the SOF and ensure the correct Landsat 9 scene was downloaded. Public Land Survey System (PLSS) shapefiles for the townships and sections were downloaded for Ouachita and Union counties from the Arkansas GIS Office website (Figure 18 and Figure 19). The downloaded shapefiles were merged into one shapefile in ESRI ArcGIS Pro v. 3.1.0 software to make the georeferencing process more efficient (Figure 20). The downloaded shapefiles were projected in UTM Zone 15 N with a WGS 1984 datum (Figure 21). These shapefiles were clipped so that only sections that matched those shown in Figure 17 were visible (Figure 22).

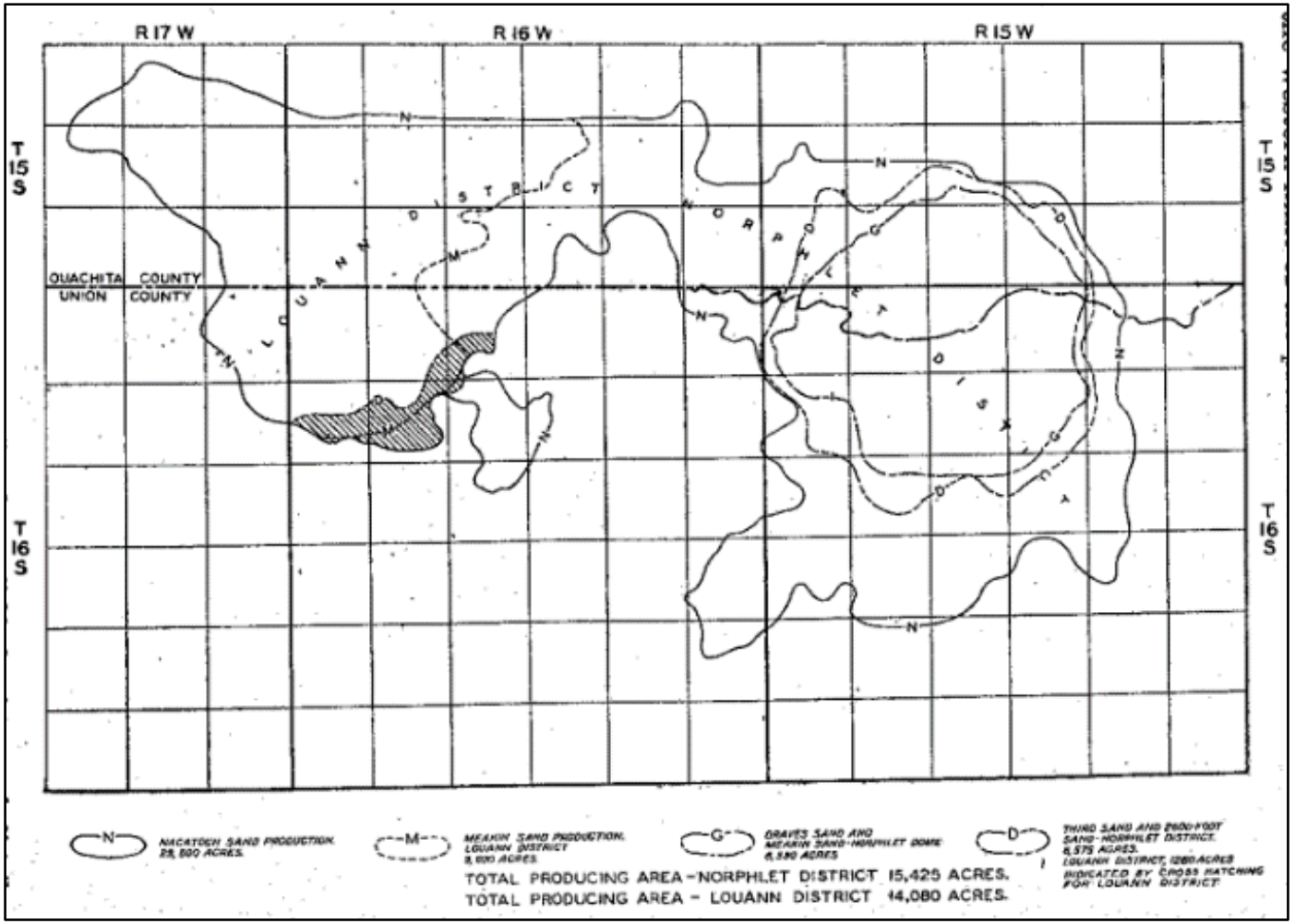

Figure 17. Smackover Oil Field map boundary from the Arkansas Geological Survey, Bulletin 2 (Spooner, 1935).

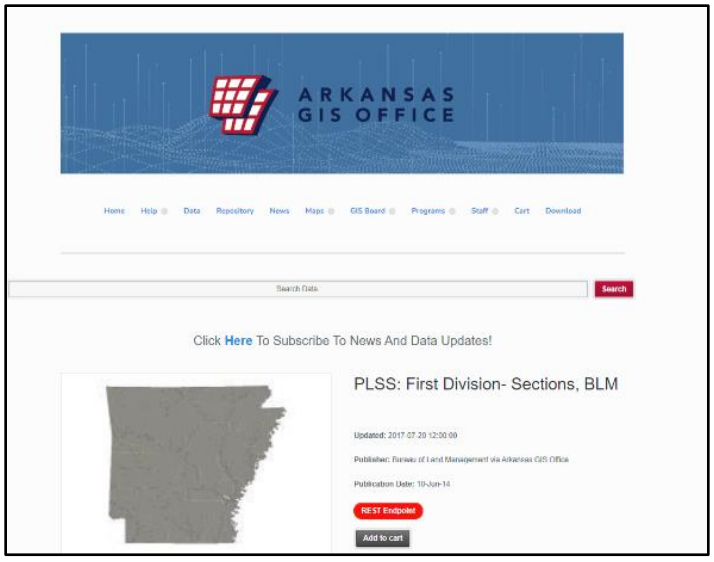

Figure 18. Public Land Survey System sections downloaded for Ouachita and Union counties from the Arkansas GIS Office, n.d..

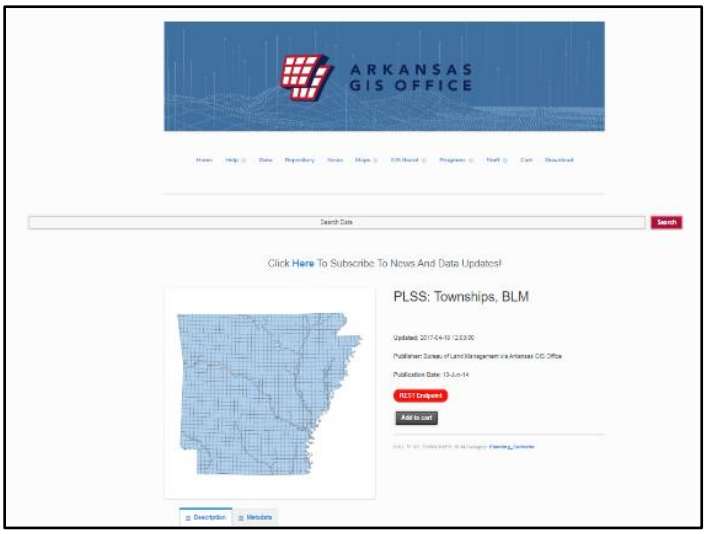

Figure 19. Public Land Survey System townships downloaded for Ouachita and Union counties from the Arkansas GIS Office, n.d.

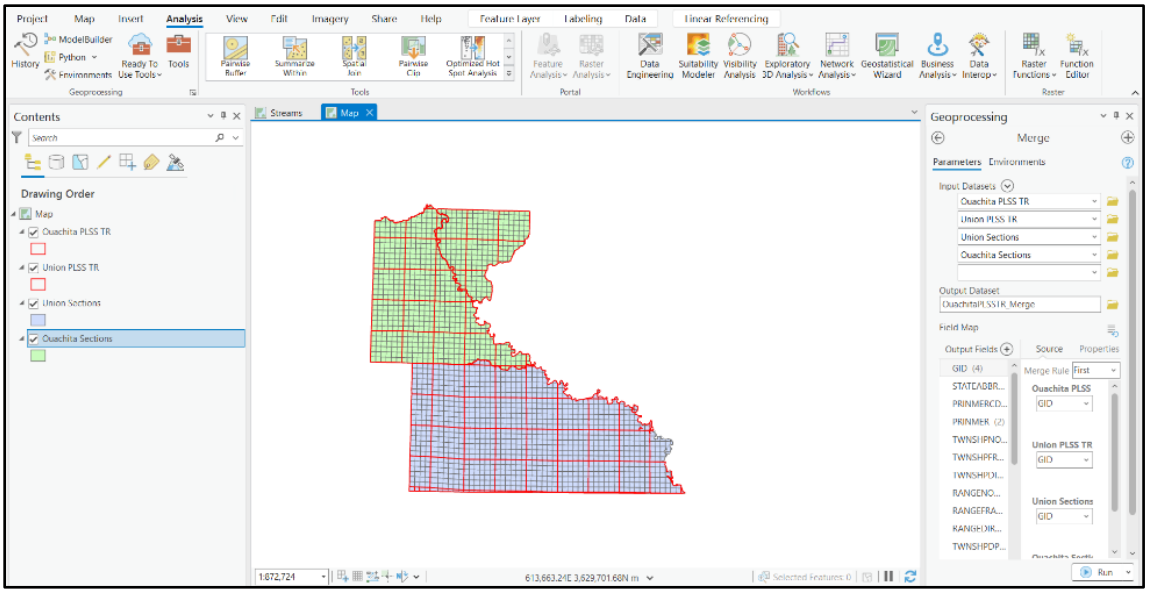

Figure 20. Merging the four PLSS related areas across the Ouachita and Union County shapefiles into one shapefile in ESRI ArcGIS Pro v. 3.1.0 software.

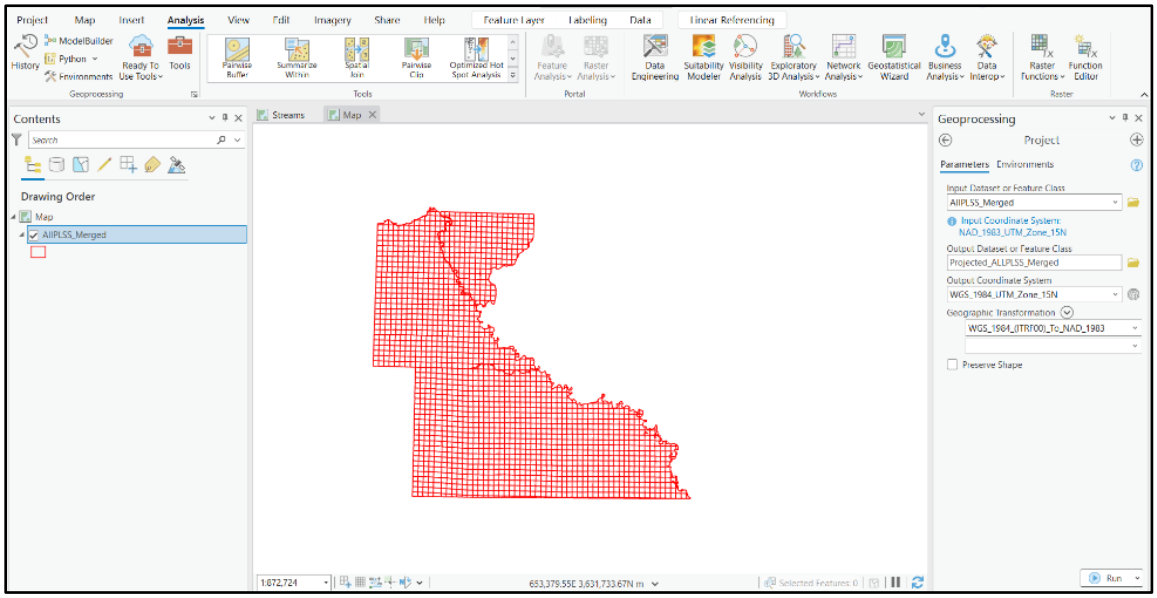

Figure 21. Projecting the merged PLSS shapefile into the UTM Zone 15 N WGS 1984 in ArcGIS Pro v. 3.1.0 software.

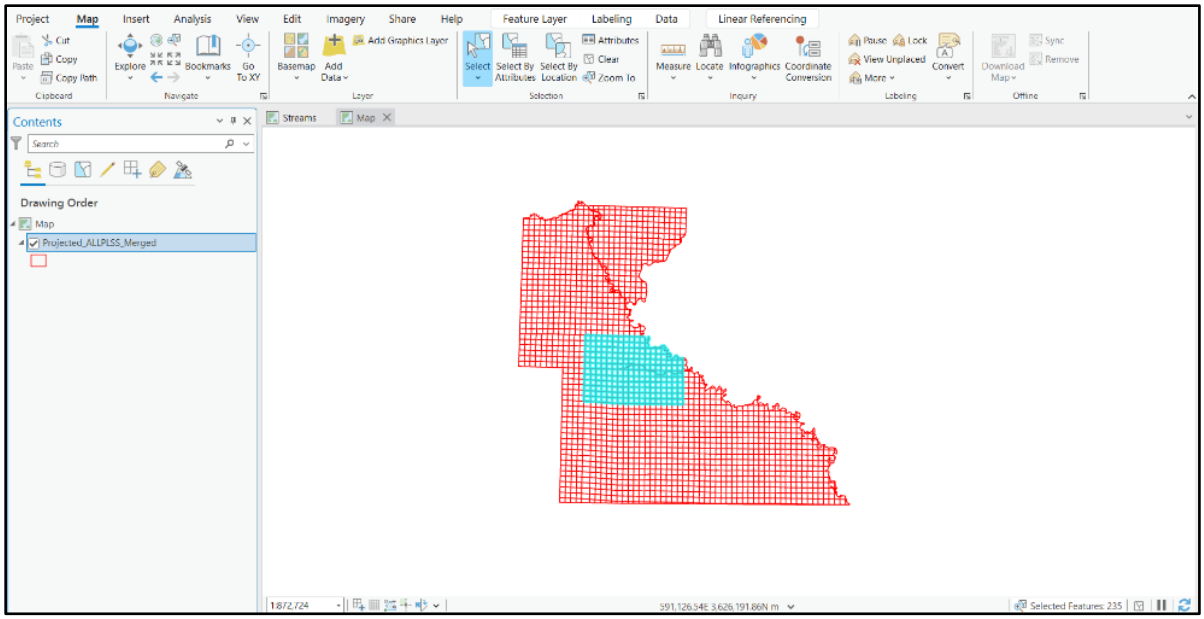

Figure 22. Exporting the PLSS sections that are consistent with sections in the Smackover Oil Field boundary in Figure 17.

Once the PLSS sections relevant to the SOF were exported into a shapefile, Figure 17 was georeferenced to the PLSS sections (Figure 23). A 1st order polynomial (affine) transformation was used on Figure 17 with 61 ground control points (GCPs) and a total RMSE error of 95.301 m. Once Figure 17 was georeferenced, the boundary of the SOF was digitized in ArcGIS Pro v. 3.1.0 (Figure 24).

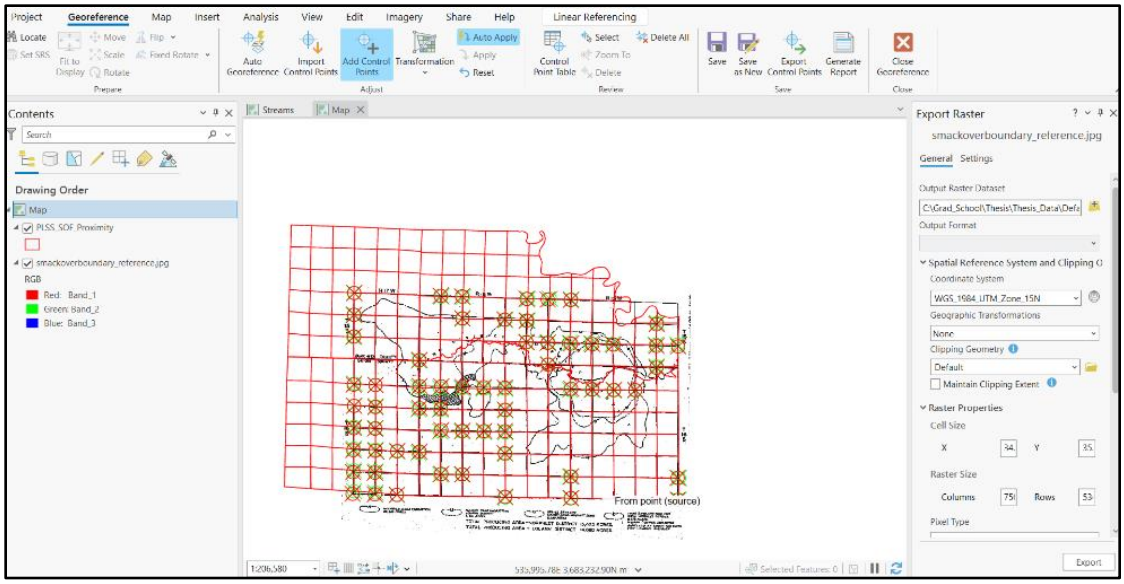

Figure 23. Figure 17 is georeferenced to the PLSS sections so that the Smackover Oil Field boundary can be digitized in ESRI ArcGIS Pro v. 3.1.0.

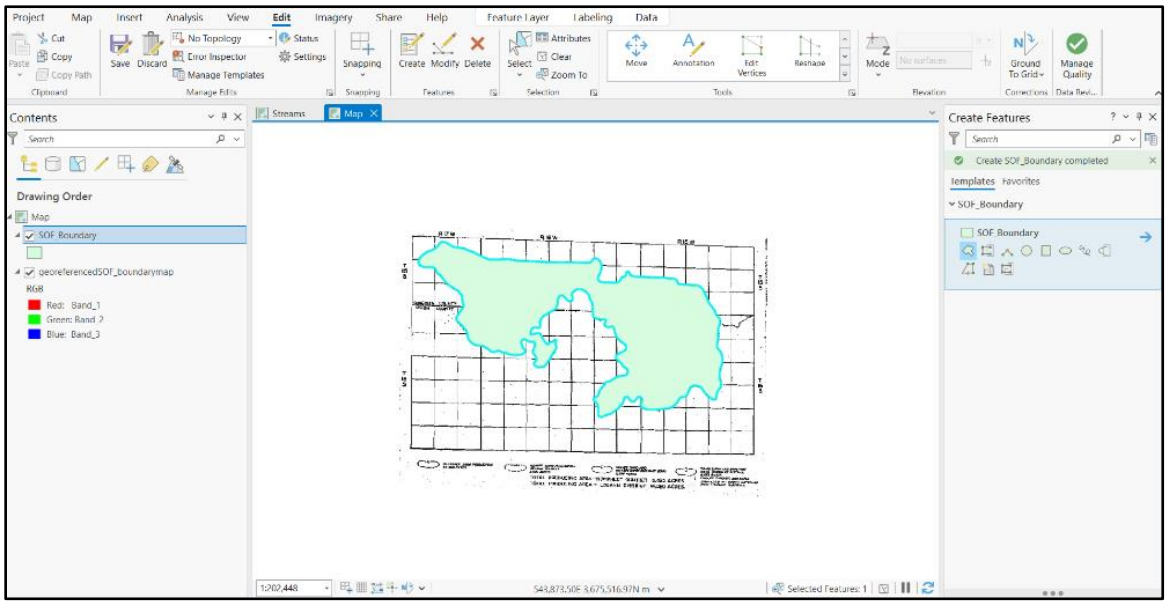

Figure 24. Digitized boundary of the Smackover Oil Field based on the historic Smackover Oil Field map boundary in ArcGIS Pro v. 3.1.0.

Landsat 9 OLI/TIRS-2

A Landsat 9 scene that included the SOF was downloaded from the USGS GloVis website (Figure 25). The spatial reference for the image was UTM Zone 15 N WGS 1984 and the image was acquired during the summer on July 26, 2022 (GloVis, n.d.). The scene was in WRS Path 024 and WRS Row 037 and possessed a scene cloud cover percentage of 8.56% (GloVis, n.d.). ERDAS IMAGINE® 2022 v. 16.7 software was used to import the multispectral Landsat 9 scene data (Figure 26) (ERDAS, 2022). The multispectral Landsat 9 scene was subset in ERDAS IMAGINE® 2022 v. 16.7 based on the previously digitized boundary of the SOF to create a digital image solely of the SOF (Figure 27). When the Landsat 9 scene was subset based on the SOF boundary, 6 spectral bands were used to create a digital image consistent with the spectral bands used for Bowe's study: blue, green, red, near-infrared, and two mid-infrared bands (Figure 28 and Figure 29) (Unger et. al., 2013).

Figure 25. A Landsat 9 OLI/TIRS-2 scene that included the SOF in the online interface, GloVis.

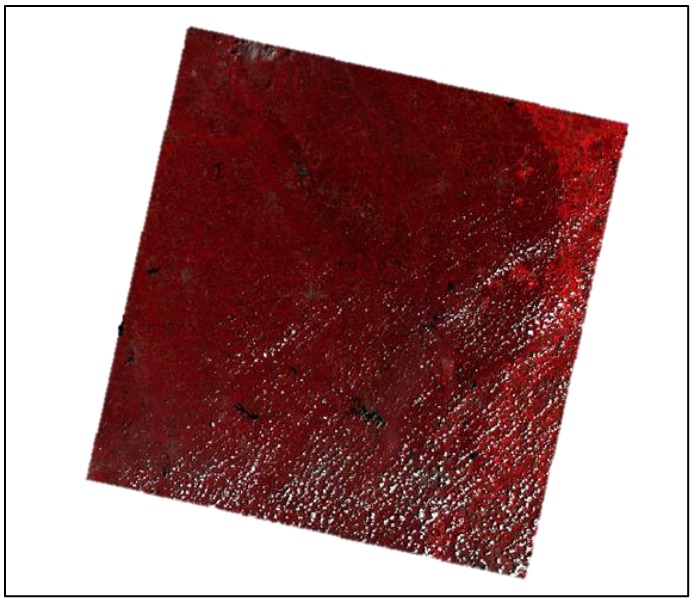

Figure 26. The downloaded Landsat 9 scene from USGS in ERDAS IMAGINE® 2022 v. 16.7.

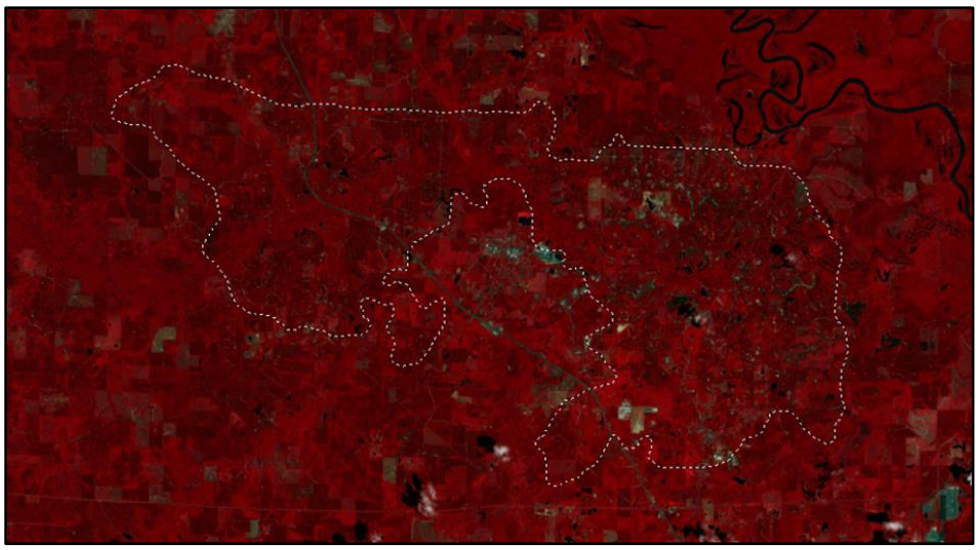

Figure 27. The area that was subset from the Landsat 9 OLI/TIRS-2 image in ERDAS IMAGINE® 2022 v. 16.7 of the Smackover Oil Field.

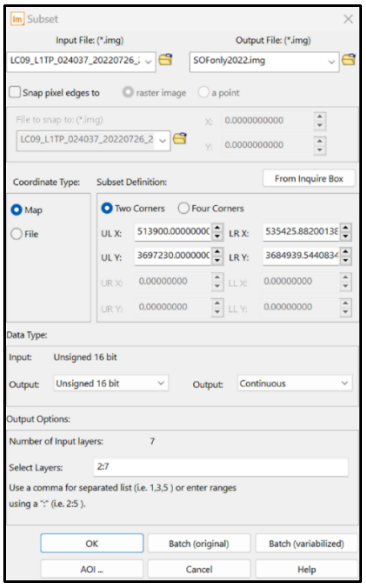

Figure 28. Creating the subset digital image and including the blue, green, red, near-infrared, and two mid-infrared bands spectral bands in ERDAS IMAGINE® 2022 v. 16.7.

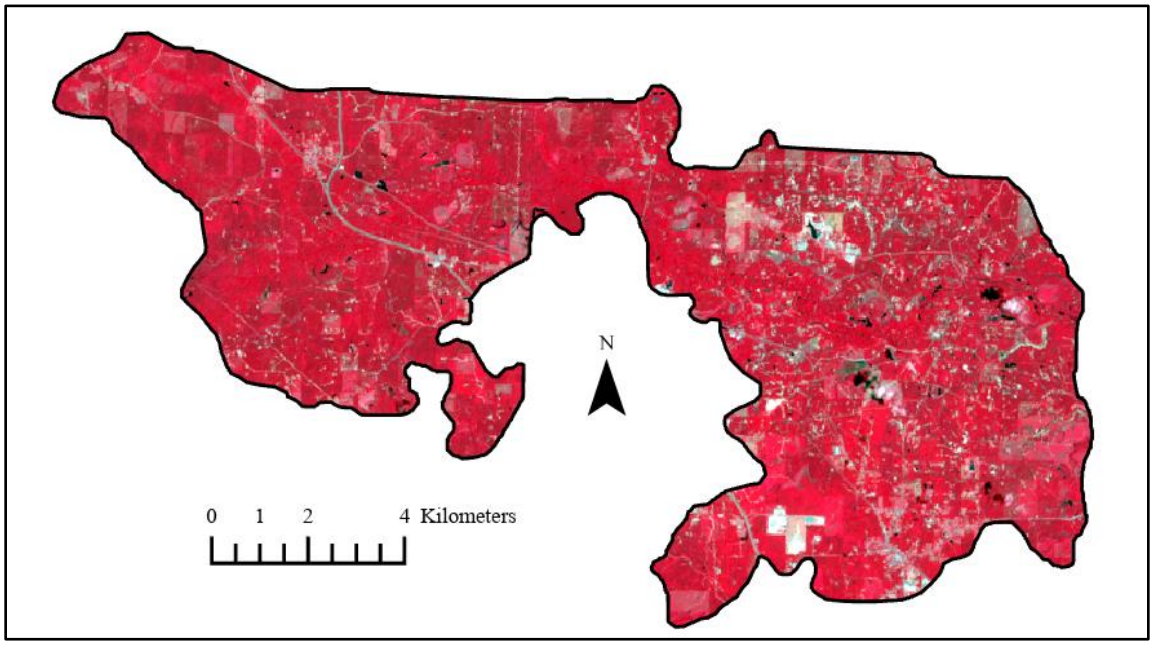

Figure 29. The 6-band multispectral digital image of the Smackover Oil Field.

Radiometric Corrections

There was no SSR bad block issue identified in the Landsat 9 scene that was used to create a subset image for the supervised classification (Figure 26). The Landsat 9 scene used was not compared to other multispectral digital imagery and as a result no radiometric corrections were performed on the Landsat scene.

Geometric Corrections

No geometric corrections were performed on the subset Landsat 9 scene depicted in Figure 29. The area was geometrically validated by ensuring that the boundary used to subset the Landsat scene was georeferenced correctly and was projected in the UTM Zone 15 WGS 1984 coordinate system (Figure 24). The subset Landsat 9 scene was compared to One Foot Digital Orthophoto Quadrangles (DOQs) from the Arkansas GIS Office. Although the data could not be directly downloaded from the Arkansas GIS Office website, the website hosted a link to a Tile Footprint of the DOQs in an ESRI ArcGIS Online web map that contained the DOQ datasets (Figure 30) (Arkansas GIS Office, n.d. & ESRI, n.d.). To efficiently select the DOQs that encompassed the SOF boundary, the SOF boundary layer was added to the web map and each tile which represented part of the SOF on the web map was downloaded (Figure 31). A total of 31 tiles were downloaded from the web map and contained a spatial reference of North American Datum (NAD) 1983 UTM Zone 15N. The “Mosaic to New Raster” tool in ESRI ArcGIS Pro v. 3.1.0 was used to mosaic the downloaded DOQs and the data was reprojected to a spatial reference of WGS 1984 UTM Zone 15N to match the spatial

reference of the subset Landsat 9 scene (Figure 32). The subset of the Landsat 9 scene that displayed the SOF and the mosaicked DOQ digital image was compared to ensure that the landscape features within the subset Landsat 9 scene visually matched (Figure 33). The subset Landsat 9 scene was not compared to other digital images in the study, so no further geometric corrections were performed on the subset Landsat 9 imagery of the SOF.

Figure 30. The One Foot Digital Orthophotographs dataset provided by the Arkansas GIS Office (Arkansas GIS Office, n.d.).

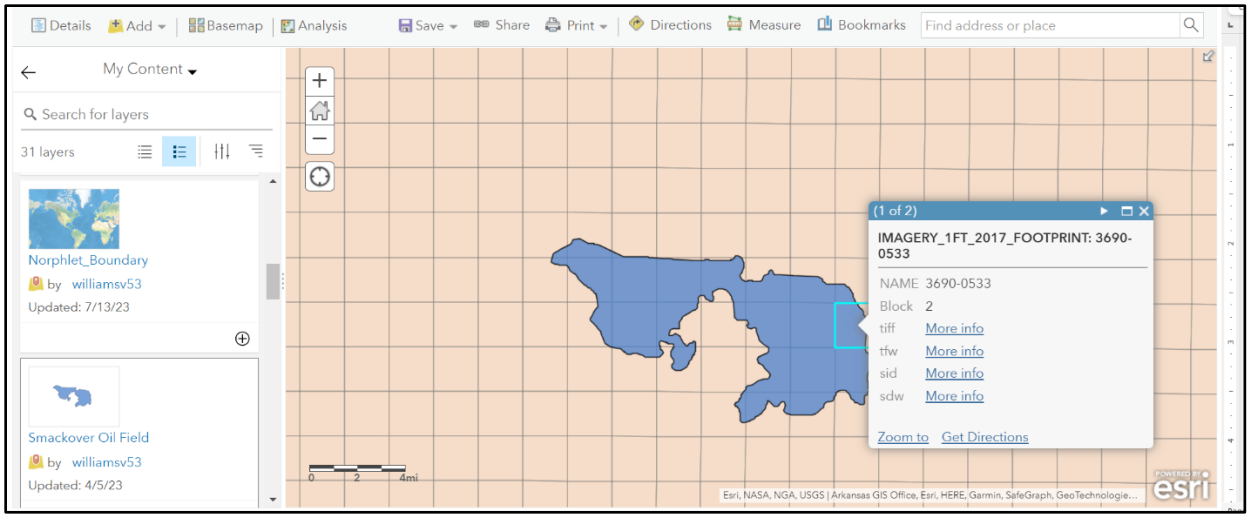

Figure 31. The process of selecting data from each relevant tile in the ESRI ArcGIS Online web map (ESRI, n.d.).

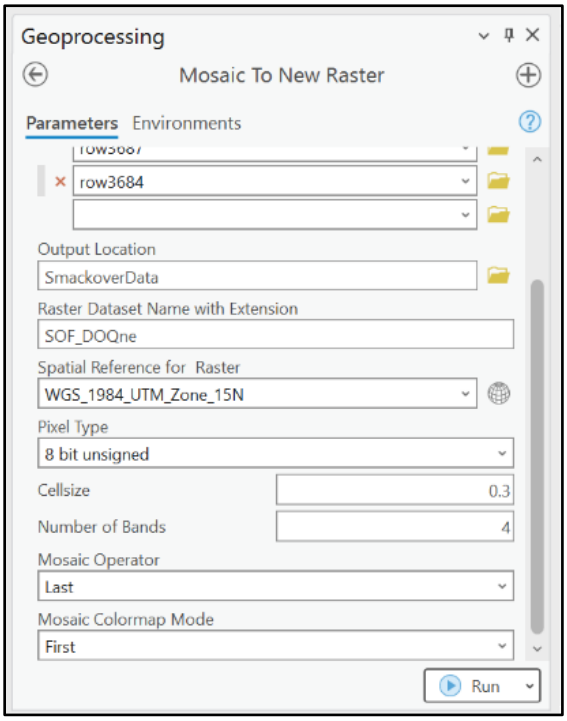

Figure 32. The Mosaic to New Raster tool in ESRI ArcGIS Pro v. 3.1.0 was used to mosaic the DOQs and reproject them into the desired spatial reference.

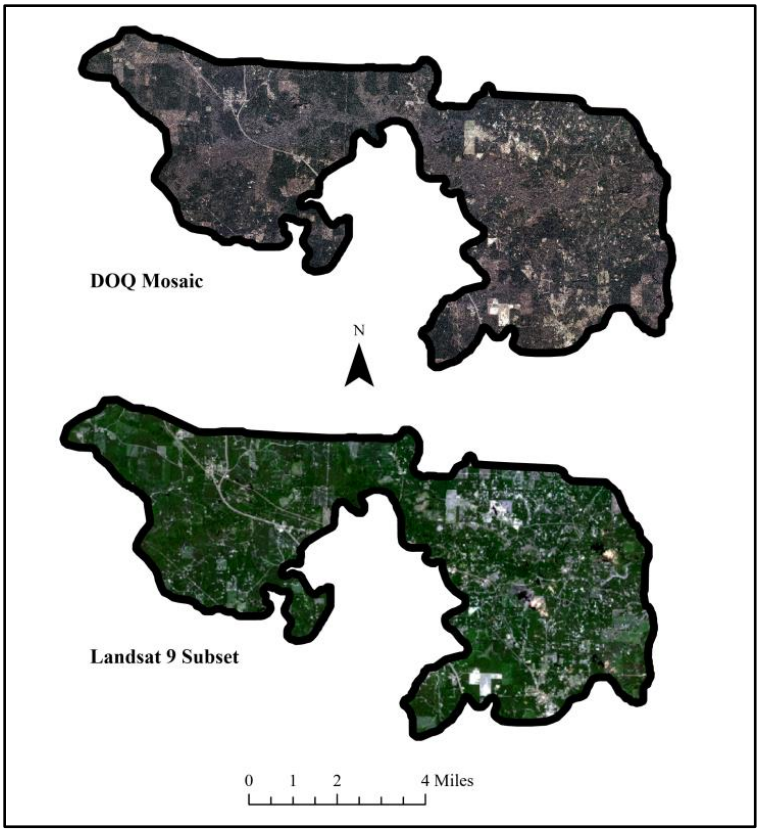

Figure 33. A comparison of landscape features between DOQ and Landsat 9 data.

Landsat 9 Image Classification

Reference Data

The reference data used for the supervised classifications were georeferenced to ensure chosen training sites were accurately located. A map depicting the 1996 earthen pit scars and creeks scars within the Norphlet District was used as reference data for the supervised classification of brine across the SOF (Figure 15) (Barrett, 2002). The location of the Norphlet District in the SOF is depicted in Figure 34. The ESRI ArcGIS Pro v. 3.1.0 software was used to georeference the reference map to the appropriate location

with a WGS 1984 UTM Zone 15N spatial reference. The reference map depicting pit and creek scarring lacked discernable enough landscape features to georeference the reference map to the correct location, so another historic map, Figure 35, which shared the same boundary as the reference map, was georeferenced first (Barrett, 2002). Figure 35 hosted streams across the Norphlet District so it was possible to match the streams in Figure 35 to streams across the Ouachita and Union counties (Figure 36). Shapefiles representing streams across the Ouachita and Union counties were retrieved from the Arkansas GIS Office website.

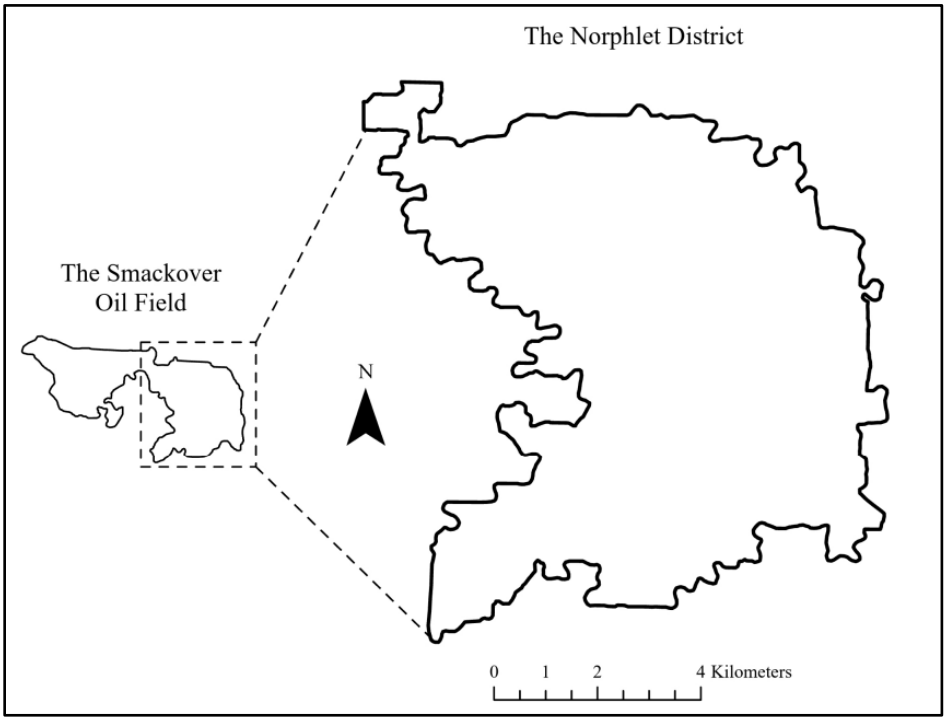

Figure 34. The Norphlet District in the eastern portion of the Smackover Oil Field.

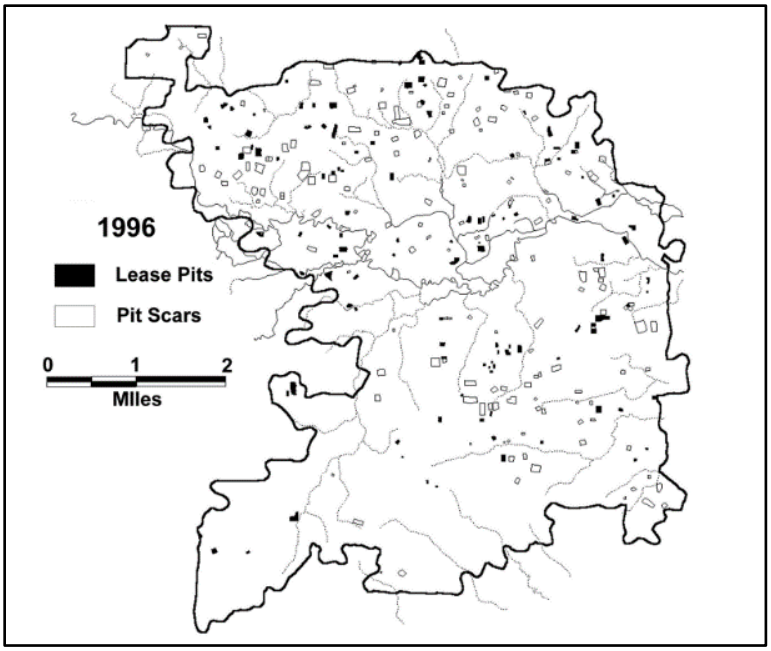

Figure 35. Norphlet District streams that were discernable in 1996 (Barrett, 2002).

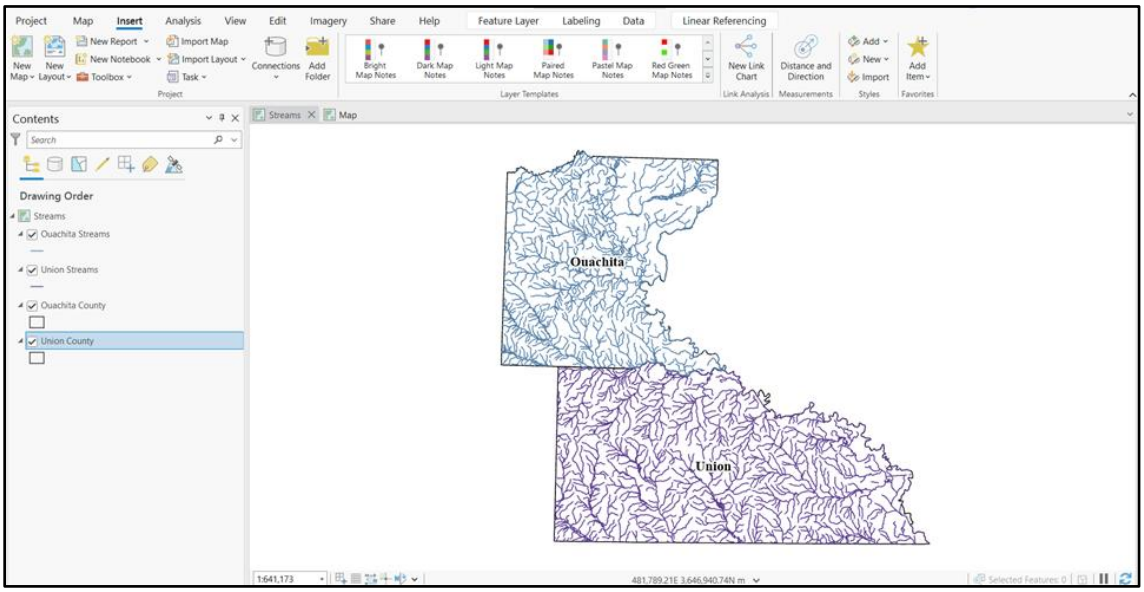

Figure 36. The streams of Ouachita and Union counties, Arkansas shown in ESRI ArcGIS Pro v. 3.1.0 and retrieved from the Arkansas GIS Office website.

The stream shapefiles for Ouachita and Union County were merged into a single shapefile using ESRI ArcGIS Pro v. 3.1.0 software (Figure 37). The merged shapefile was projected into UTM Zone 15 with a WGS 1984 Datum to match the downloaded Landsat 9 scene (Figure 38). Figure 35 was georeferenced based on the matching stream features from the Arkansas GIS office and was exported as a TIFF file with the spatial reference UTM Zone 15 N and WGS 1984 datum (Figure 40). A total of 17 GCPs were used to georeference Figure 35 with a root mean square error (RMSE) of 28.01 m using a 1st order polynomial (Affine) transformation.

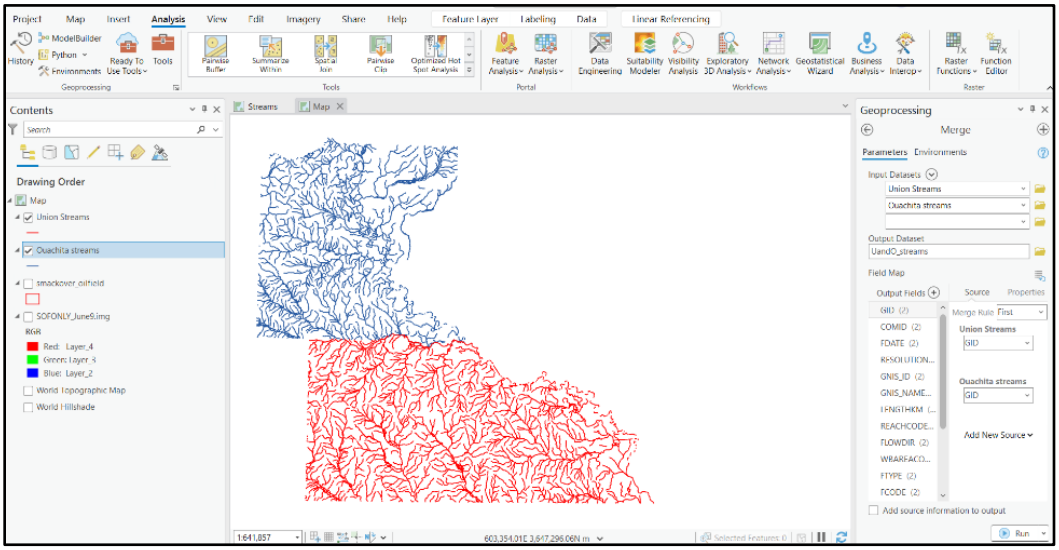

Figure 37. The streams of Union and Ouachita counties were merged into one shapefile using the Merge tool in ArcGIS Pro v. 3.1.0.

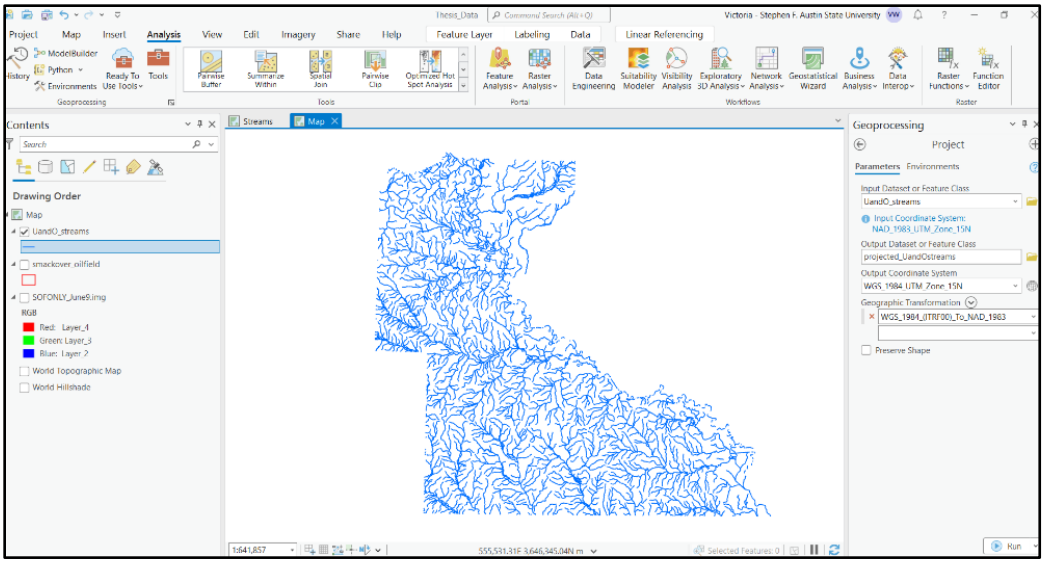

Figure 38. The Project tool was used in ESRI ArcGIS Pro v. 3.1.0 to project the merged streams into UTM Zone 15 in the datum WGS 1984.

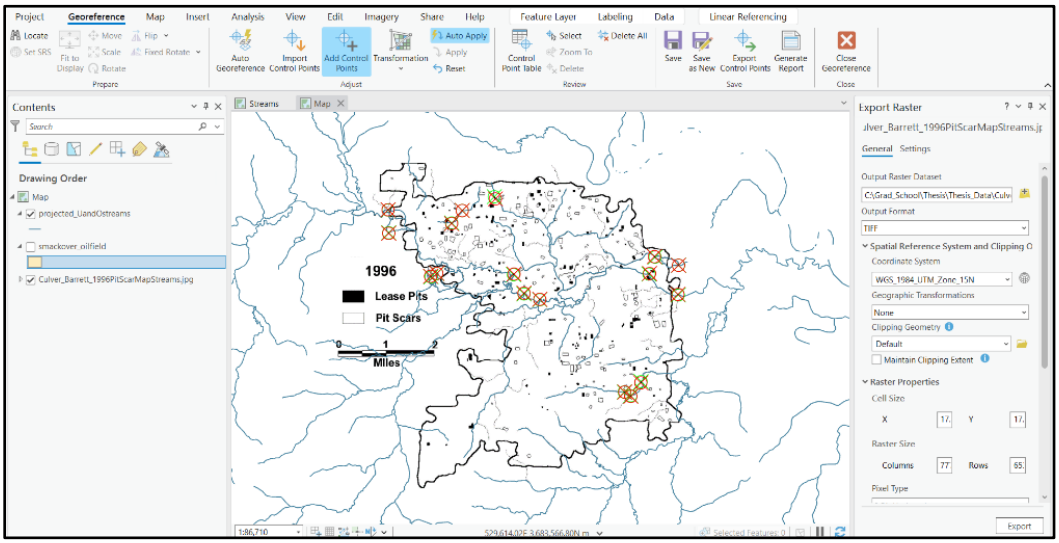

Figure 39. The streams across the 1996 map of lease pits and pit scars were georeferenced to the projected streams in Ouachita and Union counties.

After Figure 35 was georeferenced, the desired reference map, Figure 15, was georeferenced by matching the boundary of the Norphlet District to the same boundary in

Norphlet District in Figure 35. Figure 15 was transformed using a 1st Order Polynomial (affine) method with six GCPs as shown in Figure 40. There was an RMSE error of 12.10 m. Once the reference map, Figure 15, was georeferenced, it was used to identify 11 potential pit-based training sites and ten potential creek-based training sites which represented brine affected areas in the supervised classifications.

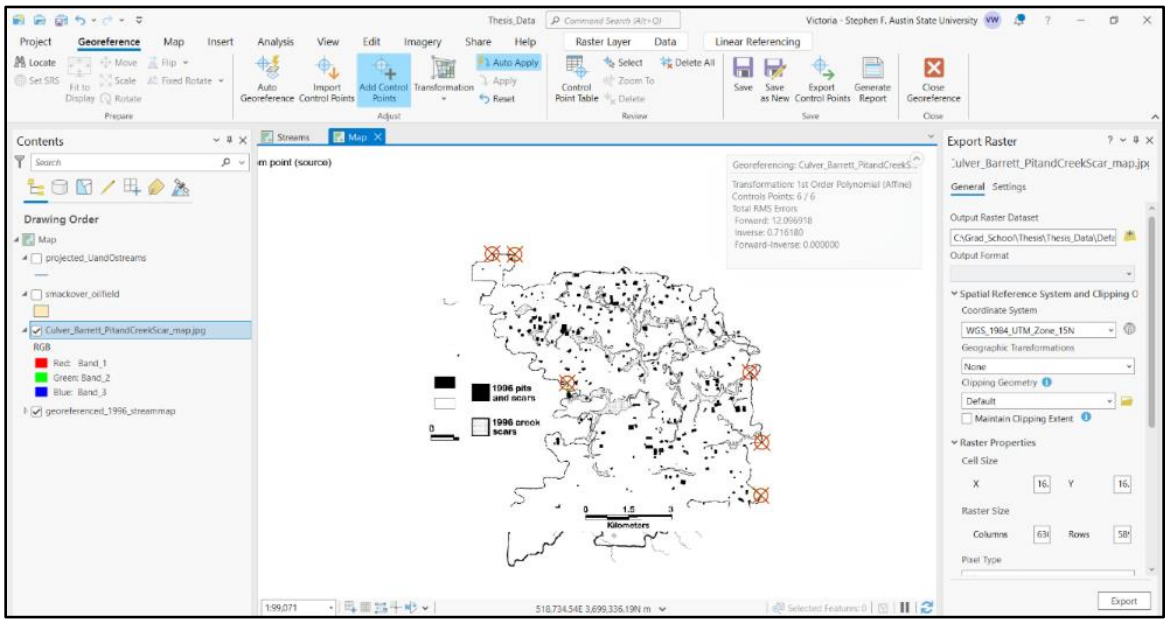

Figure 40. The reference map to identify potential training sites was georeferenced to the map containing streams across the Norphlet District using ArcGIS Pro v. 3.1.0.

Training Site Acquisition

The reference map identified pit and creeks scars that were visible in 1996. To mitigate the temporal difference between the reference map and more current data, the CONNECTexplorer™ website by EagleView Technologies was utilized to assess more current conditions of the pit and creek scars. The subset Landsat 9 scene of the SOF and the reference map were reprojected into a geographic coordinate system in ERDAS

IMAGINE® 2022 v. 16.7 so that pit and creek scars could be identified with Latitude/Longitude decimal degree coordinates in CONNECTexplorer™ (Figure 41 and Figure 42). Once potential training sites were identified in CONNECTexplorer™ based on the reference map's coordinates, the sites were evaluated to determine if they possessed an area larger than 1 acre and still showed visible signs of brine related scarring such as a lack of vegetation (Figure 43).

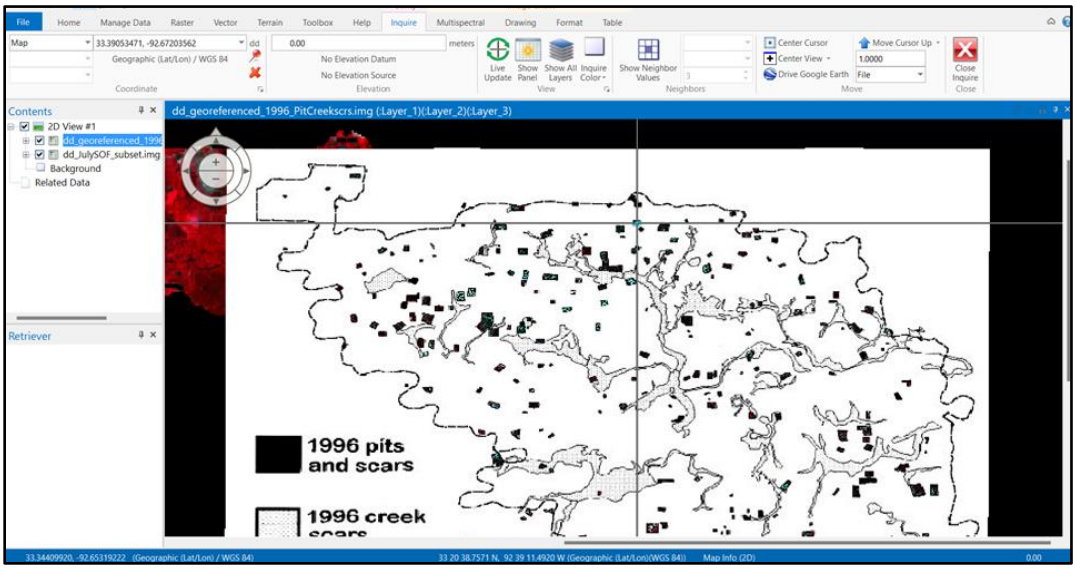

Figure 41. The coordinates of pit and creek locations were identified to facilitate locating the scarred areas in CONNECTexplorer™.

Figure 42. A potential training site located in CONNECTexplorer™ with coordinates from the reference map (EagleView Technologies, n.d.).

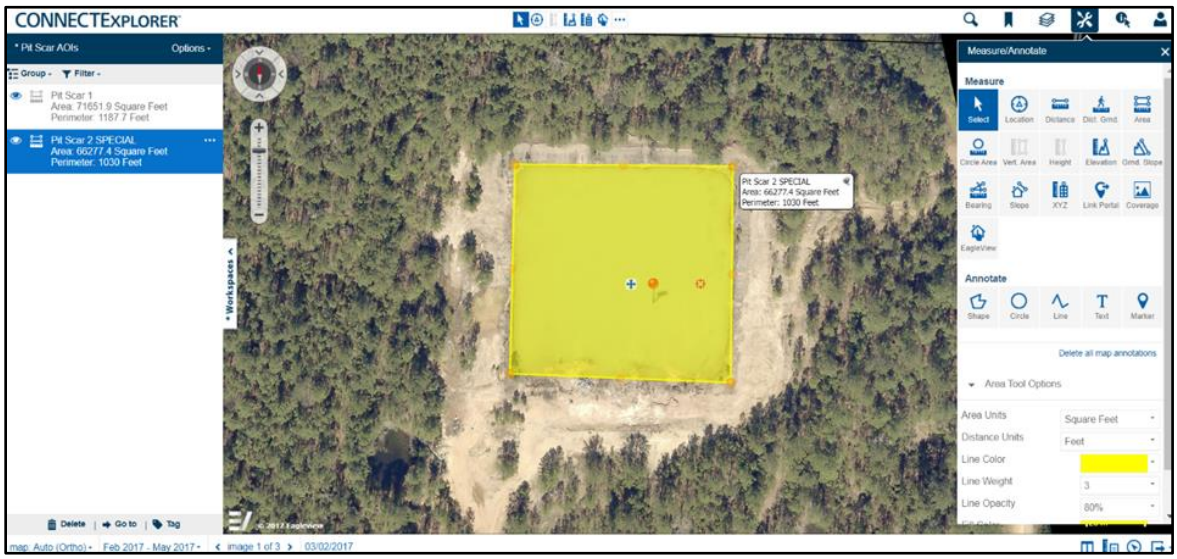

Figure 43. A potential training site located in CONNECTexplorer™ that was measured to identify acreage of the area (EagleView Technologies, n.d).

Initially, 11 training sites representative of pit scarring and ten training sites representative of creek scarring were chosen after the CONNECTexplorer™ evaluation

(Figure 44 and Figure 45). These training sites were exported as KML layers from CONNECTexplorer™ so that the training sites chosen in CONNECTexplorer™ could be converted into feature classes using the "KML to Layer" conversion tool in ESRI ArcGIS Pro v. 3.1.0. The feature classes representing the pit and creek scarring were converted into AOI layers in ERDAS IMAGINE® 2022 v. 16.7 where they would be further evaluated in a feature space layer.

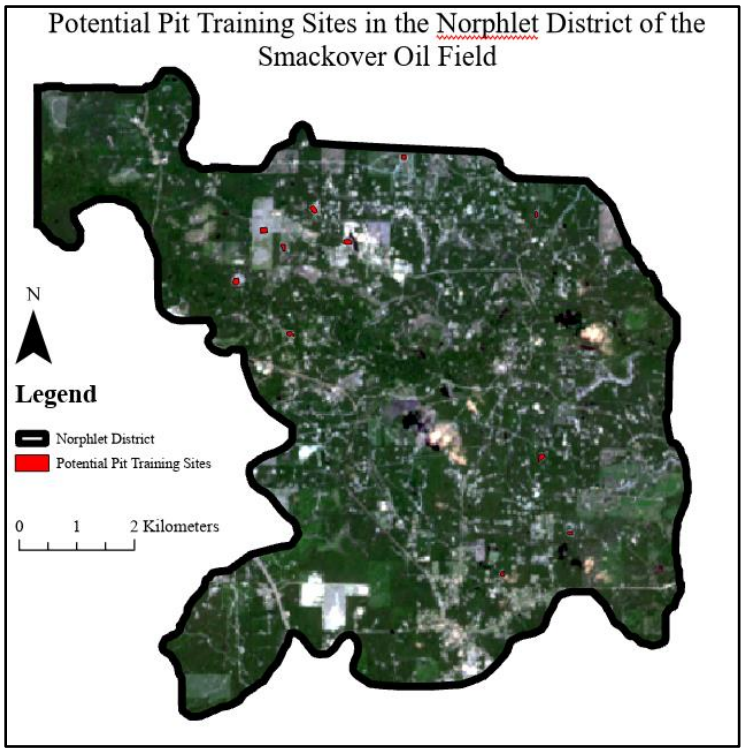

Figure 44. The 11 potential training sites which represented pit scarring across the Norphlet District.

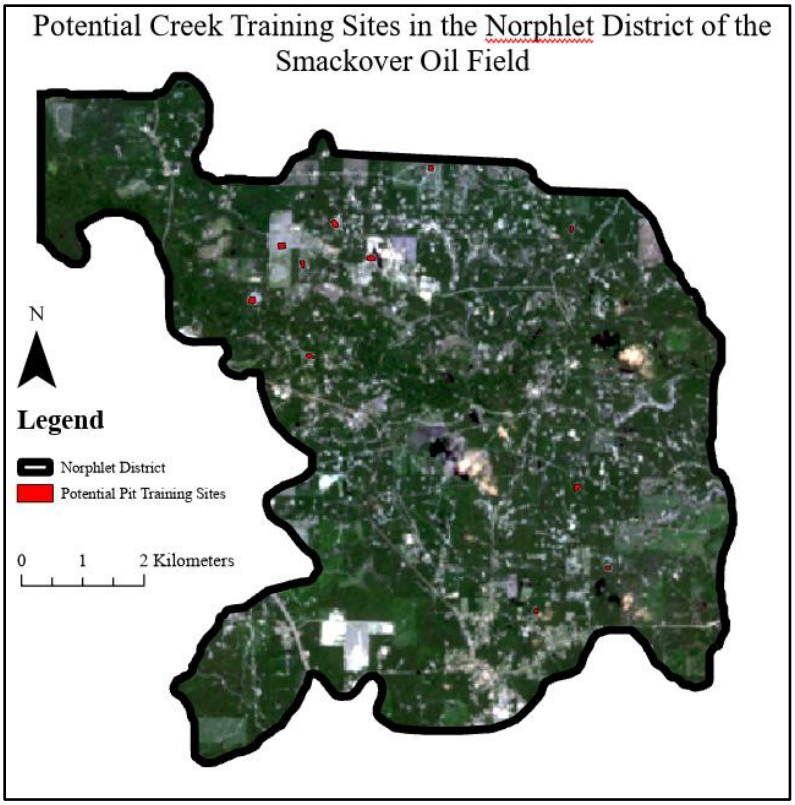

Figure 45. The ten potential training sites which represented creek scarring across the Norphlet District.

Pit Training Sites

Originally 11 potential training sites were chosen to represent brine contaminated pit scarred sites, but only four were chosen for the supervised classification. In the software, the signature editor feature was used to create a feature space layer which plotted band 1 (Blue) versus band 4 (Near-Infrared) of the subset against each other (Figure 46). Each AOI representing the pits were added individually and labelled by selecting them and adding them to the signature editor (Figure 47 and Figure 48). After all the pit AOIs were added to the signature editor, the signature objects button was used

to label and plot the ellipses of each pit to the second deviation in the created feature space layer (Figure 49 and Figure 50). The pits were visually assessed in the feature space layer and the AOIs for pit 2, 3, 5, and 8 were selected to be used as training sites for the supervised classification based on their overlap with each other and determination to not represent landscape features such as roads (Figure 51).

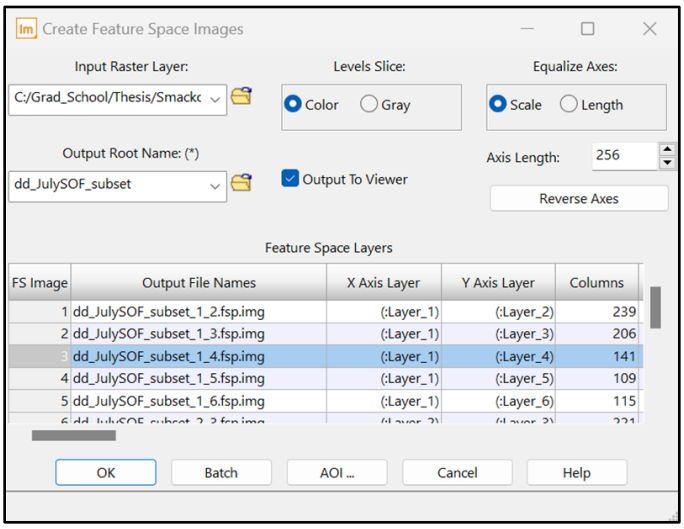

Figure 46. The blue and near-infrared bands were chosen to be plotted against each other in a feature space layer in ERDAS IMAGINE® 2022 v. 16.7.

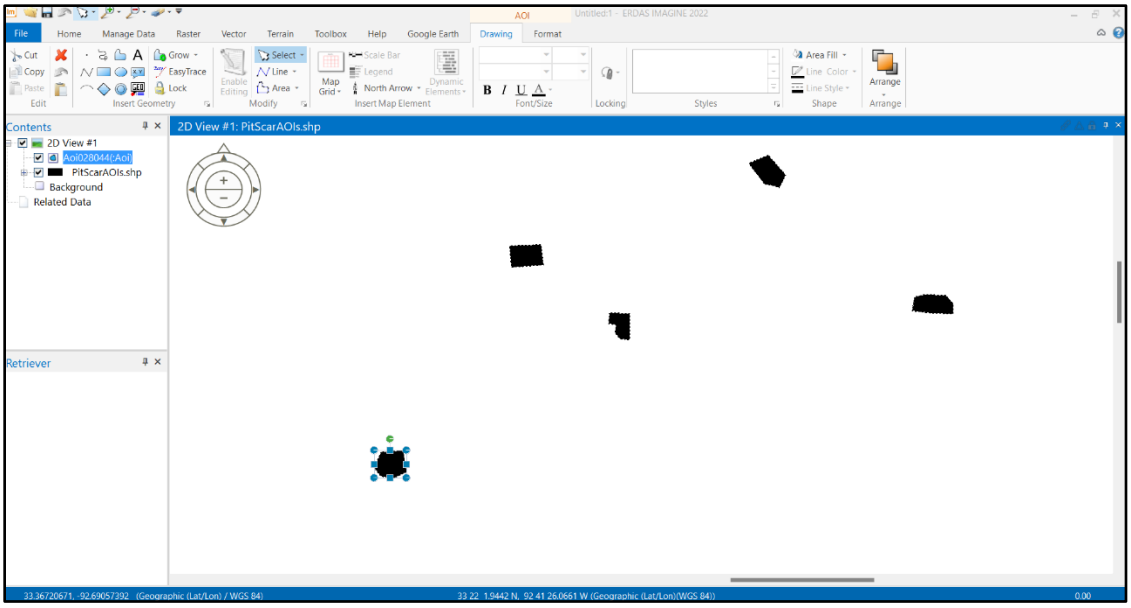

Figure 47. The selection of an individual AOI representing a the first pit scar in ERDAS IMAGINE® 2022 v. 16.7.

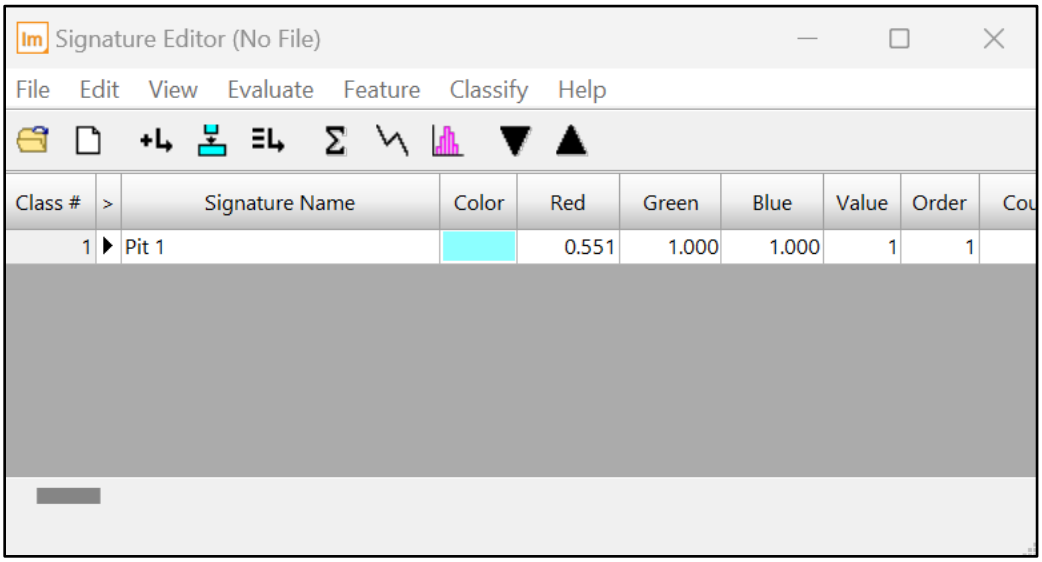

Figure 48. The first pit scar added to the Signature Editor tool in ERDAS IMAGINE® 2022 v. 16.7.

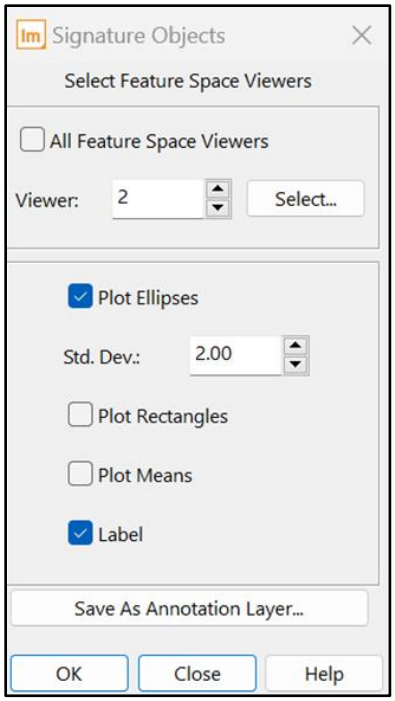

Figure 49. Each Signature Object based on the added pit AOIs were plotted and labelled at a standard deviation of 2.

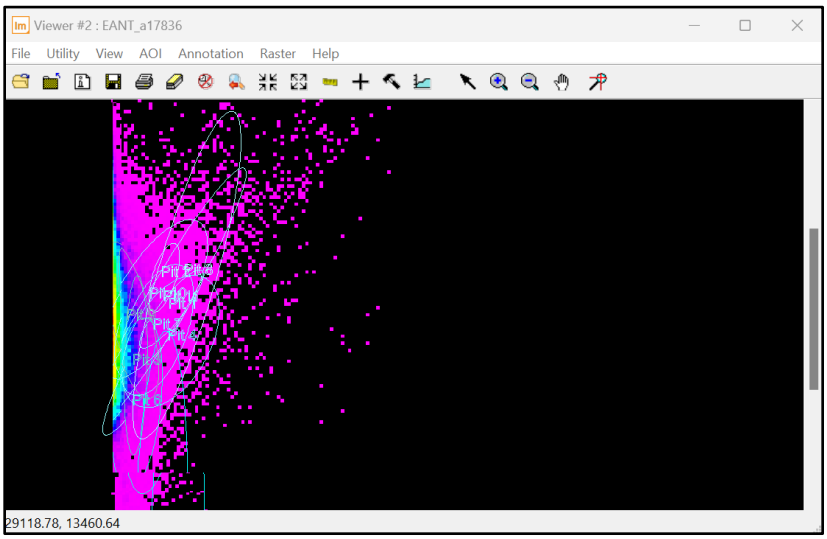

Figure 50. The Signature Objects of each pit AOI shown in the created feature space layer.

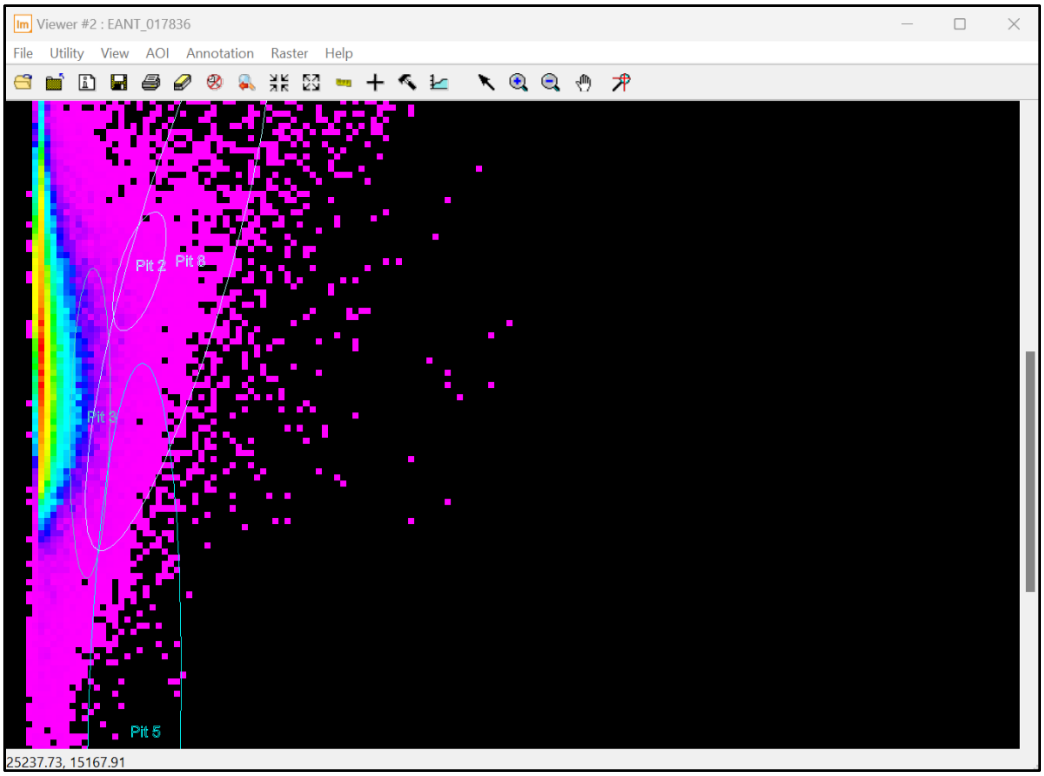

Figure 51. The Signature Objects of the chosen pit AOIs for the pit-based supervised classification.

Creek Training Sites

There were originally ten potential training sites representing brine contaminated creek scarred areas across the SOF, but only four were chosen for the supervised classification. These sites were selected individually and added to the Signature Editor tool in ERDAS IMAGINE® 2022 v. 16.7. Band 1 and Band 4 were again plotted against each other, and the Signature Object (ellipses) of each training site were labelled based on the training site they represented (Figure 52). Creek AOIs 3, 4, 6, 10 were chosen as training sites for the supervised classification of the Smackover Oil Field (Figure 53).

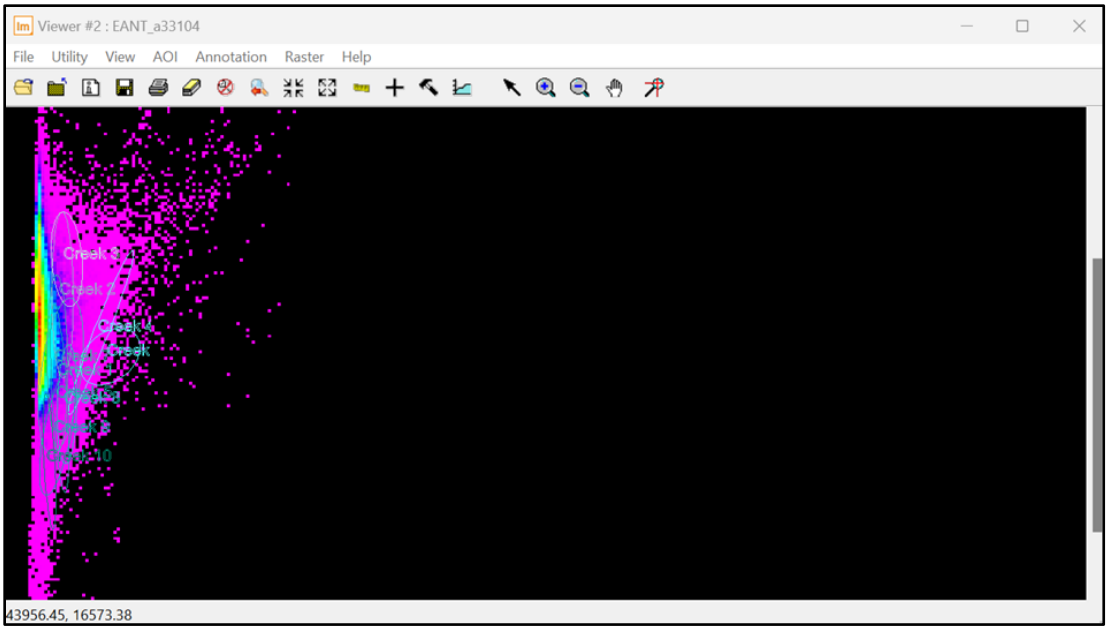

Figure 52. The Signature Objects of each creek AOI in a feature space layer in ERDAS IMAGINE® 2022 v. 16.7.

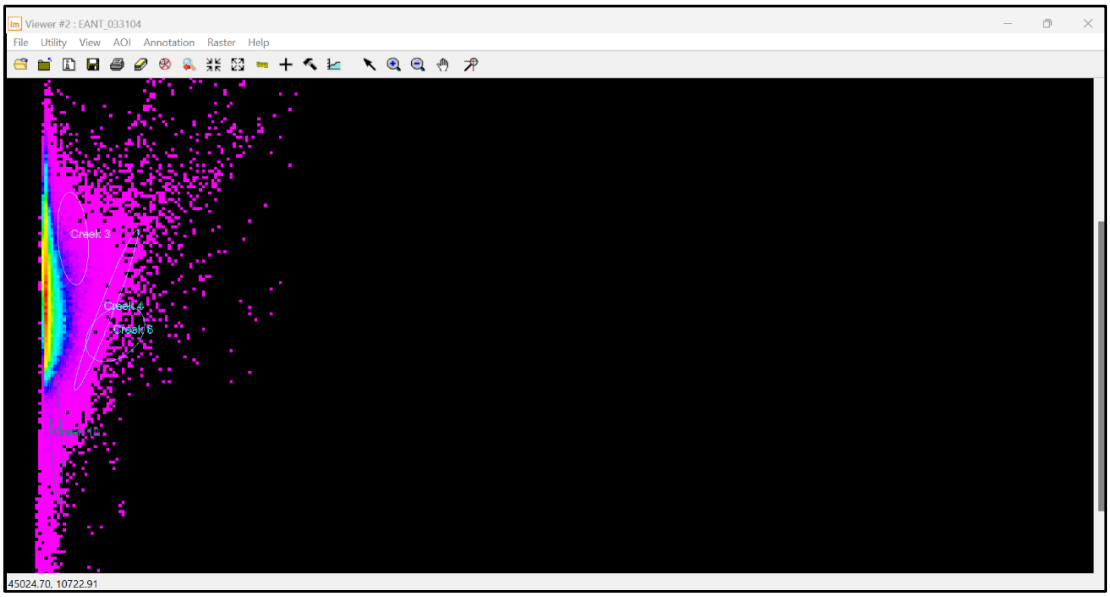

Figure 53. The Signature Objects of the chosen creek AOIs for the pit-based supervised classification.

Supervised Classification

Two supervised classifications were conducted over the Smackover Oil Field (SOF) using ERDAS IMAGINE® 2022 v. 16.7 software (ERDAS, 2022). The subset of the Landsat 9 scene which represented the SOF was used as the digital imagery for the supervised classifications (Figure 29). The same method was used for both classifications, with the only difference being the type of training sites used: pit scarred areas vs. creek scarred areas.

The two supervised classifications were run using the following decision rules: non-parametric rule- parallelepiped, overlap rule- parametric, unclassified rule- unclassified, parametric rule- maximum likelihood (Figure 54). The supervised classification based on the pit training sites is demonstrated in Figure 55 and the supervised classification based on creek training sites is demonstrated in Figure 56.

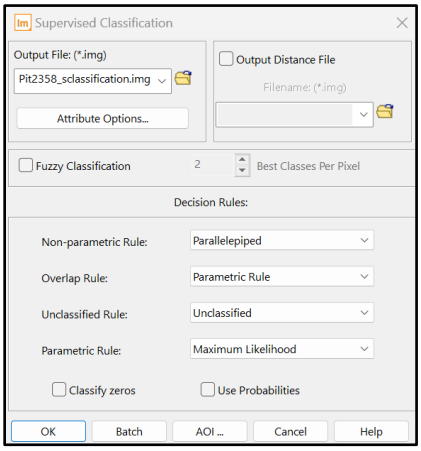

Figure 54. The decision rules selected for the pit-based and creek-based supervised classifications.

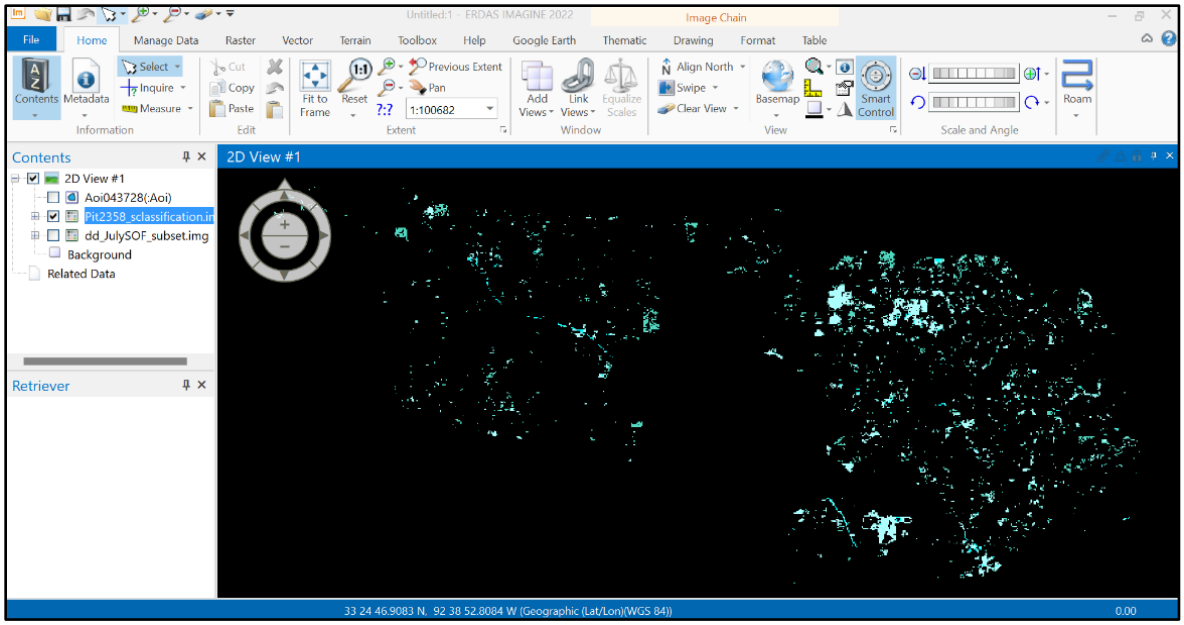

Figure 55. The supervised classification based on the chosen pit training sites.

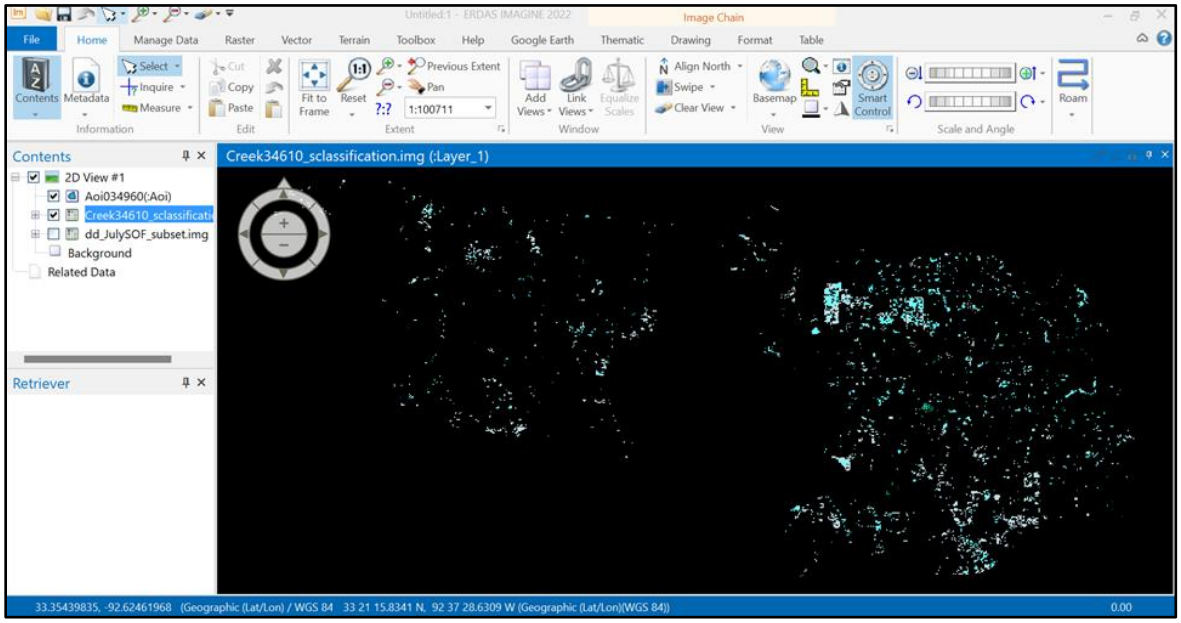

Figure 56. The supervised classification based on the chosen creek training sites.

To create a more accurate representation of brine contamination across the classification, pixels which may not truly represent brine contamination needed to be

removed. The “Clump” tool was used in ERDAS IMAGINE® 2022 v. 16.7 to create polygons of neighboring groups of pixels representing the original thematic class values, such as pit 2 and pit 3 or creek 3 and creek 4 (Figure 57). The results of the “Clump” tool for the pit- based supervised classification and creek-based supervised classification are shown in Figure 58 and Figure 59. The attribute table for each of the clumped supervised classifications was viewed to ensure each classified polygon was represented by the preselected pit or creek training sites (Figure 60).

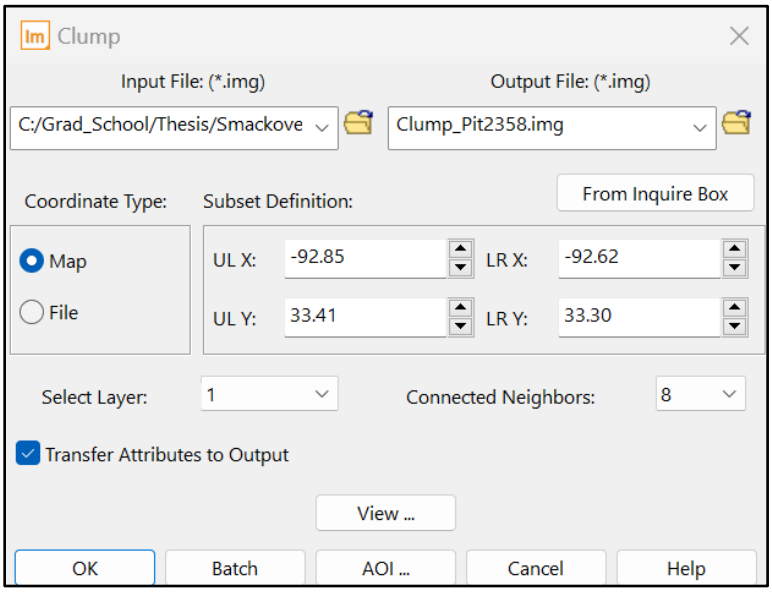

Figure 57. The Clump tool in ERDAS IMAGINE® 2022 v. 16.7 used to refine the supervised classifications.

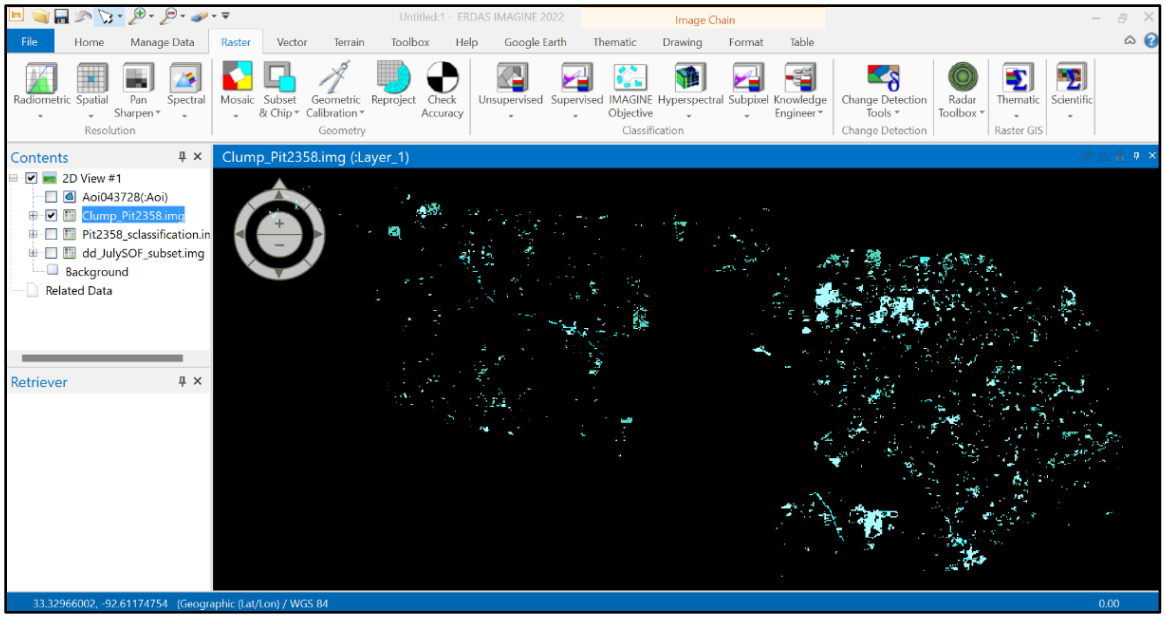

Figure 58. The pit-based supervised classification after the "Clump" tool was applied.

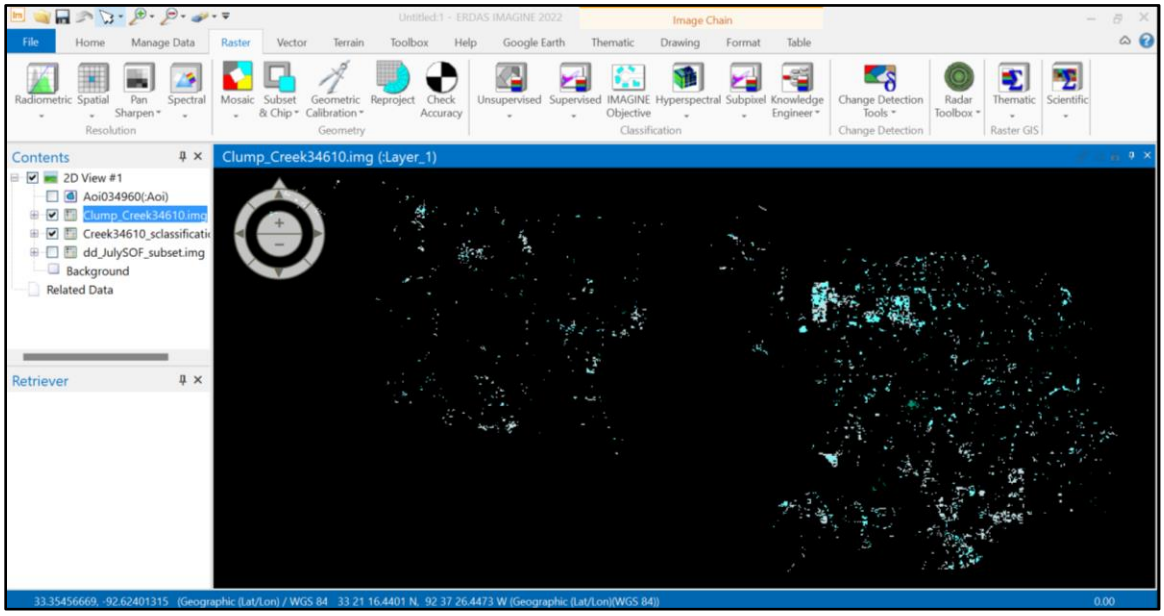

Figure 59. The creek-based supervised classifcation after the "Clump" tool was applied.

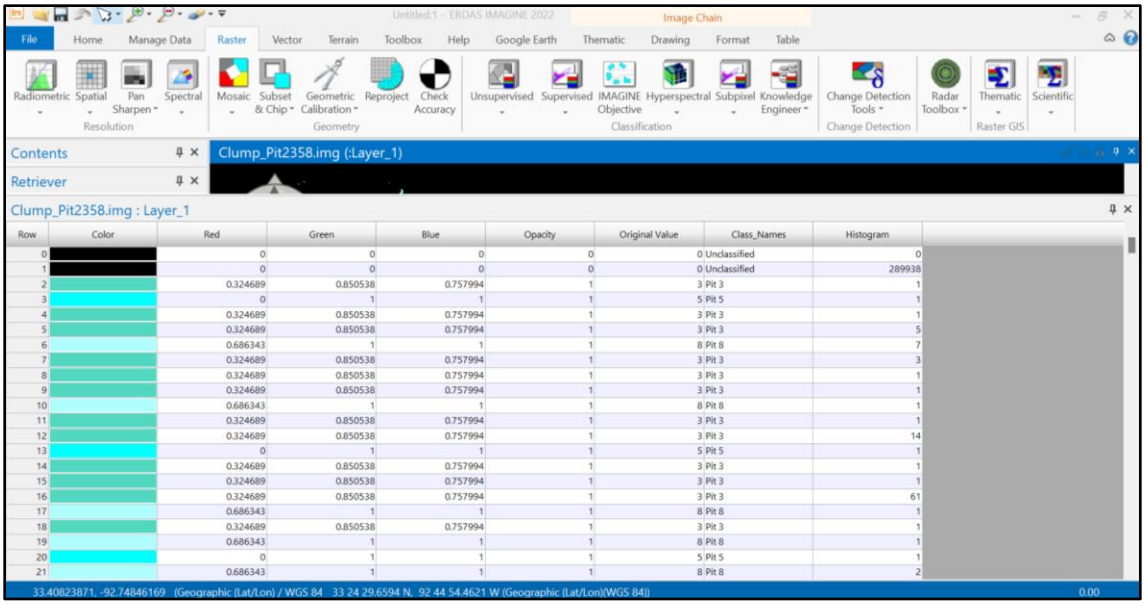

Figure 60. The attribute table for the pit-based clumped supervised classification was viewed to ensure each classified polygon was represented by the preselected pit training sites.

Following the use of the "Clump" tool in ERDAS IMAGINE® 2022 v. 16.7, the "Eliminate" tool was used to remove island polygons from the clumped classifications which represented areas less than about an acre, or 4 pixels (Figure 61). The effects of the tool "Eliminate" on the pit-based and creek-based classification are demonstrated in Figure 62 and Figure 63 respectively. To make the final classification of brine contaminated areas clearer after the "Eliminate" tool was run, all classified pixels were turned red and the opacity of classes which contained no pixels were turned to 0.

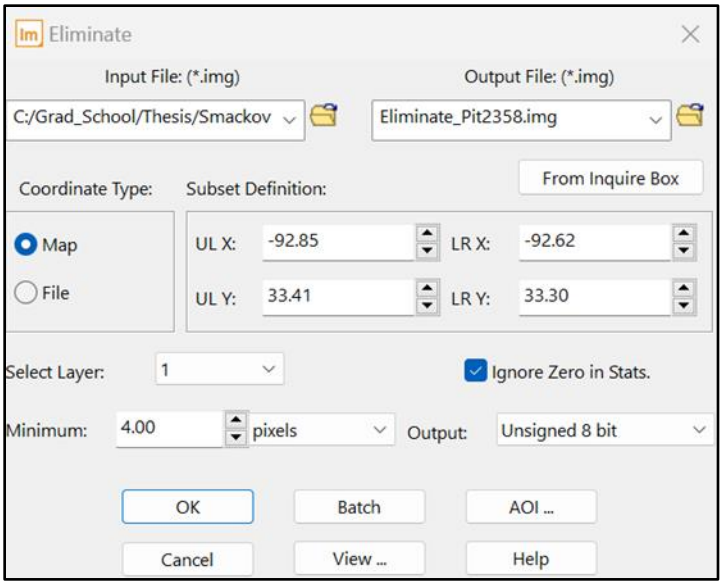

Figure 61. The Eliminate tool was used to remove island polygons from the clumped supervised classifications.

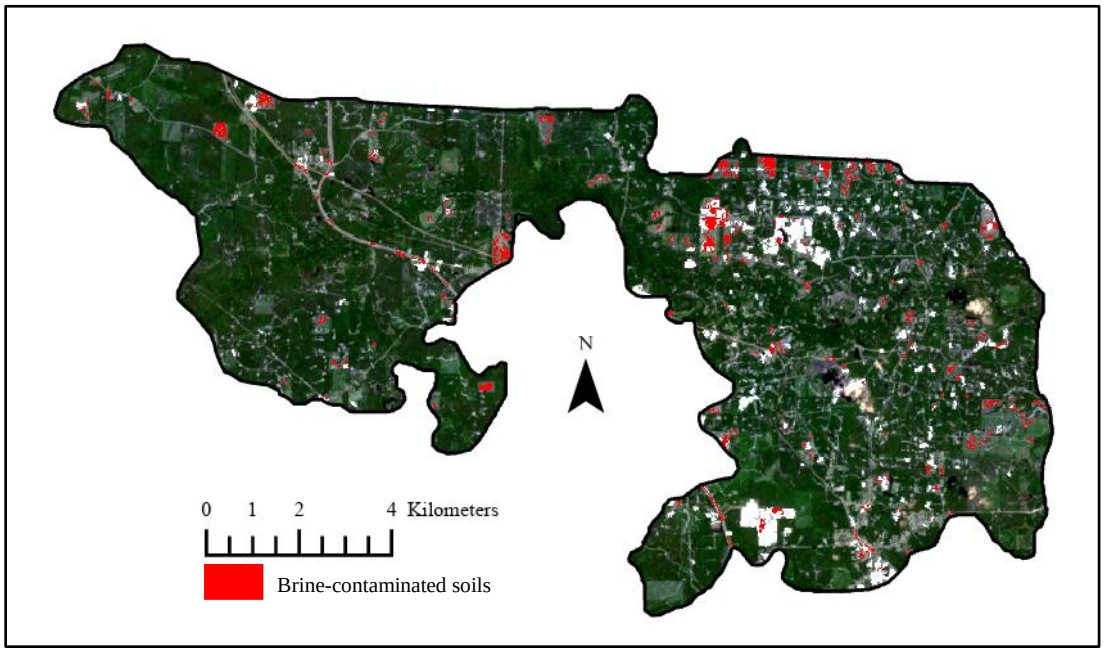

Figure 62. The effects of the Eliminate tool on the clumped pit-based supervised classification in red overlain across the subset Landsat 9 scene.

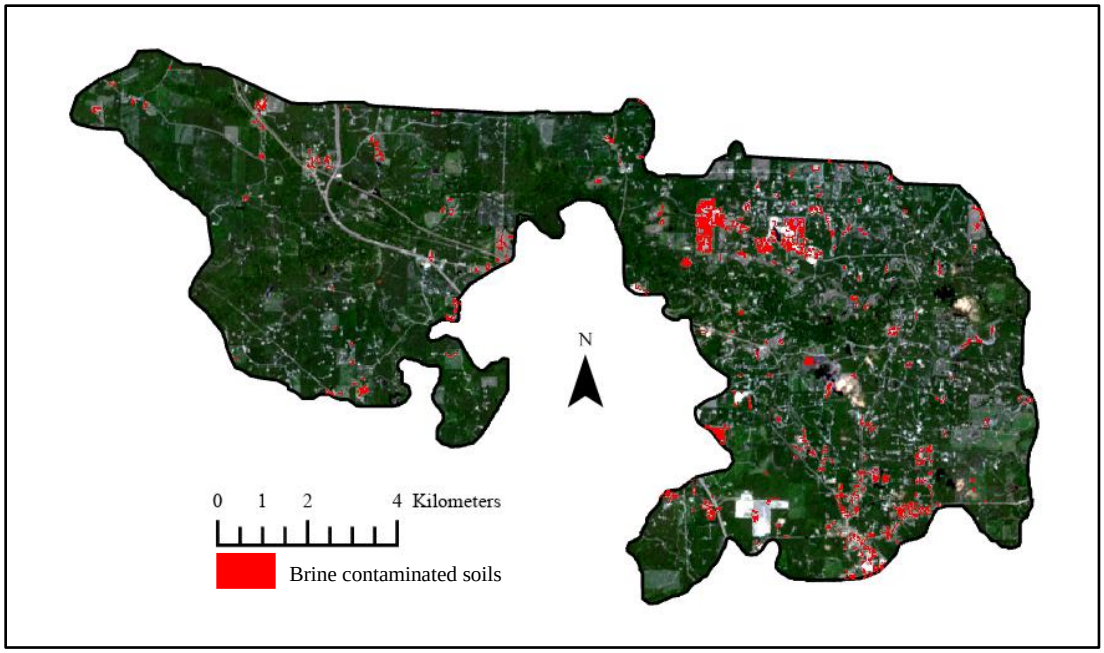

Figure 63. The effects of the Eliminate tool on the clumped creek-based supervised classification overlain in red across the subset Landsat 9 scene.

The statistics were calculated from the histogram values in the final "eliminated" supervised classifications and compared to calculated histogram values from the initial subset Landsat 9 scene to determine the percentage of pit-based and creek-based brine contamination currently present within the SOF. The initial statistics for the histogram of the subset Landsat 9 scene indicated that 136,725 pixels were present total (Figure 64). The statistics for the histogram value of the pit-based classification revealed a total of 5,374 classified pixels which indicated that 3.93% of the SOF was brine contaminated based on the pit training sites (Figure 65). The statistics for the histogram value of the creek-based classification revealed a total of 3,218 classified pixels which indicated that 2.35% of the SOF was brine contaminated based on the creek training sites (Figure 66).

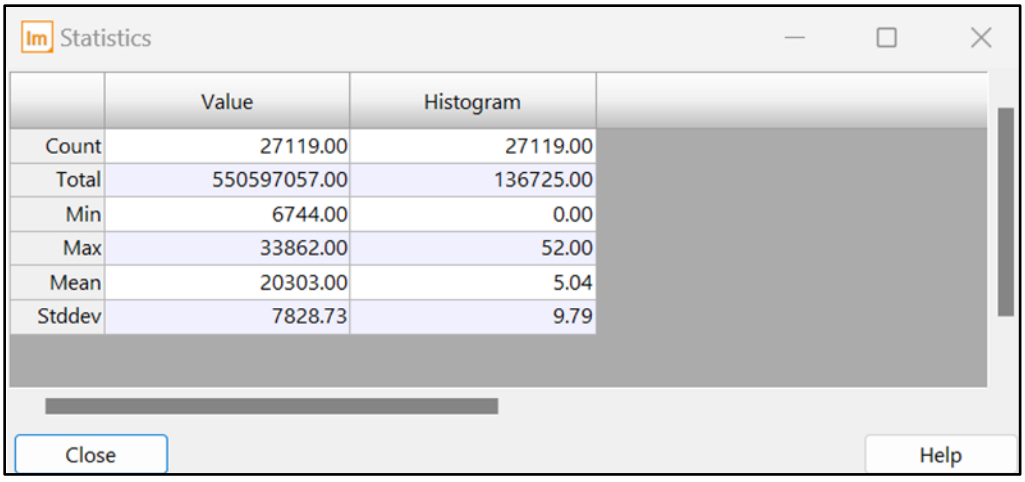

Figure 64. The initial statistics for the histogram of the subset Landsat 9 scene of the Smackover Oil Field indicated a total of 136,725 pixels in the digital image.

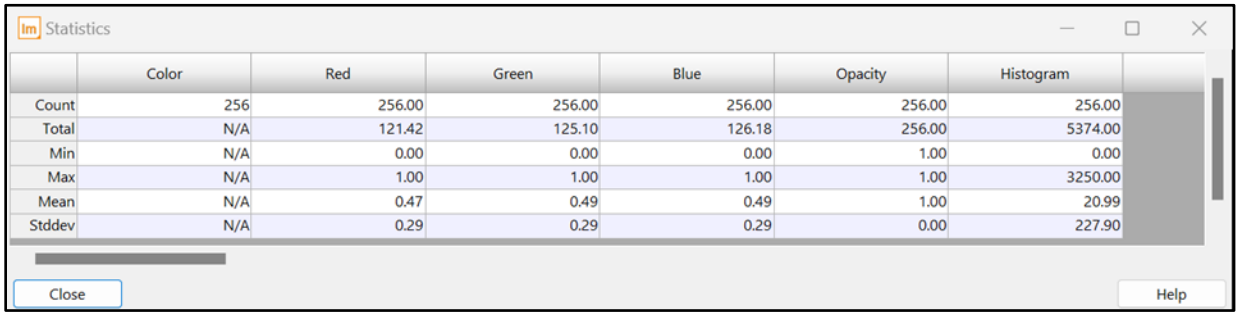

Figure 65. The statistics for the histogram value of the pit-based clumped and eliminated supervised classification revealed a total of 5,374 classified pixels.

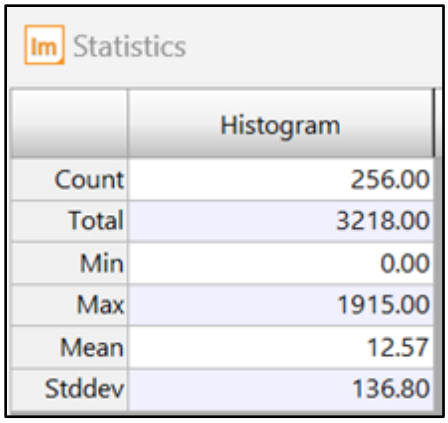

Figure 66. The statistics for the histogram value of the clumped and eliminated creek-based supervised classification revealed a total of 3,218 classified pixels.

Sample Site Selection

Access to the training sites used for the supervised classifications was denied by landowners so three publicly accessible sites were chosen based on results from the supervised classifications. The sampling sites, Louann Park, Fishing Area, and Norphlet Park are displayed in Figure 67 with yellow boundaries.

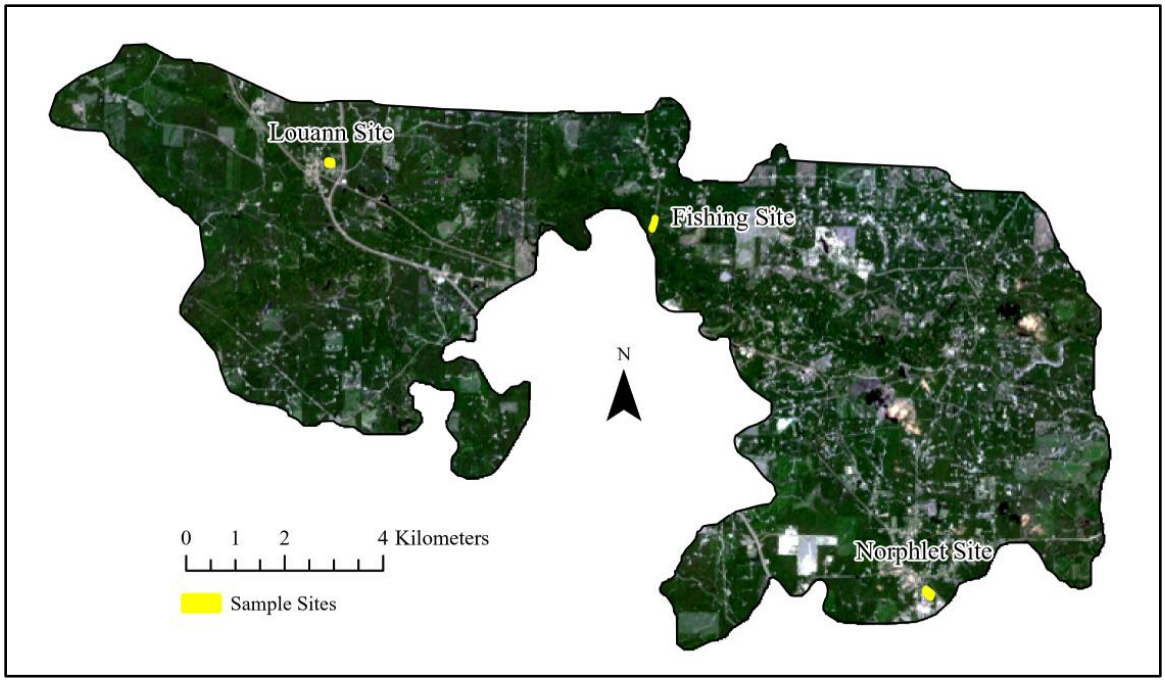

Figure 67. A map representing the three chosen sampling sites in yellow across the Smackover Oil Field.

Louann Park

The Louann Park site encompasses 1.92 acres and is in the northwestern portion of the SOF. There was a lack of vegetation other than grasses present across the site but there was vegetation bordering the sample site. The vegetation included both hardwoods and pine trees based on CONNECTexplorer™ EagleView Technologies imagery (Figure 68). This site was identified based on a public land boundary shapefile that was downloaded from the Arkansas GIS Office website. Although this part of the area was partially identified as potentially containing brine contaminated soils based on the pit-based classification, the creek-based classification visually indicated a larger extent of brine contamination compared to the pit-based classification (Figure 69). It was

determined that this sample site was brine contaminated based on the creek-based classification and would represent a brine contaminated site in the creek-based supervised classification map error matrix.

Figure 68. A CONNECTexplorer™ image of the Louann Park sampling site which displayed a lack of vegetation other than the bordering trees and was taken January 7, 2020 (EagleView Technologies, n.d.).

Figure 69. The boundary of the Louann Park site is delineated in black and brine contamination is indicated with red. The pit-based classification is displayed on the left, while the creek-based classification is displayed on the right.

Fishing Area

The Fishing Area site encompasses 1.15 acres and is located toward the center of the SOF. This site acted as a control sample as there was no brine contamination indicated by the previously created brine classifications. There were power lines, hardwood trees, and pine trees located on the sampling site based on CONNECTexplorer™ imagery (Figure 70). This site is located near a roadway known as Old Camden Road to the Smackover locales but is more widely known as Highway 67 or Ouachita Road 67. Part of this site is located adjacent to Smackover Creek and both hardwoods and pines were seen bordering the area. The Fishing Area site was identified by a Smackover City Hall employee who referred to it as a popular public fishing area.

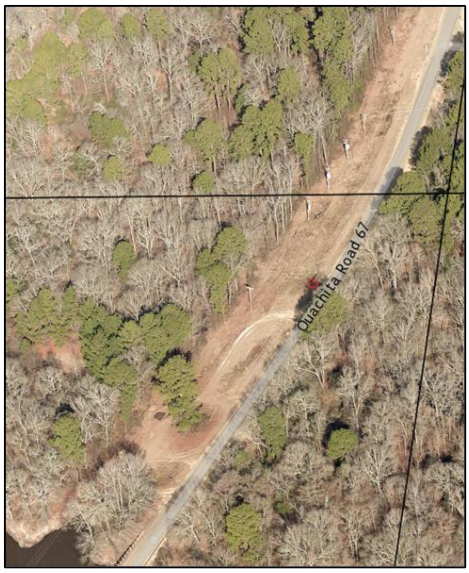

Figure 70. Fishing Area sampling site with the Smackover Creek located toward the southwestern part of the sampling site. Imagery was taken January 8, 2020 (EagleView Technologies, n.d.).

Norphlet Park

The Norphlet Park site encompasses 1.73 acres and is located toward the southeastern part of the SOF boundary. The surface across the sampling area had some grass vegetation present (Figure 71). Brine contamination for this sampling site was indicated by both creek-based and pit-based brine classifications, although for this site, the pit-based classification indicated a larger extent of brine contaminated soil across the site (Figure 72). The site was determined to be brine contaminated based on the pit-based classification rather than the creek classification. As a result, the sample site represented a brine contaminated site for the pit-based supervised classification map error matrix.

Figure 71. Norphlet Park sampling site with a lack of vegetation across the surface. A part of the Norphlet Middle School may be identified toward the southern part of the sampling site. The imagery was taken January 20, 2020 (EagleView Technologies, n.d).

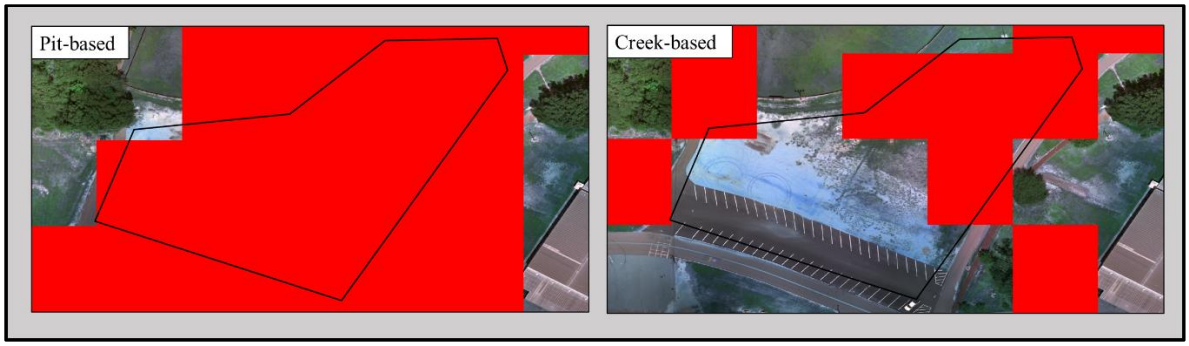

Figure 72. The boundary of the Norphlet Park site is delineated in black and brine contamination is indicated with red. The pit-based classification is located on the left, while the creek-based classification is on the right.

Soil Sampling

Soil Sample Collection

On July 17, 2023, five soil samples were collected at each sampling site to create a composite sample. To ensure that each sample was collected at a 15 cm depth, a measuring tape and a permanent marker were used to measure 15 cm from the tip of the shovel down the blade (Figure 73). As each of the five samples were taken for the sampling sites, their locations were recorded and uploaded into ESRI's Field Maps (Figure 74). The composite soil sample was mixed in a clean bucket and was then separated into three soil sample bags. A permanent marker was used to identify each soil sample map with the location, date, and time the sample was taken. A total of nine soil samples were collected once soil sampling was completed (Figure 75).

Figure 73. The 15 cm length was measured on the shovel to ensure soil samples were taken at a consistent depth.

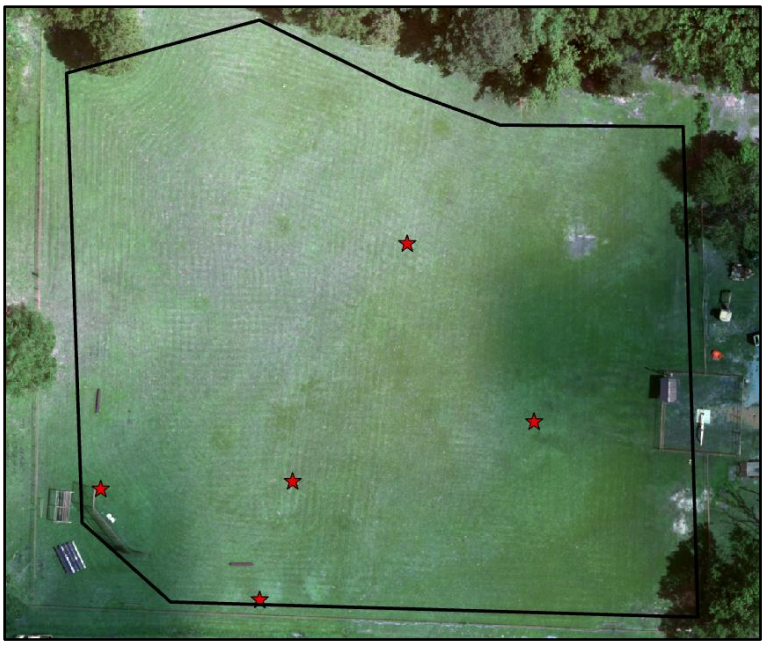

Figure 74. The five soil samples which were collected for the Louann Park sampling site and uploaded with ESRI's Field Maps displayed as red stars.

Figure 75. The composite samples from each of the three sampling sites labelled in soil bags August 2, 2023.

Soil Sample Analysis

The soil samples were taken to the SFASU Plant, Soil, and Water Analysis Laboratory. At the laboratory the samples were dried in a well-ventilated room so they could be ground (Figure 76). A soil grinder was used to remove debris and a 2 mm sieve was used to create a fine consistency in the soil samples (Figure 77). Approximately 250 mg of each sample was placed into a beaker and nanopure water was added to create a saturated paste (Figure 78). After the saturated pastes had sat overnight, the pastes were transferred into a Buchner funnel that was lined with filter paper (Figure 79). The soil samples were extracted using a vacuum to pull the leachate from the soil samples (Figure 80). The liquid extracts were tested with a Metrohm 914 pH/Conductometer for pH and EC (Figure 81). The results for the pH and EC of each sampling site are in Table 8. After

the extracts' pH and EC were measured, the extracts were analyzed with an Inductive Couple Plasma Analyzer (ICP) to determine the concentrations of elements in the solutions from each sample (Figure 82). The SAR results were calculated after this analysis and are displayed in Table 9.

Figure 76. The soil samples were dried on separate plates.

Figure 77. The grinder used to process the soil samples.

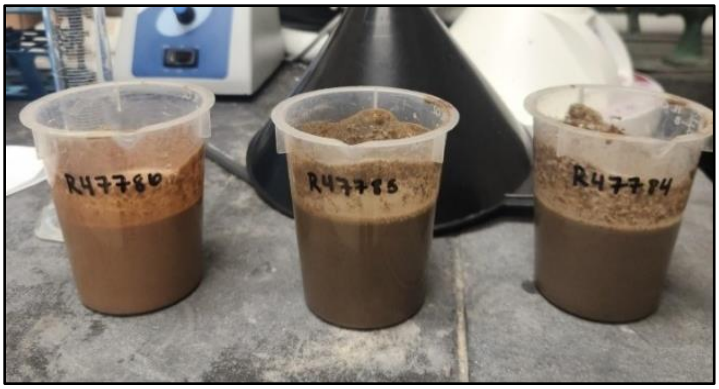

Figure 78. The saturated pastes were created by adding nano pure water to each sample.

Figure 79. The saturated soils placed in a Buchner funnel lined with filter paper.

Figure 80. The extraction of the soil samples with a vacuum setup.

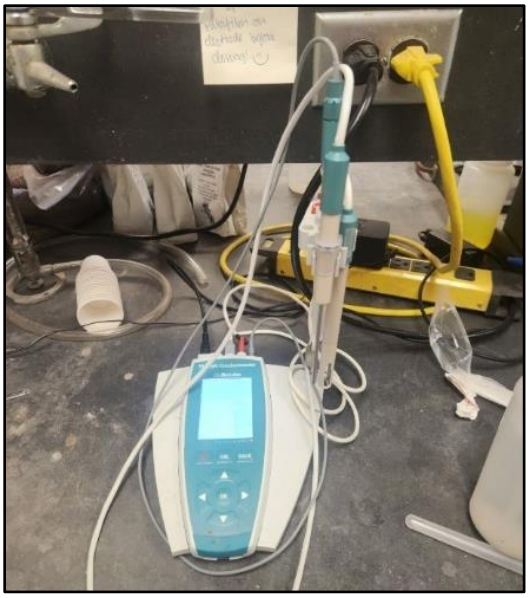

Figure 81. The Metrohm 914 pH/Conductometer was used to analyze pH and EC of the soil samples.

Table 8. The pH and Electrical Conductivity results for the sampling sites.

Lab #	Sample ID	pH	Electrical Conductivity (dS/m)
R47884	Louann Park	6.46	1.287
R47885	Fishing Area	5.43	1.385
R47886	Norphlet	5.87	8.130

Figure 82. The ICP machine used to identify the concentration of the constituents in the liquid extracts

Table 9. The concentrations of sodium, calcium, and magnesium and the SAR results for the sampling sites.

Lab #	Sample ID	Sodium Na (mg kg^{-1} soil)	Calcium Ca (mg kg^{-1} soil)	Magnesium Mg (mg kg^{-1} soil)	SAR
R47884	Louann Park	26.6	44.9	13.7	0.892
R47885	Fishing Area	10.4	6.08	1.32	0.997
R47886	Norphlet Park	14.5	1.45	1.26	2.130

Norphlet park was the only sampling site that contained an EC greater than 4 dS/m (Table 8). The pH for each of the sampling sites was below 8.5 (Table 8). The SAR results for each site were below 13 (Table 9). As none of the sites met all three EC, pH, and SAR characteristics of saline soils, the soils from each testing site were considered non-brine contaminated based on laboratory analysis (Allison et. al., 1954; Sonon et al., 2015).

P4M-RTK Image Acquisition

A total of six preprogrammed flight missions were completed with the P4M-RTK UAV on July 30, 2023. Each flight was flown at 93.54 m above ground level with an overlap of images at 80% for the front lap and 70% for the side lap (Figure 83). At each sampling site an “Inner” flight mission and “Outer” flight mission were flown to ensure that the acquired imagery fully encompassed the study areas. The imagery was collected on July 30, 2023 between 10:00 am and 2:00pm Central Time (CT) to mitigate the negative effects of shadows on aerial imagery.

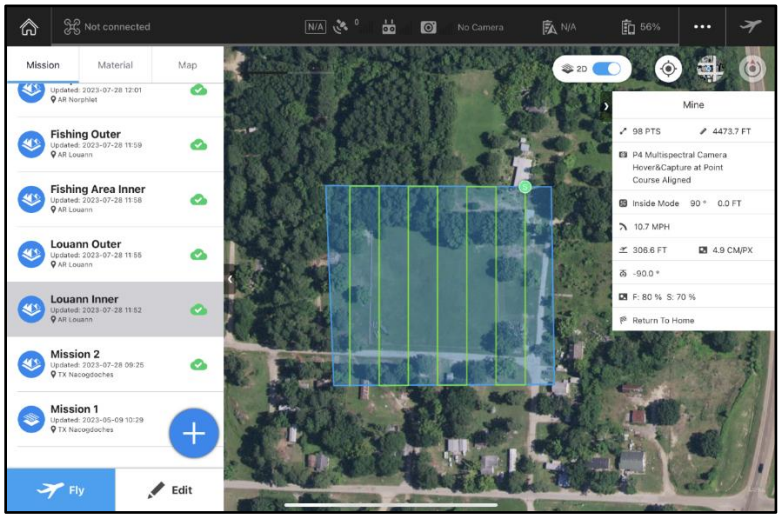

Figure 83. A preprogrammed drone flight mission for Louann Park created in the Ground Station Pro app (DJI, n.d.a).

Processing the UAV Multispectral Imagery

The multispectral imagery obtained from the P4M-RTK UAV was processed in PIX4Dmapper as “Ag Multispectral” data for each preprogrammed flight mission (Figure 84). In the processing options, the “DSM, Orthomosaic, and Index” option was chosen so

that an orthophoto mosaic of the data obtained from the flight would be created (Figure 85). The six cameras on the P4M-RTK separately collected images which resulted in separate orthophoto mosaics of the visible (standard blue, green, red) imagery, as well as the blue, green, red, red-edge, and near-infrared imagery for each preprogrammed flight mission (Figure 86).

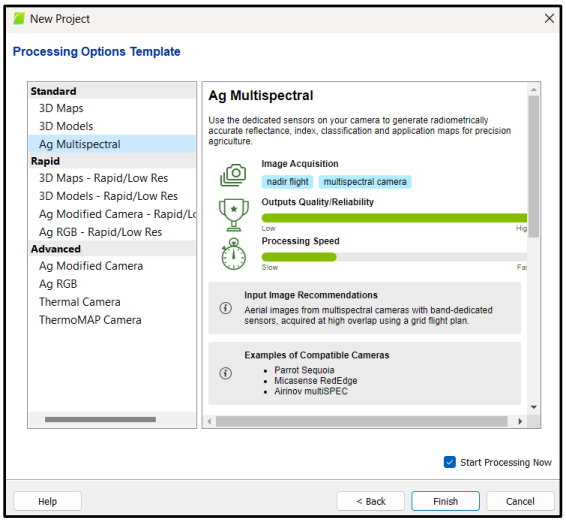

Figure 84. The Ag Multispectral procesing option chosen in PIX4Dmapper.

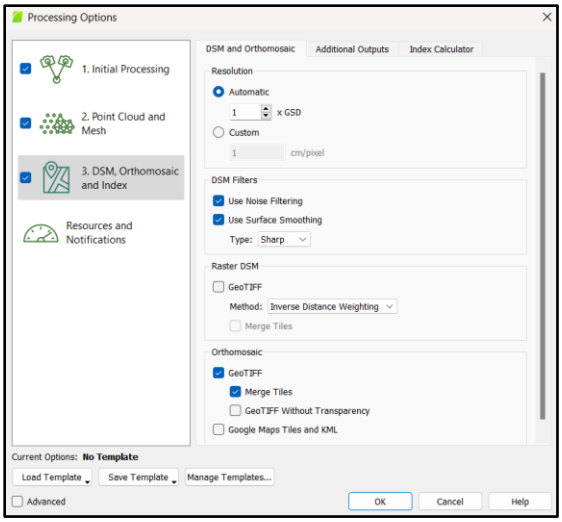

Figure 85. The DSM, Orthomosaic, and Index option was chosen so that an orthophoto mosaic of each band that was captured by the multispectral camera obtained from the flight would be created.

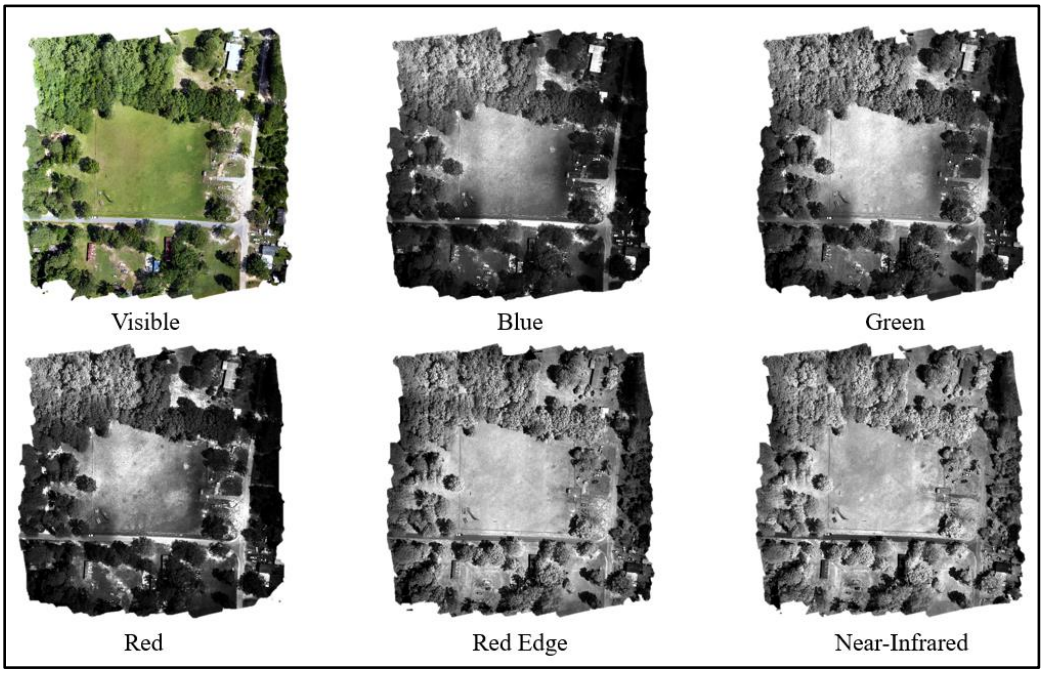

Figure 86. The orthophoto mosaic and easch individual band generated from drone imagery collected during the Louann Park Inner preprogrammed flight.

In ERDAS IMAGINE® 2022 v. 16.7, the blue, green, red, and near-infrared band were combined into a multispectral digital image with the "Layer Selection and Stacking" tool for each of the preprogrammed flight missions (Figure 87). The 4-band multispectral digital images from each preprogrammed flight mission are displayed in Figure 88. Finally, a Normalized Difference Vegetation Index for each of the multispectral digital images was conducted in ERDAS IMAGINE® 2022 v. 16.7 using the "Indices" tool (Figure 89). The NDVI for each of the preprogrammed flights is displayed in Figure 90. Areas in the image with bright white colors indicated healthy vegetation, while areas of dull white indicated unhealthy vegetation. Black areas across the NDVI images indicated that features such as roads or buildings were present. In the Louann Park NDVIs the vegetation at the northwestern portion of the sampling side was not as bright as the southeastern portion of the field. In the Fishing Areas NDVIs, there didn't visually appear to be major differences in the health and vitality of the vegetation across the site. In the Norphlet Park NDVIs the vegetation within the sampling areas seemed to be a much duller white/ greyish compared to vegetation outside of the sampling area. The NDVI was validated by comparing red and near-infrared pixel values from the multispectral digital images to the corresponding pixel value in the NDVI using Equation 3:

$$NDVI = \frac{(NIR - Red)}{(NIR + Red)} \quad (3)$$

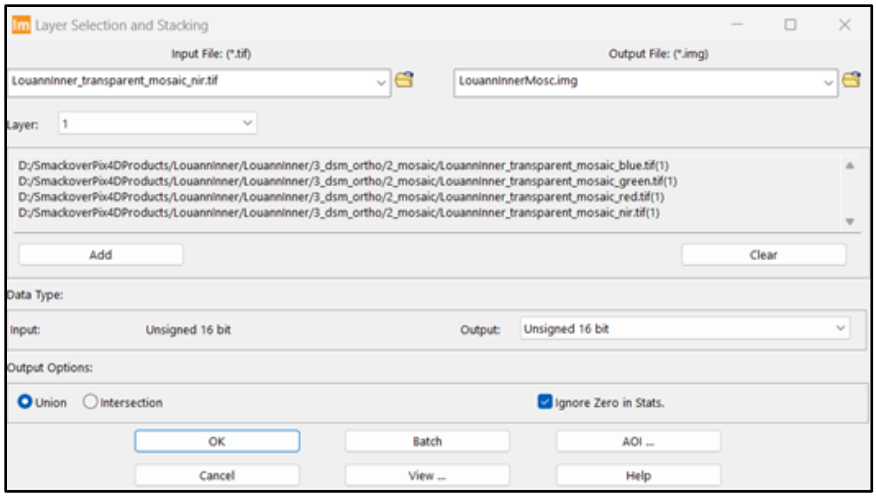

Figure 87. The blue, green, red, and near-infrared bands were combined into a multispectral digital image with the Layer Selection and Stacking tool in ERDAS IMAGINE® 2022 v. 16.7 for each dataset from the preprogrammed flights.

Figure 88. The six preprogrammed drone flights flown with the P4M-RTK each designated by a red letter: A – Louann Park Inner, B- Louann Park Outer, C- Fishing Area Inner, D- Fishing Area Outer, E- Norphlet Park Inner, F- Norphlet Park Inner.

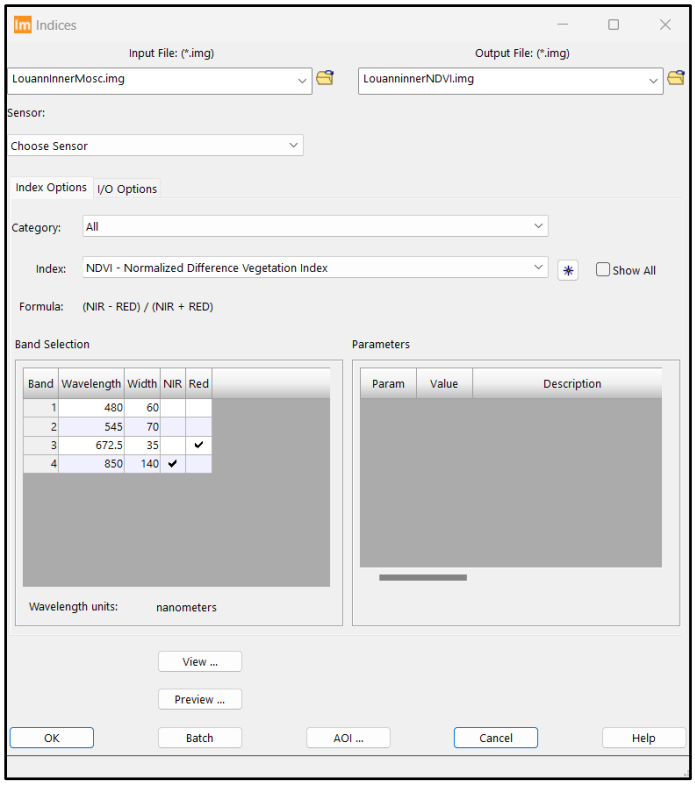

Figure 89. The Indices tool in ERDAS IMAGINE® 2022 v. 16.7 used to create the NDVI of each preprogrammed flight dataset.

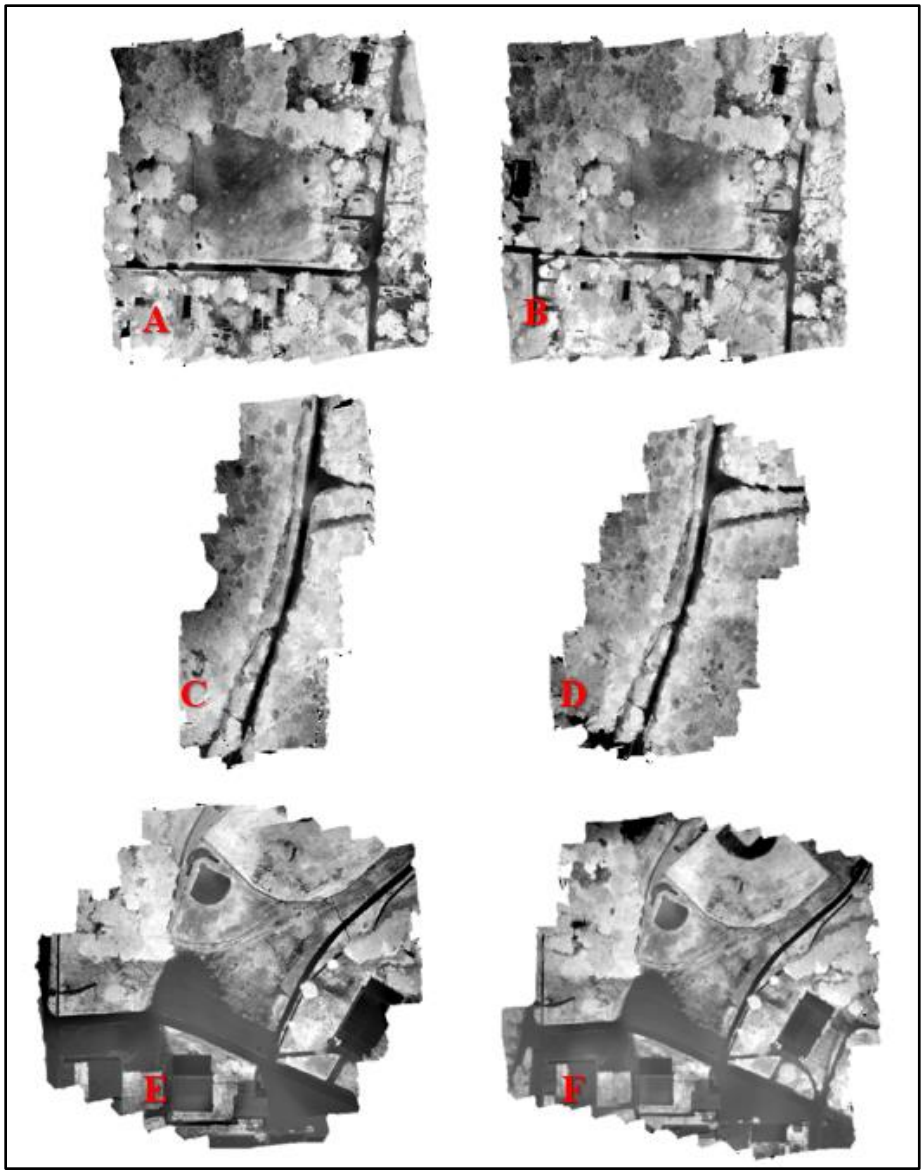

Figure 90. The created NDVI of the six preprogrammed drone flights each designated by a red letter: A – Louann Park Inner, B- Louann Park Outer, C- Fishing Area Inner, D- Fishing Area Outer, E- Norphlet Park Inner, F- Norphlet Park Inner.

P4M-RTK Image Unsupervised Classification

In ERDAS IMAGINE® 2022 v. 16.7 the 6 multispectral orthophoto mosaics from the P4M-RTK data were classified with an unsupervised classification method (Figure 91). The clustering options chosen for the unsupervised classification were: Initialize from Statistics, K Means, and a total class number of 36. The Maximum Iterations were limited to 10 iterations and a Convergence Threshold of 0.950. The result of each unsupervised classification for the six multispectral orthophoto mosaics are displayed in Figure 92. The same color palette was used for each unsupervised classification. Since the soils sample results revealed that there was no soil brine contamination across the sampling sites, precise identifications of the absence/presence of soil brine contamination based on the unsupervised classifications of the drone data could not be performed.

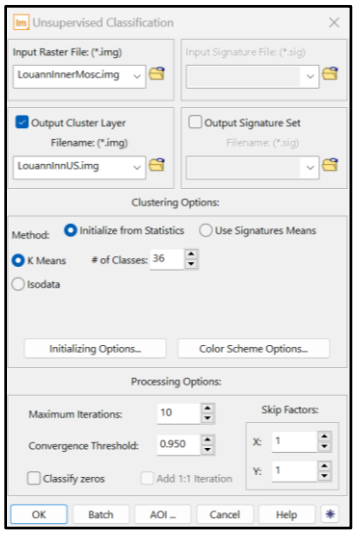

Figure 91. The clustering options chosen for the unsupervised classifications of the P4M-RTK multispectral data.

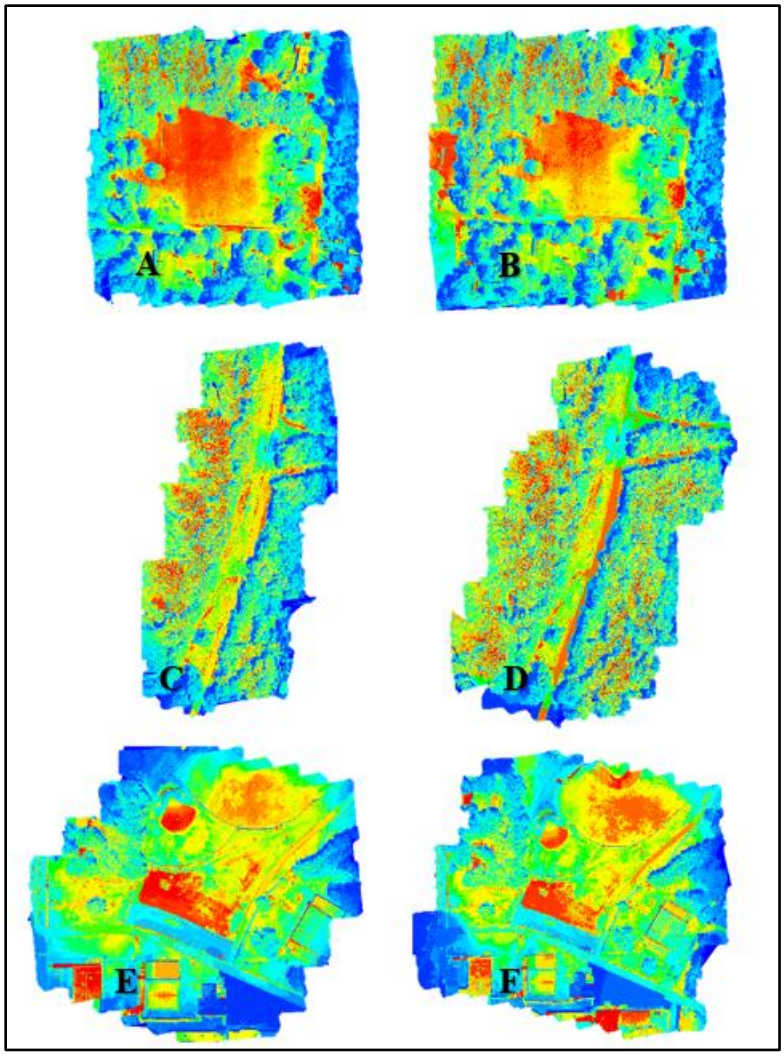

Figure 92. The created unsupervised classifications of the six preprogrammed drone flights each designated by a black letter: A – Louann Park Inner, B- Louann Park Outer, C- Fishing Area Inner, D- Fishing Area Outer, E- Norphlet Park Inner, F- Norphlet Park Inner

Accuracy Assessment

Based on the SFASU Plant, Soil, and Water Analysis Laboratory results and the supervised classification results two error matrices and two $\widehat{K}$-statistics were calculated (Table 10 and Table 11) The columns represented the results of the number of brine

contaminated vs. non-brine contaminated sites from the laboratory analysis viewpoint. The row represented the sites that were brine contaminated vs, non-brine contaminated from the user's created classification map. In Table 10, the pit-based supervised classification was assessed and in Table 11, the creek-based supervised classification was assessed.

Table 10. The error matrix, and kappa statistic for the pit-based supervised classification of the Smackover Oil Field.

		Reference Data			Accuracy	
	Class	**Brine**	**Non-Brine**	Row Total	***User's***	
Classification Map	**Brine**	0	1	1	**0%**	
	Non-Brine	0	2	2	**100%**	
	Column Total	0	3	3	**Overall**	**67%**
Accuracy	***Producer's***	**N/A**	**67%**		$\widehat{K}$**-statistic**	**0**

Table 11. The error matrix, and kappa statistic for the creek-based classification of the Smackover Oil Field.

		Reference Data			Accuracy	
	Class	**Brine**	**Non-Brine**	Row Total	***User's***	
Classification Map	**Brine**	0	1	1	**0%**	
	Non-Brine	0	2	2	**100%**	
	Column Total	0	3	3	**Overall**	**67%**
Accuracy	***Producer's***	**N/A**	**67%**		$\widehat{K}$**-statistic**	**0**

The calculated overall accuracy for both supervised classification maps identifying brine contamination was 67%. The user's accuracy in both maps was 0% for brine contaminated sites and 100% for non-brine contaminated sites. The producer's accuracy for both brine contaminated sites was not applicable for brine contaminated sites and 67% for non-brine contaminated sites.

The $\widehat{K}$-statistic for both classifications were 0 which indicated that there was a poor chance that the supervised classifications would correctly classify brine versus non-brine contaminated soils better than what could be expected by random chance assignment (Table 7) (Rwanga & Ndambuki, 2017).

DISCUSSION AND CONCLUSIONS

The overall accuracy from pit-based and creek-based classification error matrices indicates that there was a 67% chance brine and non-brine contaminated areas would be correctly classified in the supervised classification map. The User's accuracy for the brine contaminated results were 0% for the error matrices of both classified maps and the Producer's accuracy was not applicable for both error matrices, which indicated that brine contamination on the classified maps could not be accurately classified. However, the User's accuracy for non-brine contaminated areas in the error matrices was 100% and the Producer's accuracy for non-brine was 67%, which indicated that although 67% of the non-brine areas were classified as non-brine based on the maps, all the accessible sampling sites were non-brine contaminated based on the SAR laboratory analysis. Based on the calculated $\widehat{K}$-statistic for both error matrices, there was a poor chance that the supervised classification maps would correctly classify brine versus non-brine contaminated soils better than what could be expected by random chance assignment.

The statistics from the error matrices and $\widehat{K}$-statistics may not be truly representative of the completed brine identification study for several reasons. The Overall, Users, and Producer's accuracies were based on laboratory soil analysis from three publicly accessible sampling sites. Due to prohibited access, soil samples were

unable to be taken from the training sites used for the supervised classification maps. The samples were taken from publicly accessible areas. The Louann and Norphlet site were both located in public recreation areas. These sites were well maintained and regularly mowed. As these sites have been previously modified to create recreation areas it is possible fill dirt may have been brought in during their construction. Soil samples from the actual undisturbed training sites used for the classifications may have provided a better representation of the accuracy of the classified maps if they were able to be sampled. As there was no validation for the chosen training sites, the results may give the reader a misinterpretation of the results based on the error matrices and $\widehat{K}$-statistics.

Another reason the results from the error matrices and $\widehat{K}$-statistics may not be truly representative of the study is that the spatial resolution of Landsat data is 30m per pixel. The chosen training sites ranged from approximately 1 to 4 acres, representative of 4.54 to 18.18 pixels. The training sites represented areas of land across the SOF that on average were too small to accurately be classified with the mid-spatial resolution digital imagery provided by Landsat 9 data. With the mid-spatial resolution of 30m per pixel, there are several features within each pixel which represent different amounts of emitted, absorbed, or reflected electromagnetic energy, or spectral responses. This may have resulted in an error known as mixed pixels, due to the lack of uniformity in the spectral signatures from individual pixels in the Landsat 9 data.

The temporal difference between the utilized 1996 reference data and the more current 2022 Landsat 9 data may have also introduced error into the supervised

classification maps. Vegetation growth/recovery in areas which were previously delineated as brine-contaminated in the reference data may have disrupted discernable brine spectral signatures in the more current Landsat 9 data which was used for the supervised classification maps. These areas may still be brine damaged, but the soils may no longer be severely brine-contaminated enough that vegetation recovery is not possible. This study used remote sensing techniques to assess discernable brine contamination on the surface of the earth and this would not have picked up brine-contamination located at lower depths in the soils of sampling sites.

The training sites chosen were scene dependent and represented multiple small brine-contaminated areas scattered throughout the study area. In the SOF brine-contamination did not occur in areas as large as the brine-contaminated areas observed in west Texas for the study, *Detecting Oilfield Brine Contaminated Sites Using Satellite Remote* Sensing (Bowes, 2007). The training site AOI's for brine contamination in the SOF encompassed less acreage than chosen training sites for the 2007 comparison study. In the SOF study the average size of the 352 brine scars were representative of 0.48 acres, or 2.19 pixels, across the reference data (Figure 15). In Bowe's study it was determined that a minimum mapping size of 2 acres, or 9.09 pixels, was necessary to correctly classify brine-contamination with 30m spatial resolution Landsat data. Based on this, the minimum mapping size of the training sites for the SOF study were too small to effectively delineate brine and non-brine areas across the SOF in a supervised

classification map. The methodology used in Bowe's study in west Texas to identify brine contamination is not robust for oil production areas similar to the SOF.

Additionally, there is a difference in the amount of annual precipitation west Texas encounters compared to the study area, the SOF in south central Arkansas. Annually west Texas receives less than ten inches of precipitation while south central Arkansas receives an estimated 52 inches of precipitation annually (NOAA's National Weather Service, n.d.; Texas State University, n.d. The larger amount of precipitation in south central Arkansas may aid in the transport of brine contamination out of affected areas whereas the lower amounts of precipitation in west Texas may contribute to the accumulation of brine in affected areas. A higher accumulation of brine contamination in the surface soils of west Texas would make brine more identifiable than in areas which experience larger amounts of annual precipitation such as the SOF.

There are also differences in the topography between the SOF and the west Texas area analyzed in Bowes' 2007 study. The surface of the SOF is dynamic and can be separated into flood plains, hilly-uplands, and minor stream terraces, with the whole field being located in the Smackover Creek watershed (Barrett, 2002). In Bowe's study, the area of interest was located in the western portion of the Edwards Plateau ecoregion. This portion of the elevated plateau is much flatter compared to the topography of the SOF (TPWD, n.d.). The digital imagery used to classify soil brine contamination in west Texas may not have been as affected by shaded areas created from hills or large slopes.

However, the methods used to create the supervised classification maps for this study followed traditional remote sensing methods. Based on the visual analysis of training sites in the feature space layers in ERDAS IMAGINE® 2022 v. 16.7, there is confidence that the percentage of brine contamination within the SOF is correct. Training sites that visually represented brine contamination were added individually to the feature space layers to assess which training sites would best represent unique areas of brine contaminated land across the imagery and not represent similar features such as roads. Training sites that were determined to not be representative of brine contamination in the feature space layer were deleted.

In the future, to effectively delineate brine-contamination across a study area similar to the SOF, it is recommended that digital imagery with a higher spatial resolution, such as 0.65m QuickBird-2 or 1.64m GeoEye satellite imagery be used (European Space Agency, 2022a and European Space Agency, 2022b). It is also recommended that pre-authorization of potential training sites be granted to create more representative accuracy assessment results for classification maps.

LITERATURE CITED

Allison, L. E., Brown, J. W., Hayward, H. E., Richards, L. A., Bernstein, L., Fireman, M., Pearson, G. A., Wilcox, L. V., Bower, C. A., Hatcher, J. T., & Reeve, R. C. (1954). *Diagnosis and Improvement of Saline and Alkali Soils*. (L. A., Richards, Ed.) (60). U. S. Department of Agriculture. https://www.ars.usda.gov/ARSUserFiles/20360500/hb60_pdf/hb60complete.pdf

Arkansas GIS Office. (n.d.). https://gis.arkansas.gov/

Austin, R. (2011). *Unmanned Aircraft Systems: UAVS Design, Development and Deployment*. John Wiley and Sons. https://www.wiley.com/en-us/Unmanned+Aircraft+Systems:+UAVS+Design,+Development+and+Deployment-p-9780470058190

Barrett, M. (2001). The Oil Waste History of Smackover Field, Arkansas. *Environmental Geosciences*, *8*, 231-241. https://doi.org/10.1046/j.1526-0984.2001.84001.x

Barrett, M. (2002). Saltwater Waste and Landscape Change, Smackover Field, Arkansas. *Environmental Geosciences*, *9*, 17-28. https://doi.org/10.1046/j.1526-0984.2002.91003.x

Bowes, C. J., (2007). *Detecting Oilfield Brine Contaminated Sites Using Satellite Remote Sensing*. [Unpublished master's thesis]. Stephen F. Austin State University.

Chastain, R., Housman, I., Goldstein, J., Finco, M., & Tenneson, K. (2019). Empirical Cross Sensor Comparison of Sentinel-2A and 2B MSI, Landsat-8 OLI, and Landsat-7 ETM+ Top of Atmosphere Spectral Characteristics over the Conterminous United States. *Remote Sensing of Environment, 221,* 274-285. https://doi.org/10.1016/j.rse.2018.11.012

Chen, X., Vierling, L., & Deering, D. (2005). A Simple and Effective Radiometric Correction Method to Improve Landscape Change Detection across Sensors and across Time. *Remote Sensing of Environment, 98*(1), 63-79. https://doi.org/10.1016/j.rse.2005.05.021

Congalton, R. G. (1991). A Review of Assessing the Accuracy of Classifications of Remotely Sensed Data. *Remote sensing of environment, 37*(1), 35-46. https://doi.org/10.1016/0034-4257(91)90048-B

Congalton, R. G. (2010). Remote Sensing: an overview. *GIScience and Remote Sensing, 47*(4), 443-459. https://doi.org/10.2747/1548-1603.47.4.443

Culver, A. D., & Barrett, M. L. (2001). Landscape Modification of the Smackover Field, Arkansas. *Gulf Coast Association of Geological Societies Transactions, 51*, 45-53. https://archives.datapages.com/data/gcags/data/051/051001/0045.htm

Dave, C. P., Joshi, R., & Srivastava, S. S. (2015). A Survey on Geometric Correction of Satellite Imagery. *International Journal of Computer Applications*, *116*(12). 10.5120/20389-2655

DJI. (n.d.$_a$). DJI GS Pro. https://www.dji.com/ground-station-pro

DJI. (n.d.$_b$). *P4 Multispectral*. DJI. https://www.dji.com/p4-multispectral

EagleView Technologies. (n.d.). CONNECTexplorer™. https://explorer.eagleview.com/login.php

Educational Resources. (n.d.). *Global Visualization Viewer (GloVis)*. U. S. Geological Survey. https://www.usgs.gov/educational-resources/global-visualization-viewer-glovis

Environmental Systems Research Institute, Inc., (2023). ArcGIS Pro v. 3.1.0 software. https://www.esri.com/en-us/arcgis/products/arcgis-pro/overview

Environmental Systems Research Institute, Inc., (n.d.). ArcGIS Online. https://www.arcgis.com/index.html

ERDAS. (2005). *ERDAS Field Guide*. (7 ed.). Leica Geosystems GIS and Mapping LLC. http://geography.middlebury.edu/data/gg1002/Readings/Extras/ERDAS_FieldGuide.pdf

ERDAS.(2022). ERDAS IMAGINE® 2022 v. 16.7. Hexagon Geospatial, Peachtree Corners Circle Norcross. https://hexagon.com/products/erdas-imagine

EROS CalVal Center of Excellence (ECCOE). (n.d.). *Landsat Calibration and Validation*. U. S. Geological Survey. https://www.usgs.gov/calval/landsat-calibration-and-validation

European Space Agency. (2022a). GEOEye-1. *Earth Online*. https://earth.esa.int/eogateway/missions/geoeye-1#instruments-section

European Space Agency. (2022b). QuickBird-2 Overview. *Earth Online*. https://earth.esa.int/eogateway/missions/quickbird-2/description

Gharaibeh, M. A., Albalasmeh, A. A., Pratt, C., & El Hanandeh, A. (2021). Estimation of exchangeable sodium percentage from sodium adsorption ratio of salt-affected soils using traditional and dilution extracts, saturation percentage, electrical conductivity, and generalized regression neural networks. *Catena, 205*, https://doi.org/10.1016/j.catena.2021.105466

Hacker, P., & Pickell, P. (n.d.). *Fundamentals of Remote Sensing*. Bookdown. https://www.opengeomatics.ca/fundamentals-of-remote-sensing.html

Haque, M. O., Rengarajan, R., Lubke, M., Hasan, M. N., Shrestha, A., Tuli, F. T., Shaw, J. L., Denevan, A., Franks, S., Micijevic, E., Choate, M. J., Anderson, C., Thome, K., Kaita, E., Barsi, J., Levy, R., & Miller, J. (2023). ECCOE Landsat Quarterly Calibration and Validation report—Quarter 3, 2022. *US Geological Survey*, (2023-1013), 1-37. https://doi.org/10.3133/ofr20231013

Hensel, B. R., McKenna, D. P., & Adams, J. R. (1989). Environmental Impacts of Oil Field Brines in Southeastern Clay County, Illinois. *Champaign, III.: Illinois State Geological Survey*, (1989-03), 1-303. https://hdl.handle.net/2142/44899

Konkel, L. (2016). Salting the Earth: The Environmental Impact of Oil and Gas Wastewater Spills. *Environmental Health Perspectives*, *124*(12), 231-235. https://doi.org/10.1289/ehp.124-A230

Landsat Missions. (n.d.$_a$). *Landsat 7*. U. S. Geological Survey. https://www.usgs.gov/landsat-missions/landsat-7

Landsat Missions. (n.d.$_b$). *Landsat 9 Solid State Recorder Bad Block Issue*. U. S. Geological Survey. https://www.usgs.gov/landsat-missions/landsat-9-solid-state-recorder-bad-block-issue

Landsat Missions. (n.d.$_c$). *Landsat 9*. U. S. Geological Survey. https://www.usgs.gov/landsat-missions/landsat-9

Lauer, N. E., Harkness, J. S., Vengosh, A. (2016). Brine Spills Associated with Unconventional Oil Development in North Dakota. *Environmental Science and Technology*, *50*(10), 5,289-5,397. https://doi.org/10.1021/acs.est.5b06349

Li, M., Zang, S., Zhang, B., Li, S., & Wu, C. (2017). A Review of Remote Sensing Image Classification Techniques: the Role of Spatio-contextual Information. *Taylor and Francis*, *47*(1), 389-411. https://doi.org/10.5721/EuJRS20144723

Lu, H., Fan, T., Ghimire, P., & Deng, L. (2020). Experimental Evaluation and Consistency Comparison of UAV Multispectral Minisensors. *Remote Sensing*, *12*(16), 1-19. https://doi.org/10.3390/rs12162542

Lulla, K., Nellis, M. D., Rundquist, B., Srivastava, P. K., & Szabo, S. (2021) Mission to Earth: LANDSAT 9 will continue to view the world, *Geocarto International*, *36*(20), 2,261-2,263. https://doi.org/10.1080/10106049.2021.1991634

Masek, J. G., Wulder, M. A., Markham, B., McCorkel, J., Crawford, C. J., Storey, J., & Jenstrom, D. T. (2020). Landsat 9: Empowering Open Science and Applications through Continuity. *Remote Sensing of Environment, 248*, 1-13. https://doi.org/10.1016/j.rse.2020.111968

McEwen, J. A., (1970). The Geography of the Smackover Oil and Gas Field. *ProQuest Dissertations and Theses Global*. https://www.proquest.com/dissertations-theses/geography-smackover-oil-gas-field/docview/302384996/se-2

Meehan, M. A., Sedivec, K. K., DeSutter, T., Augustin, C., & Daigh, A. (2017). Environmental Impacts of Brine (Produced Water). *NDSU Extension Service, North Dakota State University*, 1-4. https://www.researchgate.net/publication/319291247_Environmental_impacts_of_brine_produced_water

National Council of Educational Research and Training (NCERT). (2006). Introduction to Remote Sensing. In S. Uppal & R. N. Bhardwaj (Eds.), *Practical Work in*

Geography Part I Textbook for Class XI, (pp. 84-106). NCERT. https://ncert.nic.in/ncerts/l/kegy307.pdf

National Space Development Agency of Japan (NASDA). (1999). *Remote Sensing Notes*. (Japan Association of Remote Sensing, Ed.). Asian Institute of Technology. http://sar.kangwon.ac.kr/etc/rs_note/rsnote/contents.htm

NOAA's National Weather Service. (n.d.). *NWS Little Rock, AR - Arkansas Yearly Climate Summary (2022)/PG1*. https://www.weather.gov/lzk/2022.htm

Norvell, P. E. (2015). The History of Oil and Gas Conservation Legislation in Arkansas. *Arkansas Law Review*, *68*(349), 349-380. https://heinonline.org/HOL/LandingPage?handle=hein.journals/arklr68&div=20&id=&page=

Nowatzki, J., Andres, R., & Kyllo, K. (2004). Agricultural Remote Sensing Basics. *NDSU Extension Service, North Dakota State University*, 1-4. https://library.ndsu.edu/ir/bitstream/handle/10365/5408/ae1262.pdf?sequence=1

Office of the State Geologist. (n.d.). *History of Discovery and Exploration.* https://www.geology.arkansas.gov/energy/crude-oil-in-arkansas.html#:~:text=The%20Smackover%20field%2C%20discovered%20in,173%2C099%2C821%20barrels%20as%20of%202016.&text=In%20south%20Arkansas%2C%20several%20wells,to%20depths%20exceeding%2016%2C000%20feet.

Omali, T. U. (2018). Impacts of Sensor Spatial Resolution on Remote Sensing Image Classification. *Global Scientific Journals*, *6*(1), 63-68. https://www.researchgate.net/profile/Thomas-Omali/publication/355208175_impacts_of_sensor_spatial_resolution_on_remote_sensing_image_classification/links/61684ab93851f9599404494c/impacts-of-sensor-spatial-resolution-on-remote-sensing-image-classification.pdf

Otton, J. K. (2006). Environmental Aspects of Produced-water Salt Releases in Onshore and Coastal Petroleum-producing Areas of the Conterminous US-A Bibliography. *U.S. Department of the Interior, U.S. Geological Survey*, (2006-1154), 5-10. http://pubs.usgs.gov/of/2006/1154/

Panigrahy, S. & Ray, S. (2005). Remote Sensing. In Chadha, K. L. & Swaminathan, M. S. (Eds.), *Agriculture and Environment* (pp. 1-15). Malhotra Publishing House. https://www.researchgate.net/publication/270565420_REMOTE_SENSING

Perumal, K., & Bhaskaran, R. (2010). Supervised Classification Performance of Multispectral Images. *Cornell University*, 124-129. https://doi.org/10.48550/arXiv.1002.4046

Runkle, J., Kunkel, K. E., Champion, S. M., Stewart, B. C., Easterling, D. R., Nielsen-Gammon, J. (2022). Arkansas State Climate Summary 2022. (Report No. 150-AR). NOAA/NESDIS. https://statesummaries.ncics.org/chapter/ar/

Rwanga, S. S., & Ndambuki, J. M. (2017). Accuracy Assessment of Land Use/Land Cover Classification Using Remote Sensing and GIS. *International Journal of Geosciences*, *8*(04), 611-622. 10.4236/ijg.2017.84033

Sathya, P., & Deepa, V. B. (2017). Analysis of supervised image classification method for satellite images. *International Journal of Computer Science Research (IJCSR)*, *5*(2), 16-19. https://www.academia.edu/download/53575833/IJCSR-050204.pdf

Sefercik, U. G., Kavzoglu, T., Colkesen, I., Adali, S., Dinc, S., Nazar, M., & Ozturk, M. Y. (2021). Land Cover Classification Performance of Multispectral RTK UAVs. *The International Archives of Photogrammetry, Remote Sensing and Spatial Information Sciences*, *XLVI-4/W5-2021*, 489-492. https://doi.org/10.5194/isprs-archives-XLVI-4-W5-2021-489-2021

Sonon, L. S., Saha, U., & Kissel, D. E. (2015). Soil salinity. Testing, Data Interpretation and Recommendations. *University of Georgia Cooperative Extension Circular*, 1019, 1-7. https://secure.caes.uga.edu/extension/publications/files/pdf/C%201019_4.PDF

Sparks, D. L., Singh, R., & Siebecker, M. G. (2024). The chemistry of saline and sodic soils. In *Elsevier eBooks* (pp. 411–438). https://doi.org/10.1016/b978-0-443-14034-1.00010-1

Spooner, W. C. (1935). Bulletin 2: Oil and Gas Geology of the Gulf Coastal Plain in Arkansas. *Arkansas Geological Survey*. *2*, 154-176. https://www.geology.arkansas.gov/publication/bulletins/b2-bulletin.html

Sukchan, S., & Yamamoto, Y. (2002). *Classification of Salt Affected Areas Using Remote Sensing and GIS*. (Report No. 30). Japan International Research Center for Agricultural Sciences. https://scholar.google.com/scholar_lookup?title=Classification+of+salt+affected+areas+using+remote+sensing+and+GIS&author=Sukchan,+S.&author=Yamamoto,+Y.&publication_year=2002&journal=JIRCAS+Working+Report&volume=30&pages=15%E2%80%9319

Tempfli, K., Huurneman, G. C., Bakker, W. H., Janssen, L. L. F., Feringa, W. F., Gieske, A. S. M., Grabmaier, K. A., Hecker, C. A., Horn, J. A., Kerle, N., van der Meer, F. D., Parodi, G. N., Pohl, C., Reeves, C. V., van Ruitenbeek, F. J. A., Schetselaar, E. M., Weir, M. J. C., Westinga, E., & Woldai, T. (2009). *Principles of remote sensing: an introductory textbook*. International Institute for Geo-Information Science and Earth Observation. http://www.itc.nl/library/papers_2009/general/PrinciplesRemoteSensing.pdf

Texas Parks and Wildlife Department (TPWD). (n.d.). *Edwards Plateau Ecological Region*.https://tpwd.texas.gov/landwater/land/habitats/cross_timbers/ecoregions/edwards_plateau.phtml

Texas State University. (n.d.). *Precipitation | Climate Dashboard*. https://www.meadowscenter.txst.edu/climatechange/climatedashboard/precipitation.html#:~:text=West%20Texas%2C%20on%20average%2C%20receives,60%20inches%20per%20year2.

Unger, D., Bowes, C., Farrish, K., & Hung, I. K. (2013). Mapping oilfield brine-contaminated sites with mid-spatial resolution remotely sensed data. *GIScience and Remote Sensing*, *50*(6), 623-632. https://doi.org/10.1080/15481603.2013.850252

Zbinden, V. (2008). Arkansas SP Murphy, J. T., No. 1 Crater: National Register of Historic Places Inventory/Nomination Form. *Arkansas Historic Preservation Program.* 1-29. https://catalog.archives.gov/id/26143857

VITA

Victoria Williams received her degree of Bachelor of Environmental Science with a minor in Geology from the Arthur Temple College of Forestry and Agriculture Stephen F. Austin State University in 2021. Following this in 2022, she entered the Graduate School at Arthur Temple College of Forestry and Agriculture at the University of Texas System, Stephen F. Austin State University to pursue a major in Environmental Science and a minor in Geospatial Sciences in Nacogdoches, Texas.

Permanent Address: 202 Bowie Street

Nacogdoches, TX 75965

This thesis was typed by Victoria Williams in an American Psychological Association, 7th edition, 2019 writing format.